LIBRARY – AIR RESOURCES BOARD

FOG, CLOUD, AND DEW CHEMISTRY

Final Report

for

The California Air Resources Board

1800 15th. St.
Sacramento, California 95814

Eric Fujita, Project Manager

Contract Number: A4–075–32

Prof. Michael R. Hoffmann

Principal Investigator

Environmental Engineering Science
W. M. Keck Laboratories
California Institute of Technology
Pasadena, California 91125

28 February 1989

TABLE OF CONTENTS

	EXECUTIVE SUMMARY
CHAPTER 1	*ACTIVE CLOUDWATER COLLECTOR*
CHAPTER 2	*INSTRUMENT TO COLLECT FOGWATER FOR CHEMICAL ANALYSIS*
CHAPTER 3	*A COMPARISON OF TWO FOGWATER COLLECTORS*
CHAPTER 4	*THE $H_2SO_4-HNO_3-NH_3$ SYSTEM AT HIGH HUMIDITIES AND IN FOGS: SPATIAL AND TEMPORAL PATTERNS IN THE SAN JOAQUIN VALLEY OF CALIFORNIA*
CHAPTER 5	*THE $H_2SO_4-HNO_3-NH_3$ SYSTEM AT HIGH HUMIDITIES AND IN FOGS: COMPARISON OF FIELD DATA WITH THERMODYNAMIC CALCULATIONS*
CHAPTER 6	*TRANSPORT AND OXIDATION OF SO_2 IN A STAGNANT FOGGY VALLEY*
CHAPTER 7	*DEPOSITIONAL ASPECTS OF POLLUTANT BEHAVIOR IN FOG AND INTERCEPTED CLOUDS*
CHAPTER 8	*CHEMISTRY AND PHYSICS OF ACID FOGS, CLOUDS, & HAZE AEROSOL*
CHAPTER 9	*KINETICS AND MECHANISMS OF CHEMICAL REACTIONS IN CLOUDS & FOGS*

CHAPTER 10 *CLOUDWATER CHEMISTRY IN SEQUOIA NATIONAL PARK*

CHAPTER 11 *IDENTIFICATION OF HYDROXYMETHANE-SULFONATE IN FOG WATER*

CHAPTER 12 *ANALYSIS OF ALDEHYDES IN NATURAL WATER SAMPLES BY HPLC WITH A POSTCOLUMN REACTION DETECTOR*

CHAPTER 13 *CARBOXYLIC ACIDS AND CARBONYL COMPOUNDS IN SOUTHERN CALIFORNIA CLOUDS AND FOGS*

CHAPTER 14 *FOGWATER CHEMISTRY AT RIVERSIDE*

CHAPTER 15 *CLOUDWATER CHEMISTRY IN THE SANTA BARBARA CHANNEL*

CHAPTER 16 *CHEMICAL COMPOSITION OF FOGWATER COLLECTED ALONG THE CALIFORNIA COAST*

CHAPTER 17 *NUTRIENT LEACHING FROM PINE NEEDLES IMPACTED BY ACIDIC CLOUDWATER*

CHAPTER 18 *CHEMICAL CHARACTERIZATION OF STRATUS CLOUDWATER AND ITS ROLE AS A VECTOR FOR POLLUTANT DEPOSITION IN A LOS ANGELES PINE FOREST*

CHAPTER 19 *FIELD INTERCOMPARISON OF FIVE TYPES OF FOGWATER COLLECTORS*

EXECUTIVE SUMMARY

Background

In our previous studies, we had established that fog– and cloudwater in Southern California was consistently acidic (pH 1.7 to 4.0). As a continuation of that work, we have expanded both the intensity of our sampling effort and the detail of our chemical characterization.

The principal objectives of this research project were:

1. to develop refined instrumentation for the collection of cloud– and fogwater and to automate the fogwater collection process,

2. to carry out multiple site sampling and analysis of aerosol, gases, clouds, and fogs in the Los Angeles (LA) coastal zone, in the Riverside area, at elevated sites in the Los Angeles basin, in the Santa Barbara Channel area, and in the southern San Joaquin Valley,

3. to characterize dew chemistry,

4. and to correlate cloud– and fogwater data with standard air quality measurements.

Our first principal objective was to construct an automated fogwater collector, which would allow fogwater monitoring to be done more conveniently. This objective has been achieved; the development effort resulted in the granting of a United States Patent (No.

4,697,462) for the design of a fog– and cloudwater collector with an associated automatic collection and field storage system. The results of this work are presented in Chapters 1, 2, and 3 of the final report.

With the aid of automated collectors, we were able to determine the spatial and temporal variation of fog/cloud chemistry within large areas of fog occurrence. The second array of principal objectives were all achieved; detailed reports of these efforts are given in Chapters 4, 5, 6, 7, 12, 13, 14, 15, 16, 17, and 18 of the final report.

After an preliminary investigation of dew chemistry in a variety of locations in the LA Basin, further investigations were halted because the relative importance of dew as a depositional pathway for atmospheric acidity was established to be negligible. Other investigators have confirmed our assessment of the importance of dew chemistry/deposition relative to dry deposition, wet deposition, and fog–derived deposition. This work has been reported in the Ph.D. thesis of J. M. Waldman (Ph.D., Caltech, 1986). With the encouragement and approval of the CARB project officers, we shifted our focus from dew to a preliminary investigation of the cloudwater chemistry in the Sierra Nevada Mountains. Results of this work are reported in Chapter 10.

Research objective number 4 was explored for fogs in the San Joaquin Valley, in the Los Angeles basin, and in the Santa Barbara Channel area. Using the techniques of multiple linear regression, a significant correlation was observed between the average nighttime cloud– and fogwater loadings of H^+ and NO_3^- and the maximum levels of O_3, NO_x, and NO recorded during the preceding days. Regression equations that were obtained were found to be reliable for predicting fogwater loadings of H^+ and NO_3^-.

Regions of high fog/cloud frequency that have been studied in detail include the Los Angeles coastal area, where previous work suggests that the highest acidities occur. the Riverside–San Bernardino area, which is subject to fog during the height of the smog season. the Santa Barbara Channel area, and the Southern San Joaquin Valley, in which the occurrence of highly acidic fogs is held in check by substantial ammonia emissions. The

limited ventilation documented by previous tracer studies of the Santa Barbara Channel and presence of fog and high humidity there suggest that rapid S(IV) (i.e. total SO_2 aqueous) oxidation in the Channel results in highly acidic fog. As predicted pH values in the vicinity of the Santa Barbara Channel have been found to range from 2.1 to 3.5. Preliminary investigations of mountain–top cloud chemistry were performed in Sequoia National Park. In conjunction with fog and cloud sampling, we have performed more detailed mesurements of deposition during fog.

In addition to determining the inorganic speciation of fog and cloudwater, we have determined the role of carboxylic and sulfonic acids in fog acidification. Our previous work has shown the covariance of very high levels of S(IV) and formaldehyde, suggesting the presence of aldehyde–S(IV) adducts (i.e. sulfonic acids). We have determined quantitatively the higher aldehydes and a series of dicarbonyls such as glyoxal, methyl glyoxal and biacetyl; furthermore we have identified a variety of sulfonic acid salts formed by reaction of S(IV) with aldehydes in the droplet phase.

Overview

Clouds, fogs, and haze aerosols are subjected to the same chemical processes because of their physical similarities. For example, cloud– and fogwater droplets are found in the size range of 2 to 50 μm, while deliquescent haze aerosol will be in the range of 0.01 to 1 μm. On the other hand, raindrops are approximately 100 times larger than cloud and fog water droplets (0.1 to 3 mm). However, a more important determinant of aqueous–phase chemistry within the droplets is the liquid water content (LWC); values of LWC range from 0.1 to 1.0 g m^{-3} in clouds, from 0.01 to 0.5 g m^{-3} in fogs, and from 10 to 100 μg m^{-3} in haze aerosols. The presence of condensation nuclei, which are composed of both soluble and insoluble materials, is essential for the formation of atmospheric water droplets. Accretion or evaporation of water to or from the condensation nuclei or droplet is forced by the difference between the ambient and

local humidities, and is affected by the droplet surface tension and the chemical potential of the solutes in the liquid phase. During droplet growth, the temperature within the droplet differs from the ambient temperature due to the release of latent heat, which in turn depends upon the instantaneous growth rate.

Fog and cloud droplets are highly effective at scavenging certain gases and particles present in the atmosphere. The overall fraction of material incorporated into fog droplets depends upon nucleation scavenging and gas transfer. The initial chemical speciation may be altered by *in situ* chemical transformations and subsequent droplet–phase scavenging. The total concentration of species i in a parcel of air is given by

$$[C_i]_T = [C_i]L + P_{C_i}(RT)^{-1} + [C_i]_a$$

where $[C_i]_T$ is the total concentration of C_i (mol m^{-3}) in the atmosphere, $[C_i]_f$ is the concentration of C_i in the droplet phase in units of mol m^{-3} ($[C_i]_f = L[C_i]$), $[C_i]_g$ is the concentration (mol m^{-3}) of C_i in the gas phase ($[C_i]_g = P_{C_i}(RT)^{-1}$), and $[C_i]_a$ is the concentration of C_i in the non–activated aerosol. R is the universal gas constant (atm m^3 mol^{-1} K^{-1}) and T is temperature in degrees K.

Fog– and cloudwater often have extremely low pH values (e.g. $1.7 < pH < 4$) and extremely high concentrations of sulfate (1 to 20 mM), nitrate (1 to 20 mM), ammonium ion (0.1 to 20 mM) and trace metals (1 to 1000 μM). Waldman et al. (1) and Munger et al. (2) have summarized concentrations reported for fogs and clouds sampled in California and elsewhere around the world. Of special interest are the high values observed for SO_4^{2-}, NO_3^-, S(IV), CH_2O, Fe, Mn, Pb and Cu in fogwater. These values and their time–dependent changes indicate that fogs and clouds provide a very reactive environment for the accumulation of HNO_3 and H_2SO_4. Concomitant incorporation of NH_3 gas and calcareous dust into the droplet phase neutralizes some of the acidity. In the pH domain typically encountered in fogs and clouds (pH 2–7), absorption of $SO_2(g)$, $HNO_3(g)$, $H_2O_2(g)$, and $NH_3(g)$ is

thermodynamically favorable because of their relatively high Henry's Law coefficients.

Of the metals commonly found in atmospheric water droplets, Fe, Mn and Cu are expected to be potential catalysts for the *in situ* oxidation of S(IV) with molecular oxygen. Iron and Mn have been found in concentrations as high as 400 μM and 15 μM in fog (1–7). Model calculations indicate that metal–catalyzed autoxidations along with oxidation by H_2O_2, O_3, and OH may contribute significantly to the overall sulfate formation rate in atmospheric droplets, particularly in the range of Fe and Mn concentrations observed in urban fog (8–10).

In addition to transition metal ions a wide variety of other chemical constituents have been found in clouds. For example, carbonyl compounds, such as aldehydes and ketones, have been found to influence liquid–phase sulfur dioxide chemistry through their reactions with SO_2 to form stable α–hydroxyalkanesulfonates. Field measurements have detected formaldehyde at concentrations of greater than 100 μM in fog– and cloudwater samples collected in Southern California (11–13). The concentrations of glyoxal and methylglyoxal occasionally approach or exceed that of CH_2O. In addition to each one of the aldehydes present the corresponding carboxylic acid has been observed, although formic and acetic acid dominate the low molecular weight carboxylic acids. They are found found in concentrations as high as 100 μM.

The presence of CH_2O and H_2O_2 ($2 - 50$ μM) in conjunction with S(IV) at levels higher than those predicted by gas/liquid solubility equilibria suggests that α–hydroxymethane-sulfonate (HMS, $HOCH_2SO_3^-$) production stabilizes a fraction of S(IV) with respect to oxidation. Equilibrium calculations using available thermodynamic and kinetic data for the reaction of SO_2 and CH_2O demonstrate that elevated concentrations of S(IV) in fog water cannot be achieved without consideration of sulfonic acid production, $HORHSO_3^-$ (11). Munger et al. (13) have identified and quantified HMSA using ion–pairing chromatography. Other S(IV) adducts which have been observed in cloudwater droplets include those formed with glyoxal, methylglyoxal, acetaldehyde, and hydroxyacetaldehyde.

Jacob et al. (14–17) have systematically characterized the interaction of H_2SO_4, HNO_3, NH_3 and in fog, aerosol, and the gas phase. The observed spatial patterns of concentrations

were shown to closely reflect the distribution of SO_2, NO_x, and NH_3 emissions within well–defined regions. Furthermore, they (16) have compared field data for the H_2SO_4–HNO_3–NH_3 system with thermodynamic calculations of the aerosol composition. Close agreement has been found between field measurements and theoretical predictions. Their field studies have shown that typical wintertime conversion rates for S(IV) in fogs were about 5 % hr^{-1} and about 1 % hr^{-1} in haze aerosol.

Gas–phase reactions of SO_2 with ozone (O_3), hydroxyl radical ($OH\cdot$), and hydroperoxyl radical ($HO_2\cdot$) are too slow to account for observed rates of sulfate production in humid urban atmospheres (18–19) and in wave clouds (20). Consequently, the catalytic autoxidation of SO_2 in deliquescent haze aerosol and hydrometeors appears to be a viable non–photolytic pathway for the rapid formation of sulfuric acid in humid atmospheres (21–26). In addition, hydrogen peroxide and ozone have been established as important aqueous–phase oxidants of dissolved SO_2 (26). Oxidation by H_2O_2 seems to be most favorable under low pH conditions (pH < 4) because of a rapid rate of reaction and a negative pH–dependence that favors the facile conversion of HSO_3^- to sulfate. In comparison, metal–catalyzed autoxidation and oxidation of S(IV) with O_3 tend to proceed more slowly with decreasing pH (27).

Limiting factors in the autoxidation pathways are the total concentration of the active metal catalyst and its equilibrium speciation as a function of pH. Los Angeles fog water contains high concentrations of iron, manganese, copper, nickel and lead (3,4,6,7). Of these metals, Fe, Mn and Cu are expected to be the most effective catalysts for the reaction of S(IV) with molecular oxygen (25–27). Model calculations indicate that metal–catalyzed autoxidations may contribute significantly to the overall sulfate formation rate in atmospheric droplets, particularly in the range of Fe and Mn concentrations observed in urban fog. However, the composition of the precursor haze aerosol or cloud condensation nuclei will determine to a large extent the observed chemical speciation of the droplet phase.

Chameides (28) has predicted based on model calculations that aqueous–phase free radical pathways can contribute substantially to the generation of acidity via the *in situ*

oxidation of S(IV) and HCHO to S(VI) and formic acid, respectively. The principal oxidants of S(IV) as identified by Chameides were H_2O_2, O_3, $\cdot OH$, and $HO_2\cdot$. Parameters found to affect the S(IV) to S(VI) conversion rate were the accommodation coefficient for the reactive species of interest, the liquid water content, and the ambient levels of SO_2 and HNO_3. Seigneur and Saxena (29) have predicted that gas–phase hydrocarbon chemistry will dominate $\cdot OH$ chemistry (i.e., aqueous–phase $\cdot OH$ chemistry due to radical scavenging appears to be inconsequential). While Mozurkewich (30) argues that nitrate radical, NO_3, is unlikely to play an important role in the nighttime chemistry of a cloud because of its low Henry's Law constant (~ 0.03 M atm^{-2}). Jacob (31) has shown that radical pathways are very important for the chemistry of remote clouds in terms of formate production and in terms of the buildup of peroxymonosulfuric acid, a S(VI)–peroxide intermediate of high oxidation potential (32).

Aqueous–phase pathways for the production of nitric acid are relatively minor contributors to nitrate accumulation in the droplet phase because of the low Henry's Law constants for NO_2 and NO and because of second–order reaction kinetics with respect to $[NO_2]$ (33–34). The pathways for S(IV) transformation involve reactions with H_2O_2, O_3, O_2 (Fe^{3+} and Mn^{2+} catalyzed), $\cdot OH$, HONO, CH_3OOH, CH_3CO_3H, PAN, $HO_2\cdot$, HCHO, and soot.

Summary of Major Observations

1. A new collector that has a lower minimum size cutoff and a higher sampling rate was designed, built, and utilized in several field sampling programs. An additional advantage of this collector, the Caltech Active Strand Collector (CASC), is the absence of external moving parts, making it safer for untended operation, and the capability of being connected to an automatic sampling system. (*vide infra*, Daube, Jr., et al., United States Patent Number 4,697,462, 1987; Chapters 1 & 2)

2. A side–by–side comparison of the previous collector, the Rotating Arm Collector (RAC) and the CASC was performed. In thin fog conditions the ratio of collection rates (CASC/RAC) exceeded the theoretical value. Because the CASC has a lower lower size cut than the RAC, it samples a greater fraction of the droplet spectrum. In thin fogs a significant fraction of the droplets may be in a size range that is only collected by the the CASC. If droplet evaporation on the strands were occurring the opposite trend would be observed. (Chapter 3)

3. Comparison of the chemical composition of the CASC and RAC samples indicated a possible size–dependent variation in droplet composition. RAC samples, which contain a greater proportion of large droplets, were enriched in Na^+, Mg^{2+}, Ca^{2+}, and Cl^-. These ions are associated with soil dust and sea salt, both of which are found in large aerosol. Concentrations of NO_3^-, SO_4^{2-}, and NH_4^+, which make up the smaller aerosol, showed no difference between the two samplers. These data suggest that large condensation nuclei lead to large droplets, thus the RAC samples, which contain a greater proportion of large drops, have higher concentrations of ions associated with the large aerosol. (Chapter 3)

4. Droplet deposition during fog has been shown to play an important role in the enhancement of acidic deposition. During stagnation episodes, pollutant removal from the Southern San Joaquin Valley requires at least 5 days, while the enhancement of deposition by fog formation leads to pollutant lifetimes on the order of 6–12 hours. Thus, in an environment characterized by flat, open landscape and low wind speed, droplet sedimentation can be the dominant removal mechanism of pollutants during prolonged stagnation episodes with fog. (Chapters 4, 5, 6 & 7)

5. Deposition rates for major species were 5 to 20 times greater during fogs than during non–foggy periods. Sulfate deposition rates (V_d) during fog ranged from 0.5 to 2 cm s^{-1} with a median value of 1.0 cm s^{-1}. Similar enhancements were observed for nitrate deposition. Ten hours of fog–induced deposition was found to be comparable to the deposition resulting from 10 cm of rainfall. (Chapter 7)

6. A systematic characterization of the atmospheric H_2SO_4–HNO_3–NH_3 system was conducted in the fogwater, the aerosol, and the gas phase at a network of site in the San Joaquin Valley. The concept of atmospheric alkalinity has been developed to interpret observed concentrations in terms of the buffering capacity of the atmosphere with respect to inputs of strong acids. The major components of fogwater alkalinity were found to be the conjugate bases of weak organic acids such as acetic acid, formic acid, lactic acid, and propionic acid. Secondary production of strong acids, H_2SO_4 and HNO_3, under stagnant conditions resulted in a complete titration of available alkalinity at the sites farthest from NH_3 sources. Steady–state SO_2 conversion rates of 0.4 to 1.1 % hr^{-1} were observed. Fog did not appear to enhance the conversion of NO_x. (*vide infra*, Jacob et al., *J. Geophys. Res.* **91**, 1073–1088, 1986; Chapter 4).

7. Concentrations of $HNO_{3(g)}$ and $NH_{3(g)}$ were determined in the field under both foggy and non–foggy conditions, simultaneously with aerosol and fogwater composition. Observed concentrations were found to compare favorably with thermodynamic model predictions. In this model, the equilibrium composition was calculated by minimizing the Gibbs free energy of a system composed of the following species: in the gas phase $H_2SO_{4(g)}$, $HNO_{3(g)}$ and $NH_{3(g)}$; in the aqueous phase H^+, HSO_4^-, SO_4^{2-}, NO_3^-, and NH_4^+; and the solid phases $NH_4HSO_{4(s)}$, $(NH_4)_3H(SO_4)_{2(s)}$, $(NH_4)_2SO_{4(s)}$, $NH_4NO_{3(s)}$, $(NH_4)_2SO_4 \cdot 3NH_4NO_{3(s)}$, and $(NH_4)_2SO_4 \cdot 2NH_4NO_{3(s)}$. (*vide infra*, Jacob et al., *J. Geophys. Res.* **91**, 1089–1096, 1986; Chapter 5).

8. The fate of SO_2 emitted in the San Joaquin Valley under stagnant foggy conditions was determined by the release of an inert tracer and the concurrent monitoring of SO_2 and SO_4^{2-} concentrations. At night, SO_2 was found to be trapped in a dense fog layer below a strong and persistent inversion base. Lack of ventilation led to the accumulation of SO_2 and sulfate in the atmosphere. The rate of oxidation of SO_2 to sulfate was determined to be ~ 3 % hr^{-1}. Production of acidity from the oxidation of SO_2 fully titrated the $NH_{3(g)}$ present before the fog and led to a progressive drop of the fogwater pH.. The tracer data indicated that about 40% of the air transported upslope in the afternoon was returned to the valley in the night–time drainage flow. (*vide infra*, Jacob et al., *Atmos. Environ.* 21, 1305–1314, 1987; Chapter 6)

9. Formaldehyde, formate, and acetate have been determined in fog and cloudwater at a number of locations in Southern California. Up to 190 μM formate and acetate was seen in samples from the San Joaquin Valley. HCHO concentrations as high as 500 μM have been observed. Fog from Riverside had maximum concentrations of 1500 and 500 μM formate and acetate while HCHO was as high as 380 μM. Average formate and acetate concentrations near Santa Barbara and San Pedro were in the range of 10 to 60 μM with HCHO ranging between 10 and 20 μM. High aqueous–phase concentrations of organic acids are observed either near sources where ambient levels are high or at sites where the cloudwater pH is high. (Chapters 11, 12 & 13)

10. Hydroxymethanesulfonate (HMS) has been determined to be an important chemical species in fog and cloud water. Concentrations of HMS as high as 300 μM have been observed. HMS was determined in fog water by a novel ion–pairing chromatographic method. HMS represents an important source of acidity for water droplets and a significant atmospheric reservoir for S(IV). (*vide infra*, Munger et al., *Science* 231.

247–249, 1986; Chapter 11)

11. Aldehydes in cloudwater samples have been analyzed by two independent methods. In the one case, dinitrophenylhydrazone derivatives were prepared and analyzed by HPLC on a C_{18} column. In the second case, the aldehydes were derivatized with 3–methyl–2–benzothiazoline hydrazone and separated on a reversed–phase C_{18} column. Using these methods we have detected substantial concentrations of formaldehyde, acetaldehyde, glyoxal, hydroxyacetaldehyde, and methylglyoxal. In addition, the biacetyl was observed at measureable concentrations. At San Pedro [HCHO] ranged from 14 to 62 μM, [CH_3CHO] ranged from 2 to 5 μM, [CHOCHO] ranged from 1 to 31 μM, and [CH_3COCHO] ranged from 5 to 27 μM. While at Riverside, [HCHO] ranged from 6 to 197 μM, [CHOCHO] ranged from 1 to 139 μM, and [CH_3COCHO] ranged from 1 to 108 μM. (Chapters 12, 13, 14)

12. Kinetic and thermodynamic data obtained for the addition of S(IV) species with several aldehydes, including benzaldehyde, glyoxal, methylglyoxal, acetaldehyde, hydroxyacetaldehyde, and glyoxylic acid, was used to predict their effectiveness as reservoirs for S(IV) in atmospheric water droplets. Equilibrium calculations in an open atmosphere indicate that hydroxyacetaldehyde, glyoxal, glyoxylic acid, and to a smaller extent, methylglyoxal, lead to potentially significant enrichment of S(IV) in the liquid phase, although HMS is an even better reservoir for S(IV). Scavenging of SO_2 from the gas–phase due to hydroxyalkylsulfonate formation becomes important at high liquid water contents, pH $\geq$ 5, and when an excess partial pressure of the aldehyde is present. The overall dissolution of RCHO and SO_2 into a droplet and the subsequent formation of the hydroxyalkylsulfonate, also results in a net increase in acidity, which in a weakly buffered solution, can be more than a unit drop in pH.

13. Acidic cloudwater was consistently observed in intercepted stratus collected along the Santa Barbara Channel coast. Ventura and Pt. Mugu, which are immediately adjacent to the coast, were the most acidic. Casitas Pass, which is further inland was somewhat less acidic. (Chapter 15)

14. Nitrate is equivalent to or slightly greater than sulfate in the Santa Barbara Channel intercepted stratus. The NO_3^-:SO_4^{2-} ratio was found to be ≤ 2. In contrast the ratio of NO_x to SO_2 in local emissions and in the LA basin is ≥ 2. (Chapter 15)

15. Fogwater collected at Riverside was highly concentrated. Ammonium concentrations ranged from 8 to 26 mN; NO_3^- ranged from 6 to 29 mN; and SO_4^{2-} ranged from 1.4 to 6.2 mN. (Chapter 14)

16. pH values in Riverside fogwater dropped to 2.3, despite the presence of excess NH_3 in the gas phase during the day. HNO_3 is the dominant acid. At night, reduced vertical mixing and drainage flows would isolate the sampling site from the NH_3 emission area. Continued production of HNO_3 via NO_3^- and N_2O_5–pathways could then acidify the fog. Fog on the floor of the basin may still be in contact with the NH_3 emissions and would not be acidic. This mechanism implies that there could be a region of acidic fogwater on the slopes surrounding the Riverside/San Bernardino basin. (Chapter 14)

17. The preexisting aerosol is not completely scavenged by the fog forming at Riverside. Scavenging efficiencies computed from fogwater loading and concurrent or prior aerosol samples are typically < 50%. These radiation fogs never achieve high enough supersaturations to activate all of the aerosol. (Chapter 14)

18. Cloudwater samples collected in Sequoia National Park varied widely in chemical composition, both within the course of one event and from one event to another. The pH of the samples ranged from 4.4 to 5.7. The most acidic sample was not the sample with the highest ionic loading, indicating the importance of the varying composition of the sample in determining its acidity. (Chapter 10)

19. Organic acids were seen to be important contributors to the overall composition of many of the samples collected in Sequoia National Park. In some instances the concentrations of formate and acetate were comparable to those of nitrate and sulfate. (Chapter 10)

20. The advance of cold fronts into the Park seems to lead to higher aerosol and gas–phase concentrations than would be seen under normal mountain–valley circulation patterns, particularly during the night and morning hours. The arrival of these increased concentrations prior to and during cloud impaction on the mountain slopes leads to higher cloudwater concentrations than would otherwise be expected. (Chapter 10)

21. A size–fractionating inlet on the Caltech Active Strand Collector was used to collect intercepted stratus on San Pedro Hill. Ions associated with soil dust and sea salt (Ca^{2+}, Mg^{2+}, and Na^{+}) were enriched in the large droplet fraction. The secondary aerosol ions (NH_4^{+}, SO_4^{2-}, and to some extent H^{+}) were enriched in the small droplet fraction. Ions that are associated with gas-phase species (HCl and HNO_3) showed mixed behavior. The concentrations of several components that exist partly in the gas phase (e.g. Cl^{-}, HCOOH, and CH_3COOH) appear to be independent of droplet size.

22. Multiple linear regression analysis has shown that $[H^+]$ in the droplet phase in the Santa Barbara Channel area, as an example, can be predicted by

$$[H^+]_{aq} = 29.2(O_3) + 33.8(NO_x) - 35.8(NO) - 157.1$$

where $[H^+]_{aq}$ is the average nightly cloudwater loading of H^+ expressed in neq m^{-3} and (O_3), (NO_x), and (NO) are the maximum hourly gas–phase concentrations of O_3, NO_x, and NO, respectively, in parts per hundred million (pphm). The correlation coefficient for this relationship is 0.84. Similar equations are available for other components and for different locations.

Conclusions

1. Riverside California, which often has high pH fogwater and is near emission sources, had the highest concentrations of carbonyl compounds and organic acids reported to date in the literature. Low pH fogs (~ 2) can arise in the Riverside area due to downslope flow of polluted air that is depleted in ammonia.

2. The formation of hydroxymethanesulfonate (HMSA) contributes to high concentrations of CH_2O observed in fogwater.

3. Oxidation of aromatic hydrocarbons and ozonolysis of isoprene appear to be the two important sources of the dicarbonyl compounds found in fogs.

4. The pre–existing aerosol, which is the principal determinant of fogwater composition, is not completely scavenged by the radiation fogs due to the relatively low water supersaturation levels. High degrees of supersaturation are necessary to activate all of

the aerosol. Coastal stratus clouds are highly efficient scavengers of pre–existing aerosol.

5. Cloudwater is routinely acidic (pH $\cong$ 3) in the Santa Barbara Channel area.

6. HCl is volatilized from sea–salt aerosol by exchange with HNO_3; when clouds appear the HCl is rescavenged.

7. Sources for acidity in the Santa Barbara Channel appear to be the oxidation of local emissions of NO_x and SO_2, or transport of polluted air from Los Angeles.

8. Some of the variability in cloudwater chemical composition can be explained by changes in cloud liquid water content. Changes in concentration can also occur during periods of relatively constant liquid water content. Removal by drizzle results in decreases in concentration. Wind shifts, enhanced turbulence, or entrainment from aloft may account for increases in concentration.

9. Differences in the composition of size–fractionated cloudwater samples indicate that large droplets are formed from sea salt and soil dust, which are large aerosol, and small droplets are formed on small secondary aerosol composed of primarily ammonium sulfate and ammonium nitrate.

10. Model calculations show that a reduction in sources of NH_3 in the LA Basin will result in the production of uniformly acidic fogs with pH $\cong$ 2. This scenario could become a reality with the commercial and residential development of land in the Chino area. A similar situation exists in the Southern San Joaquin Valley.

Recommendations for Future Research

Two areas for future research are the size–dependence of droplet chemical composition, and turbulent mixing processes in cloud and fog layers. A size–fractionating inlet has been developed for use with the Caltech Active Strand Collector. Samples collected from one coastal stratus cloud event indicate that large droplets are derived from large sea–salt and soil–dust aerosol and small droplets are formed from secondary ammonium sulfate and nitrate aerosol. Future work should refine the size–fractionating inlet in order to provide a sharper size cut and verify the performance of the inlet. A comprehensive experiment to determine the size dependence of droplet composition would include size–fractionated aerosol sampling, measurement of aerosol and droplet size distributions, cloud liquid water content. An adequate means for determining liquid water content in ground–based sampling is not presently available. Gravimetric methods for LWC determination do not allow sufficient time resolution to follow fluctuations in LWC from due to the turbulence in the cloud. Other locations, with different aerosol characteristics need to be investigated.

Results presented here and results of other studies indicate that entrainment from aloft is an important factor controlling cloud and fog chemical composition. Formation of HNO_3 via the $NO_2 + NO_3 \longrightarrow N_2O_5$ reaction is likely in the inversion layer above the cloud or fog. The mountains surrounding the Riverside basin and the coastal mountains in Los Angeles and the Santa Barbara Channel are ideal sites to study this phenomenon. A comprehensive experiment to identify the role of above–cloud reaction and entrainment mixing would include a vertical array of aerosol, gas, and cloudwater samplers and meteorological instruments.

Publications

The points summarized above are discussed in detail in the relevant chapters of the of the main body of the report. The primary data collected as a part of this research has been

documented in the Appendices of the Ph.D. theses of J. M. Waldman (1986), D. J. Jacob (1985), and J. W. Munger (1989). Copies of these theses can be obtained for a nominal charge from University Microfilms in Ann Arbor, Michigan. In addition the following publications have resulted directly from research activity related to this contract:

D. J. Jacob, Ph.D. Thesis, "The Origins of Inorganic Acidity in Fog," California Institute of Technology, Pasadena, 331 pages, 1985.

J. M. Waldman, Ph.D. Thesis, "Depositional Aspects of Pollutant Behavior in Fog," California Institute of Technology, Pasadena, CA, 322 pages, 1986.

J. W. Munger, Ph.D. Thesis, "The Chemical Composition of Fogs and Clouds in Southern California," California Institute of Technology, Pasadena, 395 pages, 1989.

J. M. Waldman, J. W. Munger, D. J. Jacob, and M. R. Hoffmann, "Chemical Characterization of Stratus Cloudwater and its Role as a Vector for Pollutant Deposition in a Los Angeles Pine Forest." *Tellus,* **37B**, 91–108 (1985).

D. J. Jacob, J. M. Waldman, M. Haghi, M. R. Hoffmann, and R. C. Flagan, "An Automatable Instrument to Collect Fogwater for Chemical Analysis." *Rev. Sci. Instr.,* **56**, 1291–1293 (1985).

D. J. Jacob, J. M. Waldman, J. W. Munger, and M. R. Hoffmann, "Chemical Composition of Fogwater Collected along the California Coast." *Environ. Sci. Tech.,* **19**, 730–735 (1985).

D. J. Jacob, J. M. Waldman, J. W. Munger, and M. R. Hoffmann, "The H_2SO_4–HNO_3–NH_3 System at High Humidities and in Fogs: I. Spatial and Temporal Patterns in the San Joaquin Valley of California." *J. Geophys. Res.* **91D**, 1073–1088 (1986).

D. J. Jacob, J. M. Waldman, J. W. Munger, and M. R. Hoffmann, "The H_2SO_4–HNO_3–NH_3 System at High Humidities and in Fogs: II. Comparison of Field Data with Thermodynamic Calculations." *J. Geophys. Res.* **91D**, 1089–1096 (1986).

J. W. Munger, C. Tiller, and M. R. Hoffmann, "Identification and Quantification of Hydroxymethanesulfonic Acid in Atmospheric Water Droplets," *Science,* **231**, 247–249 (1986).

M. R. Hoffmann, "Fog and Cloud Water Deposition," in ***Materials Degradation Caused by Acid Rain***, R. Baboian, ed., American Chemical Society Symposium Series, **318**, 64–91, (1986).

M. R. Hoffmann, J. M. Waldman, J. W. Munger, and D. J. Jacob, "The Chemistry and Physics of Acid Fogs, Clouds, and Haze Aerosol," in ***Aerosols: Research, Assessment and Control Strategies***, S. D. Lee, T. Schneider, L. D. Grant, and P. J. Verkerk, eds., Lewis Publishers, Chelsea, MI (1986).

M. R. Hoffmann and J. M. Waldman, "The Chemistry, Microphysics, and Physics of Enhanced Pollutant Deposition in Dew, Fog, and Intercepted Clouds," in ***Sources and Fates of Aquatic Pollutants***, R. A. Hites and S. J. Eisenreich, eds., Advances in Chemistry Series, American Chemical Society, Washington,79–130 (1987).

D. J. Jacob, F. H. Shair, J. M. Waldman, J. William Munger, and M. R. Hoffmann "Transport and Oxidation of SO_2 in a Stagnant Foggy Valley," *Atmos. Environ.* **21**, 1305–1313 (1987).

B. C. Daube, Jr., R. C. Flagan, and M. R. Hoffmann (1987) "Active Cloudwater Collector," United States Patent, Patent Number: 4,697,462; Date: Oct. 6, 1987.

S. V. Hering, D. L. Blumenthal, R. L. Brewer, A. Gertler, M. Hoffmann, J. A. Kadlecek, and K. Pettus, "Field Intercomparison of Five Types of Fog Water Collectors," *Atmos. Environ.*, **21**, 654–663 (1987).

J. M. Waldman, J. W. Munger, D. J. Jacob, and M. R. Hoffmann, "A Field Study of Pollutant Deposition in Radiation Fog," in the *The Chemistry of Acid Raand Atmospheric Processes,"* R. Johnson, ed., ACS Symposium Series, American Chemical Society, Washington, DC, **239**, 250–257 (1987).

M. Igawa, J. W. Munger, and M. R. Hoffmann, "Analysis of Aldehydes in Cloudwater Samples by HPLC with a Postcolumn Reaction Detector," in press, *Environ. Sci. Technol.* (1989).

J. W. Munger, J. Collett, B. C. Daube and M. R. Hoffmann, "Carboxylic Acids and Carbonyl Compounds in Southern California Clouds and Fogs," in press, *Tellus* (1989).

J. Collett, B. C. Daube, J. W. Munger, and M. R. Hoffmann, "Cloudwater Chemistry in Sequoia National Park" in press, *Atmos. Environ.* (1989).

J. M. Waldman and M. R. Hoffmann, "Nutrient Leaching from Pine Needles Impacted by Acidic Fogwater," *Water, Air and Soil Pollution*, **37**, 193–201 (1988).

T. M. Olson and M. R. Hoffmann, "Hydroxyalkylsulfonate Formation: Its Role as a S(IV) Reservoir in Atmospheric Water Droplets," in press, *Atmospheric Environment* (1989).

J. M. Waldman, J. W. Munger, D. J. Jacob, and M. R. Hoffmann, "A Field Study of Pollutant Deposition in Radiation Fog," submitted to *Atmos. Environ.* (1988).

J. W. Munger, J. Collett, B. Daube, and M. R. Hoffmann, "Fogwater Chemistry at Riverside California," in press, *Atmos. Environ.* (1989).

J. Collett, J. W. Munger, B. Daube, and M. R. Hoffmann, "A Comparison of Two Cloudwater/fogwater Collectors," in press, *Atmos. Environ.* (1989).

Table 1. Fogwater Concentrations in Riverside

	Vol	pH	Na^+	NH_4^+	Ca^{2+}	Mg^{2+}	Cl^-	NO_3^-
	ml	←				μN		→
				23 January 1986				
N	8	8	8	8	8	8	8	8
Min	18	2.33	30	8660	100	27	100	7580
Max	59	3.70	123	19800	362	86	371	20100
Avg $_{vol\ wt}$		2.99	52	11096	175	43	158	819
				28 February 1986				
N	4	4	4	4	4	4	4	4
Minimum	16	4.24	35	8340	106	23	130	6050
Maximum	92	5.22	64	18100	209	55	384	13300
Avg $_{vol\ wt}$		4.59	48	9588	122	27	178	7050

23 January 1986

	SO_4^{2-}	S(IV)	CH_2O	H_2O_2	HFo	HAc	HMSA	−/+	LWC
	μN	←			μM		→		g m^{-3}
N	8	8	8	8	8	4	8	8	
Min	1430	13	165	0	106	56	49	0.90	
Max	3960	64	279	0	346	237	103	1.01	
Avg $_{vol\ wt}$	1929	40	194	0	—	—	73	0.96	0.074

28 February 1986

N	4	4	4	4	4	4	NA	4	
Min	1810	5	175	6	357	134	NA	0.94	
Max	3660	15	370	25	576	267	NA	0.97	
Avg $_{vol\ wt}$	2096	11	221	14	444	163		0.95	0.109

Table 2. Cloudwater Composition Along the Santa Barbara Channel

Laguna Peak Cloudwater *5 August – 14 August 1986*

	Vol	pH	Na^+	NH_4^+	Ca^{2+}	Mg^{2+}	Cl^-	NO_3^-	SO_4^{2-}	$SO_{4\,xs}^{2-}$ *
	ml		←			μN				→
N		20	20	20	20	20	20	20	20	20
Min		2.69	9	143	4	3	46	344	276	275
Max		3.46	318	686	73	88	350	1410	1340	1335
Avg		3.07	68	337	16	20	122	702	590	582
$Avg_{vol\ wt}$		3.16	47	276	11	15	105	579	472	466

	S(IV)	CH_2O	H_2O_2	HFo	HAc	H^+	–/+	LWC
	←			μM		→		$g\ m^{-3}$
N	15	15	15	16	16	20	20	20
Min	0	7	0	24	12	347	0.75	0.02
Max	0	33	6	103	44	2042	1.57	0.39
Avg	0	17	2	42	18	941	1.05	0.21
$Avg_{vol\ wt}$	0	17	1	39	17	775	1.02	

Laguna Road Cloudwater *5 August – 14 August 1986*

	Vol	pH	Na^+	NH_4^+	Ca^{2+}	Mg^{2+}	Cl^-	NO_3^-	SO_4^{2-}	$SO_{4\,xs}^{2-}$ *
	ml		←			μN				→
N	20	20	20	20	20	20	20	20	20	20
Min		2.58	119	445	21	28	102	612	425	407
Max		3.49	1070	1780	162	247	758	2140	2630	2500
Avg		3.06	367	857	65	90	325	1030	1000	956
$Avg_{vol\ wt}$		3.12	319	807	59	79	299	926	860	822

	S(IV)	CH_2O	H_2O_2	HFo	HAc	H^+	–/+	LWC
	←			μM		→		$g\ m^{-3}$
N	18	18	17	16	20	20	20	
Min	0	4	0	21	7	324	0.81	
Max	12	15	21	74	34	2630	1.31	
Avg	2	11	7	40	15	1054	1.03	
$Avg_{vol\ wt}$	2	10	7	29	11	872		

Table 2. (continued)

Ventura Hill Cloudwater *30 July – 14 August 1986*

	Vol	pH	Na^+	NH_4^+	Ca^{2+}	Mg^{2+}	Cl^-	NO_3^-	SO_4^{2-}	$SO_{4\ xs}^{2-\ *}$
	ml		←			μM				→
N	32	32	32	32	32	32	32	32	32	32
Min	33	2.74	74	405	18	23	104	247	267	246
Max	188	4.92	5720	2990	1400	1450	4290	6480	3220	2528
Avg	111	3.12	745	959	154	181	684	1430	948	858
$Avg_{vol\ wt}$		3.05	471	833	87	112	463	1161	797	740

	S(IV)	CH_2O	H_2O_2	HFo	HAc	H^+	–/+	LWC
	←			μM		→	g m^{-3}	
N	30	30	29	16	17	32	32	32
Min	0	5	0	31	3	12	0.58	0.02
Max	0	27	29	96	173	1820	1.08	0.18
Avg	0	13	11	60	32	971	0.99	0.10
$Avg_{vol\ wt}$	0	13	10	56	30	896		

Casitas Pass Cloudwater *31 July – 14 August 1986*

	Vol	pH	Na^+	NH_4^+	Ca^{2+}	Mg^{2+}	Cl^-	NO_3^-	SO_4^{2-}	$SO_{4\ xs}^{2-\ *}$
	ml		←			μM				→
N		32	32	32	32	32	32	32	32	32
Min		3.33	12	149	8	6	22	147	108	106
Max		4.52	176	1130	170	52	164	892	769	753
Avg		3.97	47	613	29	18	58	406	329	277
$Avg_{vol\ wt}$		3.90	41	552	24	15	53	369	295	290

	S(IV)	CH_2O	H_2O_2	HFo	HAc	–/+	H^+	LWC
	←		μM		→	μM	g m^{-3}	
N	32	30	22	25	25	32	32	32
Min	0	3	3	16	4	0.83	30	0.05
Max	0	13	16	58	15	1.02	468	0.28
Avg	0	8	6	27	10	0.93	131	0.14
$Avg_{vol\ wt}$	0	7	4	19	7	0.94	126	

$SO_{4\ xs}^{2-\ *}$ = Excess Sulfate = Total Sulfate – Marine Sulfate

Table 3. Fogwater Concentrations at Elevated Sites in the Los Angeles Basin

San Pedro Hill 1987

	V(mL)	pH	Na^+	NH_4^+	Ca^{2+}	Mg^{2+}	Cl^-	NO_3^-	SO_4^{2-}	CH_2O	−/+	LWC
			‖⟵			μN			⟶‖	μM		g m^{-3}
N	240	242	241	242	225	231	242	242	242	80	241	227
Min	1	2.42	6	44	3	1	11	28	39	5	0.73	0.00
Max	69	4.98	3796	9383	1143	1151	2096	8191	5796	51	1.84	0.34
Avg	49	3.25	404	775	82	107	369	1185	917	23	1.09	0.14
Avg vol wt		3.15	263	632	51	65	256	941	736	—	—	0.103

	V(mL)	pH	S(IV)	CH_2O	H_2O_2	HCOOH*	CH_3COOH*
			‖⟵		μM		⟶‖
N	21	21	—	20	16	21	21
Min	9	3.14	—	5	4	12	6
Max	59	3.83	—	38	72	43	31
Avg	38	3.58	—	13	42	20	10

* RCOOH = [RCOOH] + [RCO_2^-]

Henninger Flats 1987

	V(mL)	pH	Na^+	NH_4^+	Ca^{2+}	Mg^{2+}	Cl^-	NO_3^-	SO_4^{2-}	CH_2O	−/+	LWC
			‖⟵			μN			⟶‖	μM		g m^{-3}
N	76	76	76	76	76	76	76	76	76	17	76	72
Min	7	2.62	3	273	7	2	18	231	36	53	0.46	0.01
Max	65	4.78	1652	4085	985	435	975	5472	2606	109	1.33	0.40
Avg	50	3.25	166	1203	118	57	142	1206	689	71	0.94	0.14
Avg vol wt		3.29	82	845	74	31	86	855	511	—	—	0.09

Table 4. Fogwater Concentrations in the San Joaquin Valley

Bakersfield 1984

	pH Range	Na^+	NH_4^+	Ca^{2+}	Mg^{2+}	Cl^-	NO_3^-	SO_4^{2-}	HFo	−/+	LWC
		‖⟵			μN			⟶‖	μM		g m^{-3}
N	16	16	16	16	16	16	16	16	16		16
Avg	5.1–6.9	42	3270	169	33	122	819	2070	45		0.06

McKittrick 1984

	pH Range	Na^+	NH_4^+	Ca^{2+}	Mg^{2+}	Cl^-	NO_3^-	SO_4^{2-}	HFo	−/+	LWC
		‖⟵			μN			⟶‖	μM		g m^{-3}
N	58	58	58	58	58	58	58	58	58		58
Avg	2.7–5.2	11	480	39	5	15	250	345	22		0.11

Buttonwillow 1984

	pH Range	Na^+	NH_4^+	Ca^{2+}	Mg^{2+}	Cl^-	NO_3^-	SO_4^{2-}	HFo	−/+	LWC
		‖⟵			μN			⟶‖	μM		g m^{-3}
N	7	7	7	7	7	7	7	7	7		7
Avg	5.0–6.8	13	1067	82	10	47	522	760	144		0.05

Visalia 1984

	pH Range	Na^+	NH_4^+	Ca^{2+}	Mg^{2+}	Cl^-	NO_3^-	SO_4^{2-}	HFo	−/+	LWC
		‖⟵			μN			⟶‖	μM		g m^{-3}
N	13	13	13	13	13	13	13	13	13		13
Avg	5.5–7.2	6	1080	17	2	115	341	265	53		0.05

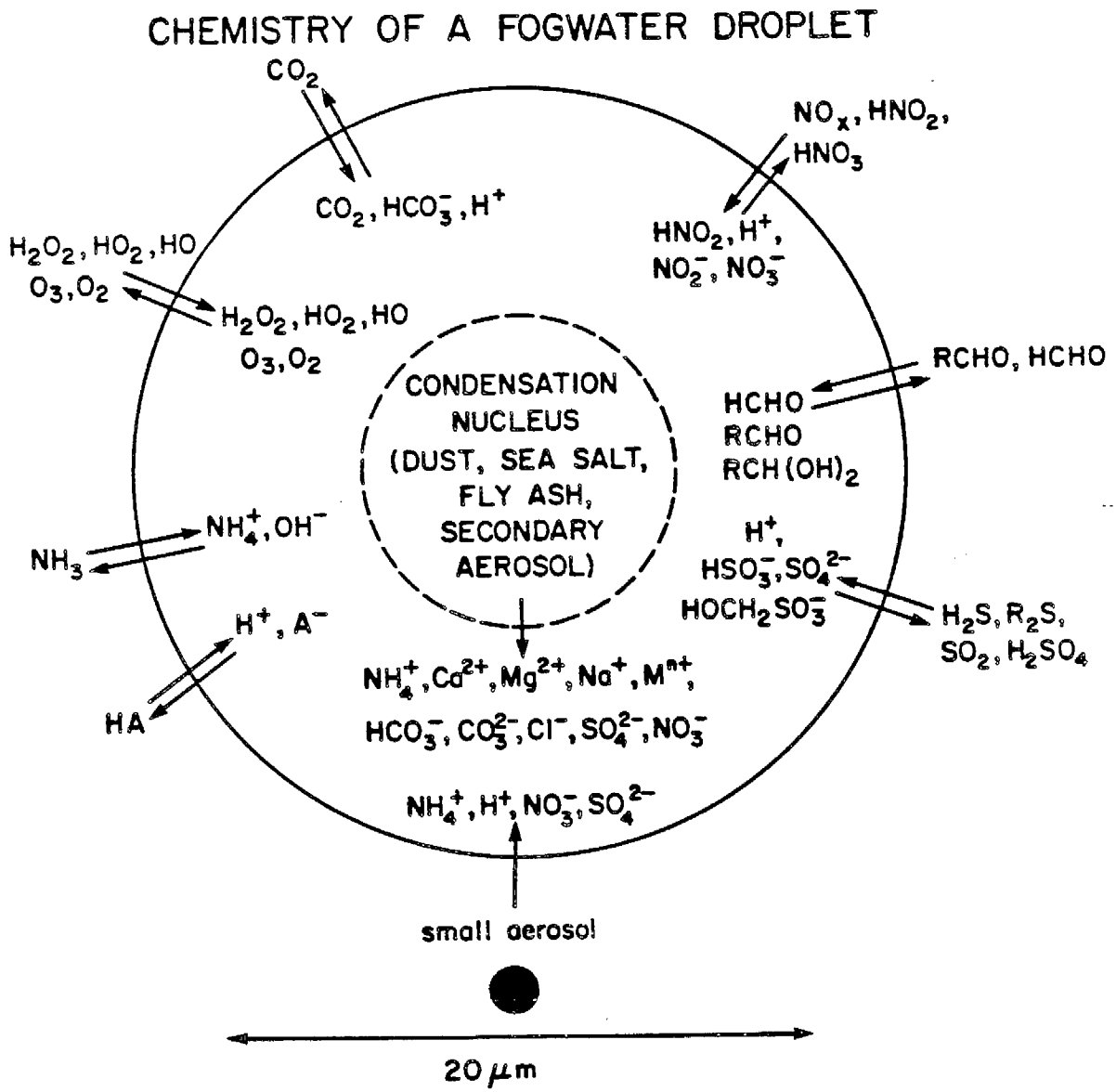

Figure 1. The chemistry of a fogwater droplet is indicated schematically. Important chemical processes involve a multiphasic system that includes solid, liquid, and gas phases.

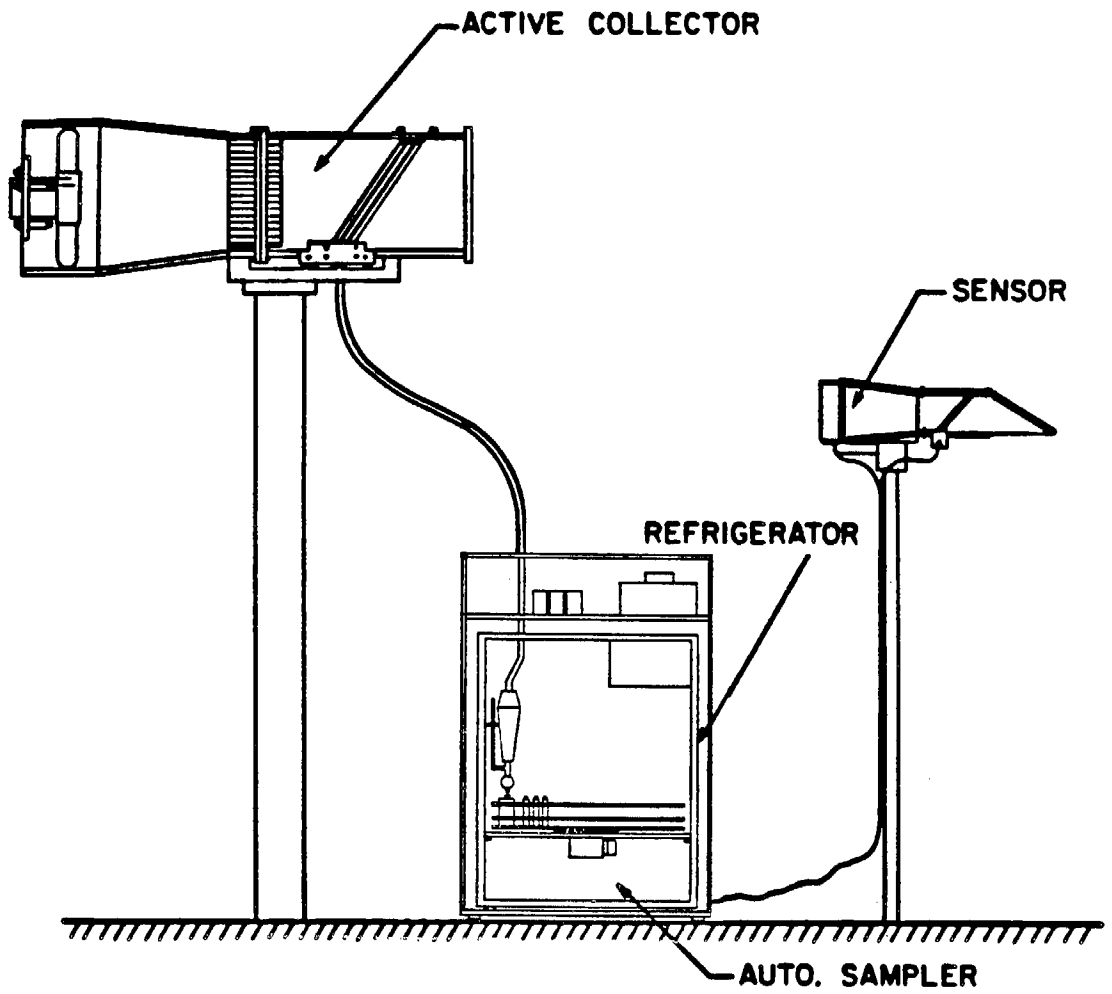

Figure 2. A schematic diagram of the automatic fogwater collection system. Details are provide in Chapter 1.

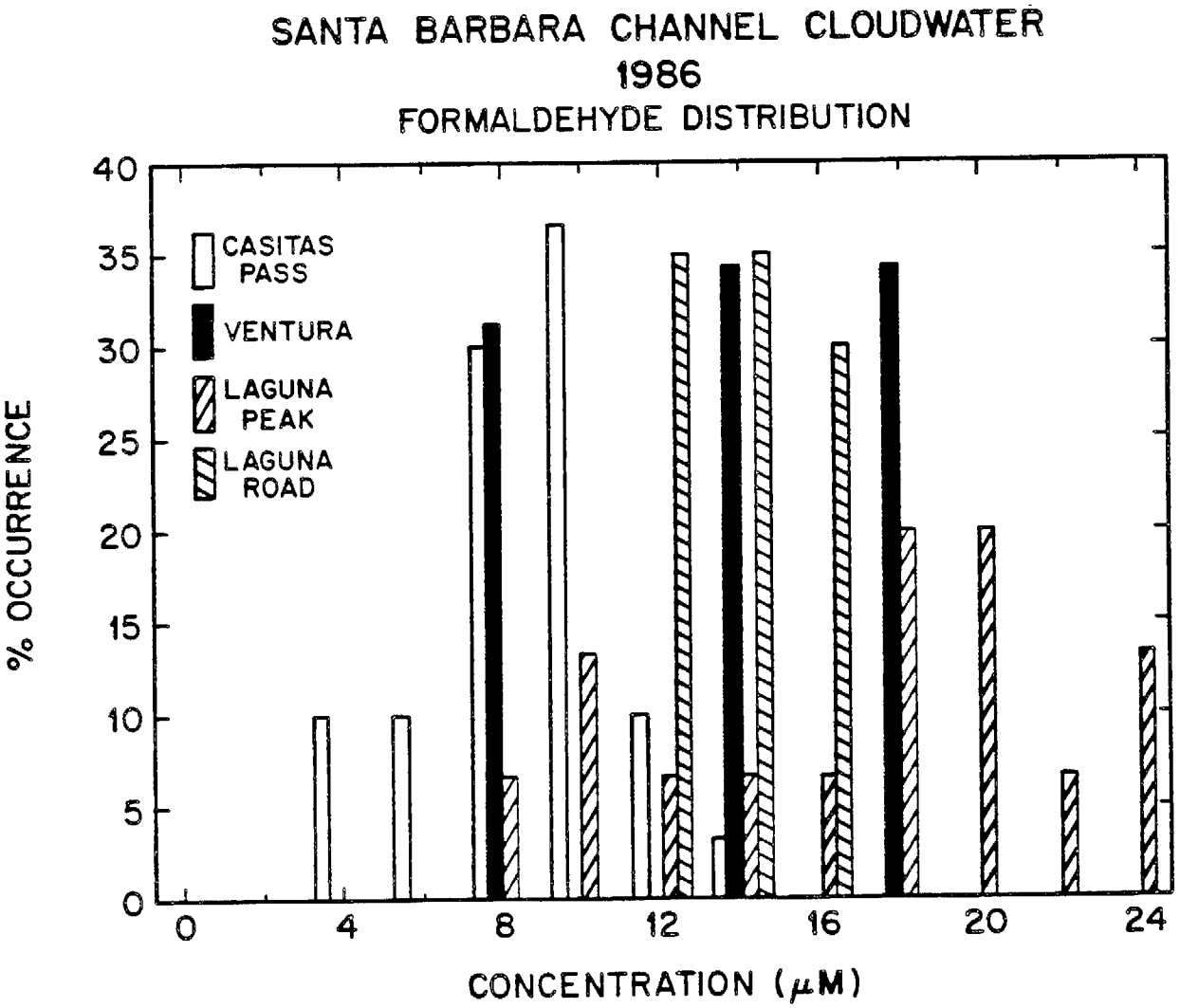

Figure 3. A frequency distribution of formaldehyde concentrations observed in Santa Barbara Channel cloudwater at four different locations. Results of the cloudwater study conducted in the Santa Barbara Channel are discussed in detail in Chapter 15.

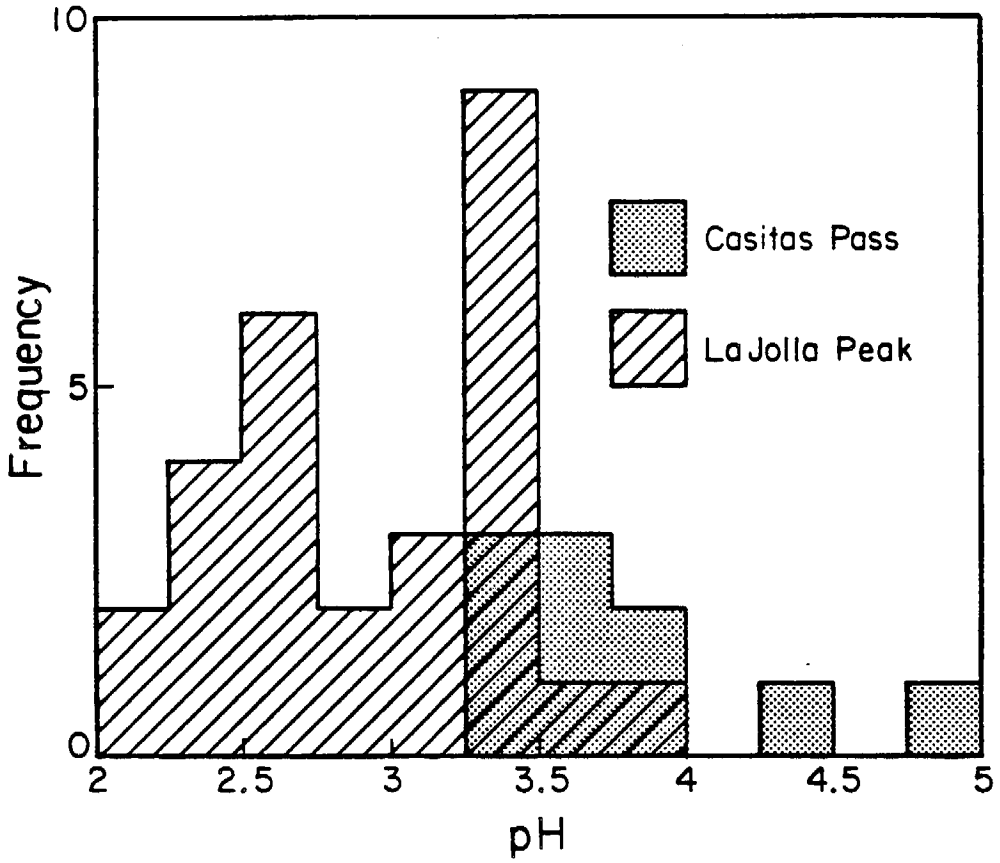

Figure 4. A frequency distribution for pH values in Santa Barbara Channel cloudwater at three two locations. Details are provided in Chapter 15.

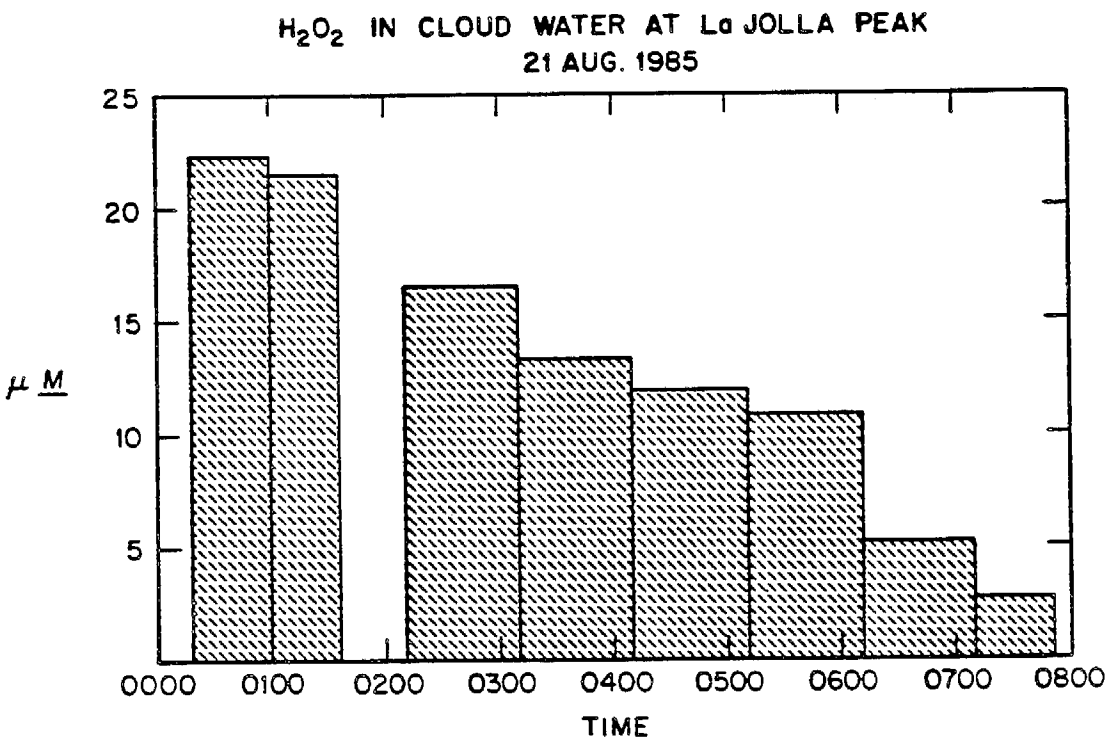

Figure 5. A concentration vs. time profile for hydrogen peroxide concentration as a function of time in Santa Barbara Channel cloudwater collected at LaJolla Peak. Detailed results of the cloudwater study conducted in the Santa Barbara Channel are provided in Chapter 15.

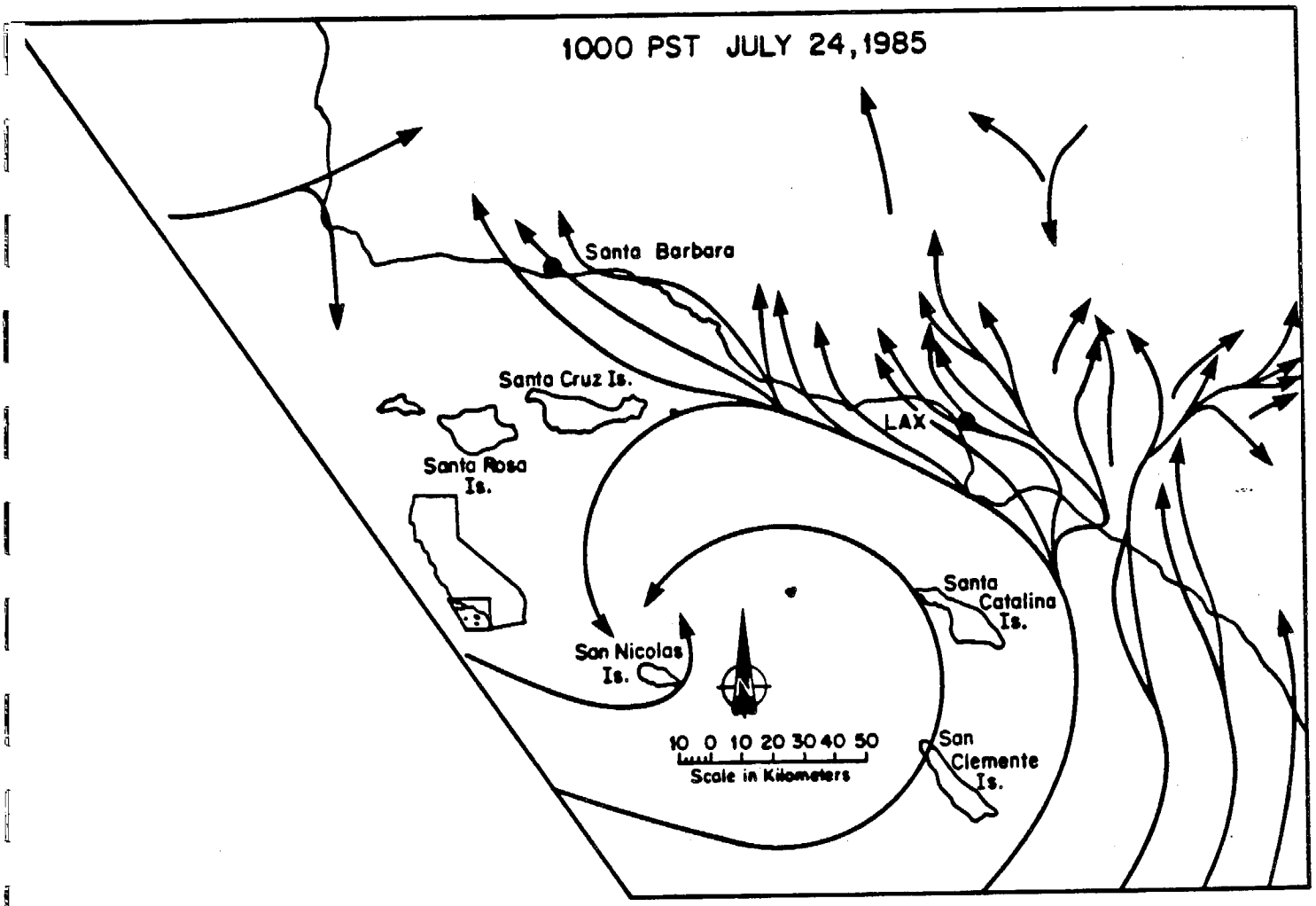

Figure 6. Streamlines calculated for the prevailing winds recorded during the morning of 24 July 1985 during a period of heavy stratus cloud impaction along the coast. The streamlines indicate that a portion of the Los Angeles air mass transported out to sea at night can be transported north into the Santa Barbara Channel. The chemical composition of the cloudwater at elevated sites along the coast is characteristic of LA cloudwater.

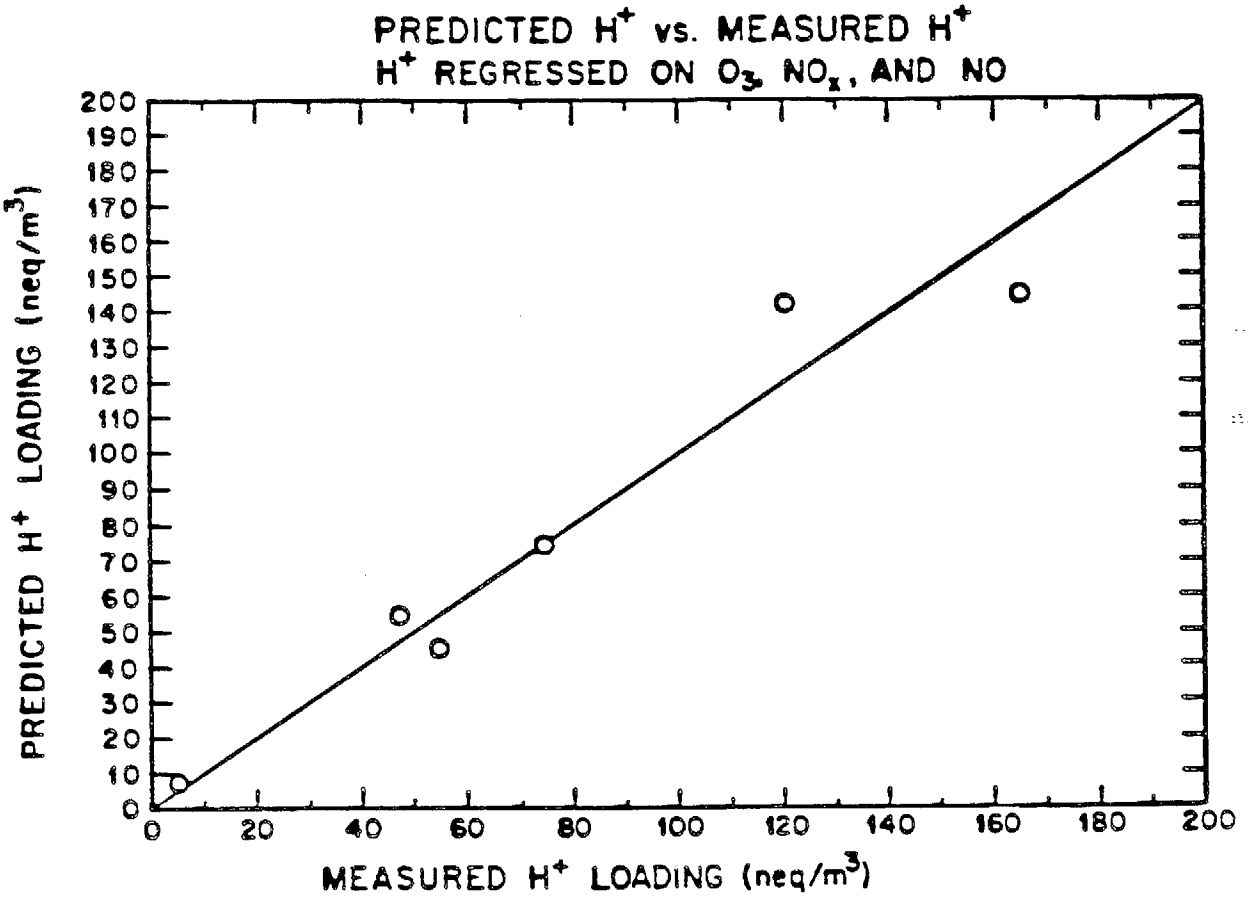

Figure 7. Average nightly cloudwater loadings (solid line) of H^+ predicted using maximum hourly O_3, NO, and NO_x concentrations observed the preceding day, and the actual observations at Ventura for 6 nights during the summer of 1986.

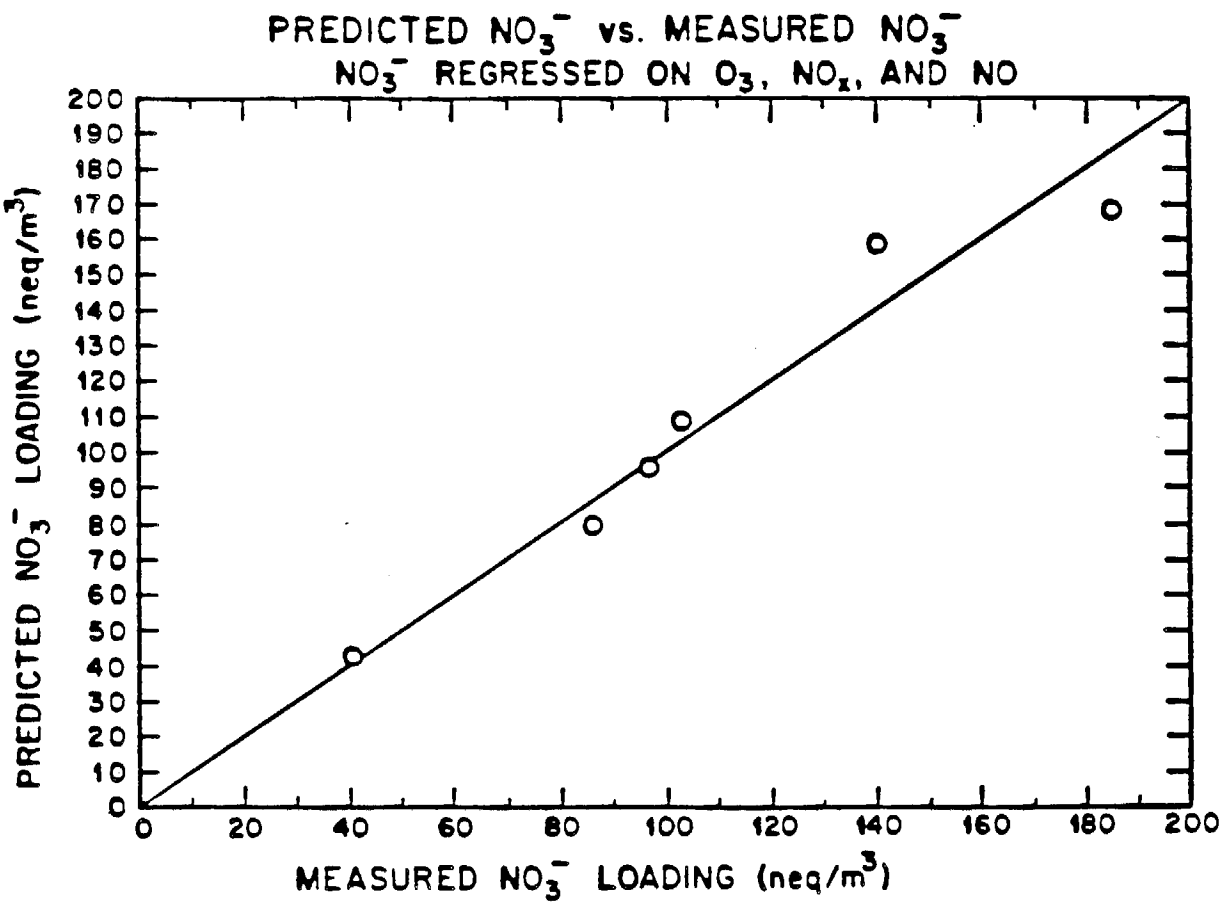

Figure 8. Average nightly cloudwater loadings (solid line) of NO_3^- predicted using maximum hourly O_3, NO, and NO_x concentrations observed the preceding day, and the actual observations at Ventura for 6 nights during the summer of 1986.

References

1. Liljestrand, H. M. Ph.D. Thesis, California Institute of Technology, Pasadena, 1980.

2. Liljestrand, H. M.; Morgan, J. J. *Environ. Sci. Technol.* 1981, **15**, 333–338.

3. Waldman, J. M.; Munger, J. W.; Jacob, D. J.; Hoffmann, M. R. *Tellus* 1985, **37B**, 91–108.

4. Munger, J. W.; Jacob, D. J.; Waldman, J. W.; Hoffmann, M. R. *J. Geophys. Res.* 1983, **88C**, 5109–5121.

5. Jacob, D. J.; Wang, R. T.; Flagan, R. C. *Environ. Sci. Tech.* 1984, **18**, 827–833.

6. Jacob, D. J.; Waldman, J. M.; Munger, J. W.; Hoffmann, M. R. *Environ. Sci. Technol.* 1985, **19**, 730–735.

7. Waldman, J. M.; Munger, J. W.; Jacob, D. J.; Flagan, R. C.; Morgan, J. J.; Hoffmann, M. R. *Science,* **218**, 677–680.

8. Jacob, D. J.; Hoffmann, M. R. *J. Geophys. Res.* 1983, 88, 6611–6621.

9. Jacob, D. J. Ph.D. Thesis, California Institute of Technology, Pasadena, 1985.

10. Hoffmann, M. R.; Jacob, D. J.; in "SO_2, NO and NO_2 Oxidation Mechanisms: Atmospheric Consideration"; Calvert, J. G., Ed.; ***Acid Precipitation Series*** Vol. 3, Butterworth Publishers: Boston, 1984; 101–172.

11. Munger, J. W., Jacob, D. J., and Hoffmann, M. R., *J. Atmos. Chem.* 1984, **1**, 335–350.

12. Waldman, J. M. Ph.D. Thesis, California Institute of Technology, Pasadena, CA, 1986.

13. Munger, J. W.; Tiller, C.; Hoffmann, M. R. *Science* 1986, **231**, 247–249.

14. Jacob, D. J.; Waldman, J. M.; Munger, J. W.; Hoffmann, M. R. *Tellus* 1984, **36B**, 272–285.

15. Jacob, D. J.; Waldman, J. M.; Munger, J. W.; Hoffmann, M. R. *J. Geophys Res.* 1986, **91D**, 1089–1096.

16. Jacob, D. J.; Munger, J. W.; Waldman, J. M.; Hoffmann, M. R. *J. Geophys Res.* 1986, **91D**, 1073–1088.

17. Jacob, D. J.; Shair, F. H.; Waldman, J. M.; Munger, J. W.; Hoffmann, M. R. *Atmos. Environ.* 1987, **21**, 1305–1313.

18. Calvert, J. G. SO_2, NO, and NO_2 Oxidation Mechanisms: Atmospheric Considerations, ***Acid Precipitation Series***, Vol. 3, Butterworth Publishers, Stoneham MA (1984).

19. Cass, G. R., Ph.D. Thesis, California Institute of Technology, Pasadena, CA (1977).

20. Hegg, D. A.; Hobbs, P. V. *Atmos. Environ.* 1982, **16**, 2663–2668.

21. Hegg, D. A. and Hobbs, P. V. *Atmos. Environ.* 1978, **12**, 241–253.

22. Kaplan, D. J., Himmelblau, D. M. and Kanaoka, C. *Atmos. Environ.* 1981, **15**, 763–773.

23. Penkett, S. A., Jones, B. M. R. and Eggleton, A. E. J. *Atmos. Environ.* 1979, **13**, 139–147.

24. Penkett, S. A., Jones, B. M. R., Brice, K. A. and Eggleton, A. E. J. *Atmos. Environ.* 1979, **13**, 123–137

25. Beilke, S. and Gravenhorst, G. *Atmos. Environ.* 1978, **12**, 231–239.

26. Martin, L. R. "Kinetic Studies of Sulfite Oxidation in Aqueous Solution," in SO_2, NO, and NO_2 Oxidation Mechanisms: Atmospheric Considerations, ***Acid Precipitation Series***, Vol. 3, Butterworth Publishers, Stoneham, MA (1984).

27. Hoffmann, M. R. and Boyce, S. D. "Catalytic Autoxidation of Aqueous Sulfur Dioxide in Relationship to Atmospheric Systems," in Trace Atmospheric Constituents: Properties, Transformations and Fates, S. E. Schwartz, ed. Adv. *Environ. Sci. Technol.* 1983, **12**, 147–189.

28. a. Chameides, W. L. and D. D. Davis, *J. Geophys. Res.,* 1982, **87C**, 4863–4877.

    b. Chameides, W. L., *J. Geophys. Res.,* 1984, **89D**, 4739–4755.

    c. Chameides, W. L., *J. Geophys. Res.* 1986, **91D**, 5331–5337.

29. Seigneur, C. and P. Saxena, *Atmos. Environ.* 1984, **18**, 2109–2124.

30. Mozurkewich, M., *J. Geophys. Res.* 1986, **91D**, 14569–14570.

31. Jacob, D. J., *J. Geophys. Res.* 1986, **91D**, 9807–.

32. Lee, Y. N. and Schwartz, S. E., *J. Geophys. Res.,* 1981, **86**, 11971–11983.

33. Schwartz, S. E., "Gas–Aqueous Reactions of Sulfur and Nitrogen Oxides in Liquid–Water Clouds," in *SO_2, NO and NO_2 Oxidation Mechanisms: Atmospheric Considerations*, Calvert, J. G., Ed.; Butterworth: Boston, 1984; Vol. 3, pp. 173–208.

34. Hoffmann, M. R. and Calvert, J. G. "Chemical Transformation Modules for Eulerian Acid Deposition Models Vol.II: The Aqueous–Phase Chemistry," EPA/NCAR Report DW 930237, March (1985).

35. Betterton, E. A. and Hoffmann, M. R. "Rapid Oxidation of Aqueous SO_2 by Peroxymonosulfate," submitted to, *J. Phys. Chem.* (1988).

CHAPTER 1

United States Patent [19]

Daube, Jr. et al.

[54] **ACTIVE CLOUDWATER COLLECTOR**

[75] Inventors: **Bruce C. Daube, Jr.; Richard C. Flagan; Michael R. Hoffmann,** all of Pasadena, Calif.

[73] Assignee: **California Institute of Technology,** Pasadena, Calif.

[21] Appl. No.: **867,820**

[22] Filed: **May 27, 1986**

[11] **Patent Number: 4,697,462**

[45] **Date of Patent: Oct. 6, 1987**

[57] **ABSTRACT**

A cloud water collector is disclosed comprised of a sampler duct having a plurality of spaced Teflon strands, in the form of screens, mounted across the conduit at an acute angle facing the open inlet of the conduit. Droplets in a cloud sample are drawn into the conduit by a fan located at the back end of the conduit, impact upon the Teflon strands and are drawn down to the lower ends of the strands, where they drop and the accumulated droplets are diverted to a sample bottle for collection. The cloud water collector can be automated to collect a plurality of successive cloud water samples by an automated sampler containing a reservoir into which cloud water obtained in the cloud water collector is discharged. A motor-driven turntable is provided which holds a plurality of sample bottles. When the reservoir is filled to a predetermined volume, apparatus, such as a liquid level sensor, actuates a valve to open same and discharge the liquid sample from the reservoir into one of the bottles at a filling station on the turntable. The valve then closes and the turntable rotates to index the next bottle beneath the reservoir at the filling station, and the operation is repeated to fill the latter bottle. When all of the bottles on the turntable have been filled, the indexing mechanism is deactivated and liquid accumulating in the reservoir is diverted to an overflow bottle.

United States Patent [19]

Daube, Jr. et al.

[11] **Patent Number: 4,697,462**

[45] **Date of Patent: Oct. 6, 1987**

[54] **ACTIVE CLOUDWATER COLLECTOR**

[75] Inventors: **Bruce C. Daube, Jr.; Richard C. Flagan; Michael R. Hoffmann,** all of Pasadena, Calif.

[73] Assignee: **California Institute of Technology,** Pasadena, Calif.

[21] Appl. No.: **867,820**

[22] Filed: **May 27, 1986**

[51] **Int. Cl.**[4] **G01N 1/24;** G01N 1/14; G01N 1/18

[52] **U.S. Cl.** ..... **73/863.21;** 73/863.02; 73/863.31; 73/864.34; 73/170 R; 55/185; 55/259; 55/528

[58] **Field of Search** ..... 73/863.21, 863.22, 863.23, 73/863.24, 863.25, 863.02, 863.03, 863.31, 864.34, 864.35, 170 R; 55/185, 257 PV, 259, 528

[56] **References Cited**

U.S. PATENT DOCUMENTS

2,699,679	1/1955	Munger	73/863.21
3,462,995	8/1969	Weiss	73/863.21
3,593,583	7/1971	Anderson et al.	73/863.21 X
3,889,532	6/1975	Pilie et al.	73/863.22
4,159,635	7/1979	Sehmel	73/863.22
4,570,494	2/1986	Dunn et al.	73/863.22

FOREIGN PATENT DOCUMENTS

500504	5/1976	U.S.S.R.	73/863.22

OTHER PUBLICATIONS

"A Technique for the Experimental Measurement of Collection Efficiency"; Conference on Cloud Physics Fort Collins, Colo., Aug. 24–27, 1970, paper reprint, pp. 139–142; J. R. Adam et al.

"A Linear Impactor for Fog Droplet Sampling"; *Atmospheric Environment,* vol. 14, No. 7, pp. 797–801; Sandra Fuzzi et al; 1980.

Primary Examiner—Tom Noland

Attorney, Agent, or Firm—Max Geldin

[57] **ABSTRACT**

A cloud water collector is disclosed comprised of a sampler duct having a plurality of spaced Teflon strands, in the form of screens, mounted across the conduit at an acute angle facing the open inlet of the conduit. Droplets in a cloud sample are drawn into the conduit by a fan located at the back end of the conduit, impact upon the Teflon strands and are drawn down to the lower ends of the strands, where they drop and the accumulated droplets are diverted to a sample bottle for collection. The cloud water collector can be automated to collect a plurality of successive cloud water samples by an automated sampler containing a reservoir into which cloud water obtained in the cloud water collector is discharged. A motor-driven turntable is provided which holds a plurality of sample bottles. When the reservoir is filled to a predetermined volume, apparatus, such as a liquid level sensor, actuates a valve to open same and discharge the liquid sample from the reservoir into one of the bottles at a filling station on the turntable. The valve then closes and the turntable rotates to index the next bottle beneath the reservoir at the filling station, and the operation is repeated to fill the latter bottle. When all of the bottles on the turntable have been filled, the indexing mechanism is deactivated and liquid accumulating in the reservoir is diverted to an overflow bottle.

25 Claims, 17 Drawing Figures

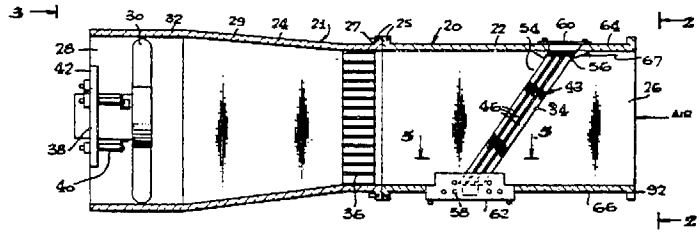

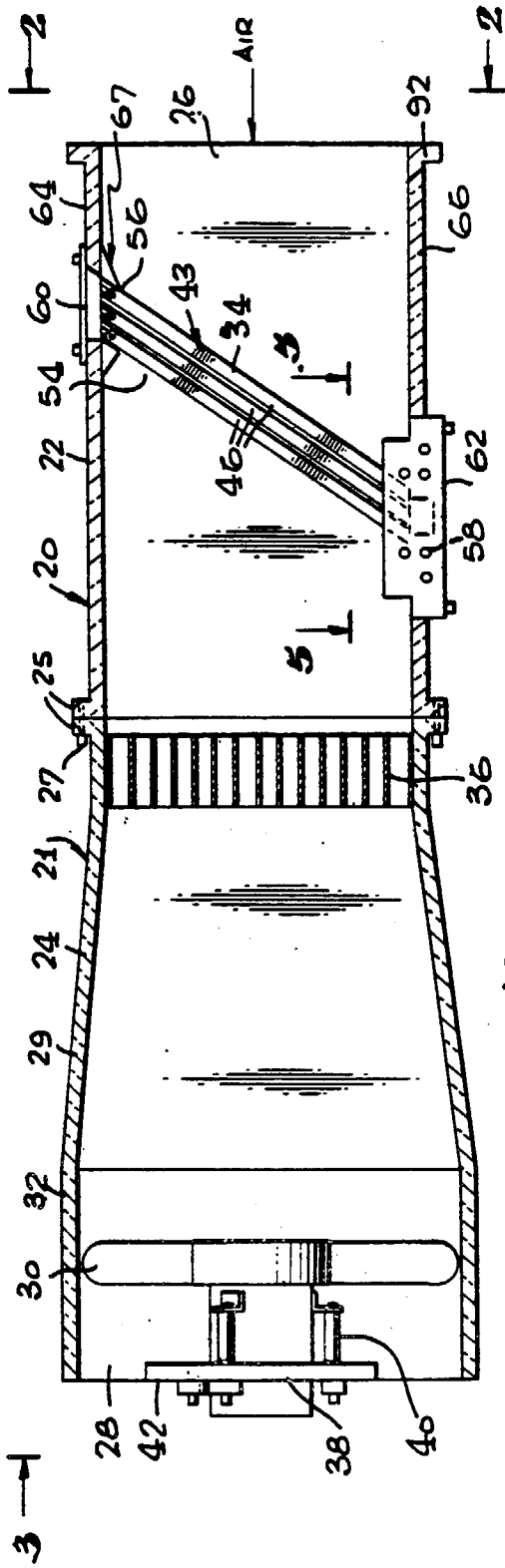

FIG. 1

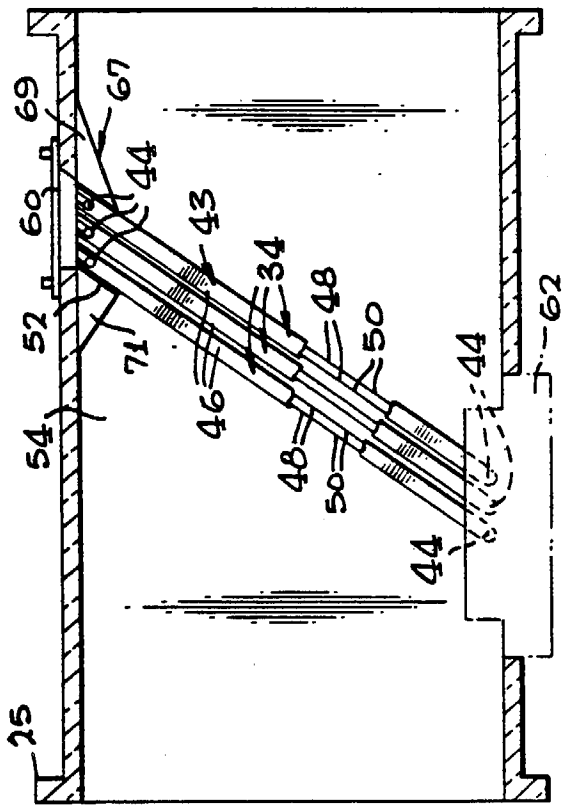

FIG. 1a

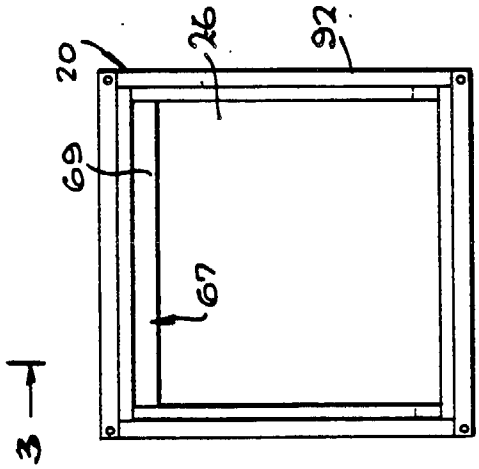

FIG. 2

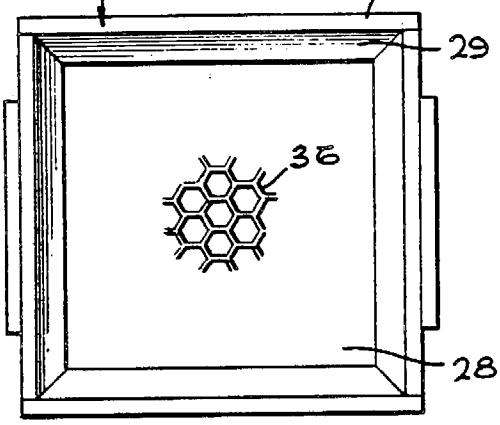

FIG. 3

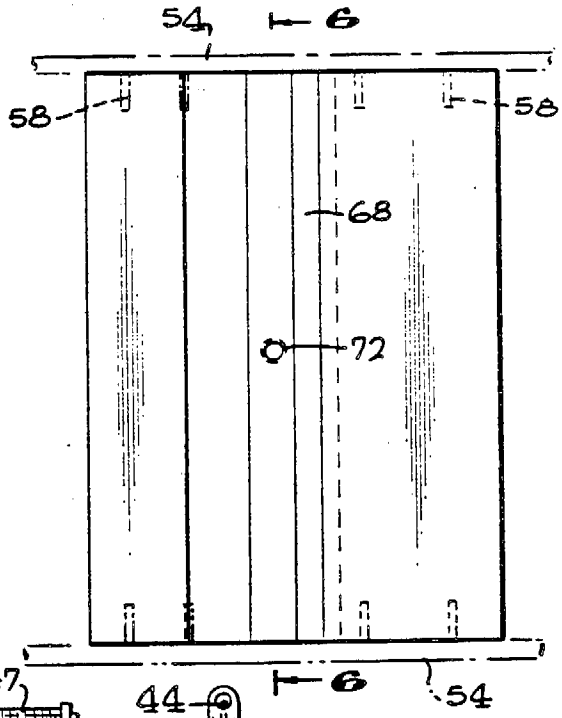

FIG. 5

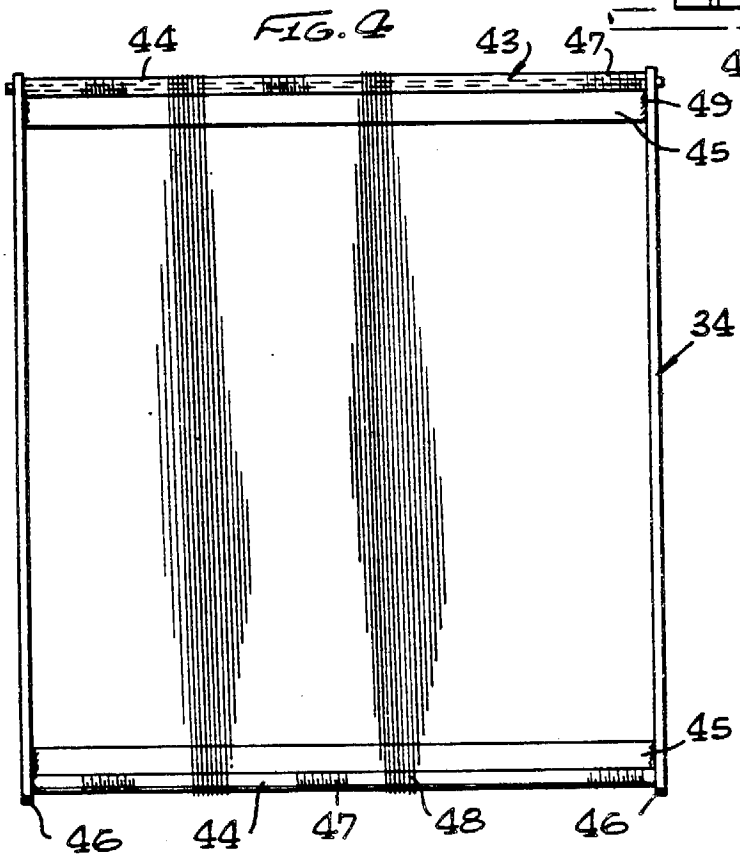

FIG. 4

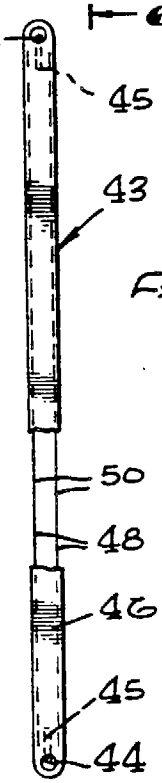

FIG. 4a

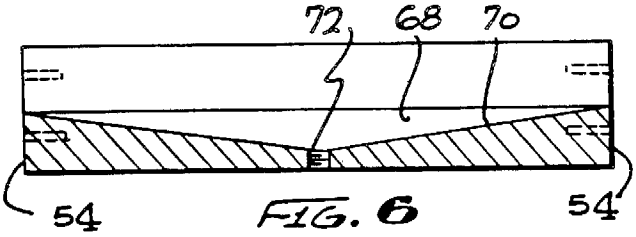

FIG. 6

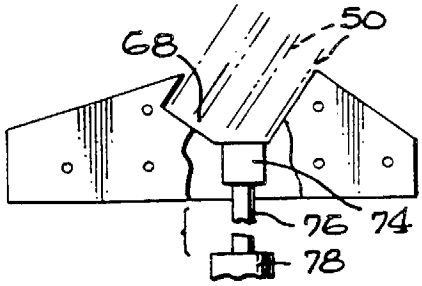

FIG. 7

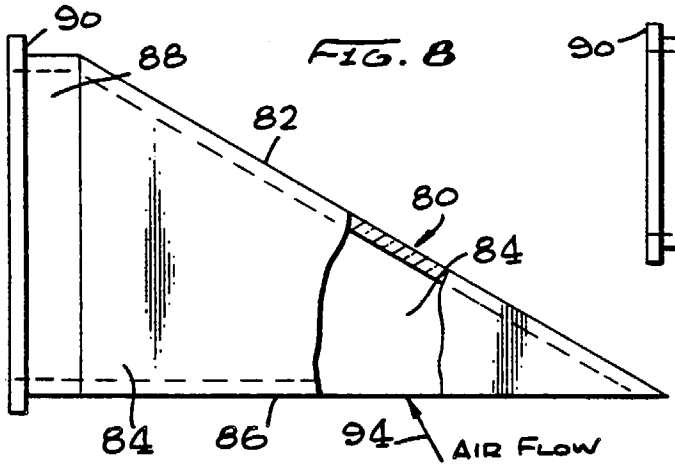

FIG. 8

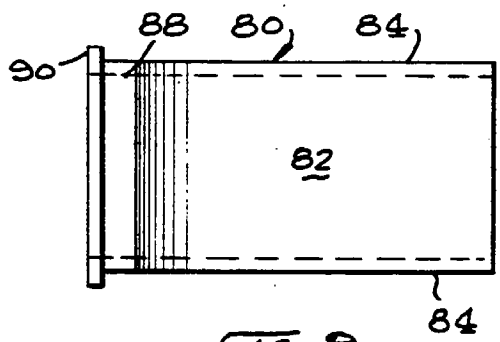

FIG. 9

FIG. 10

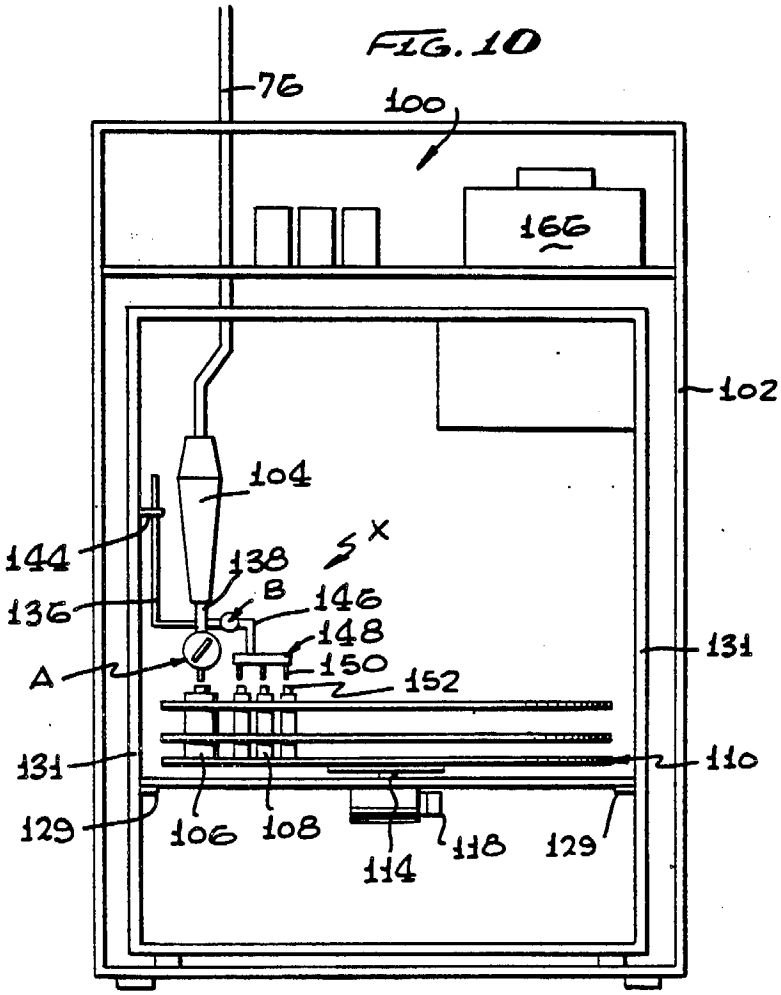

FIG. 11

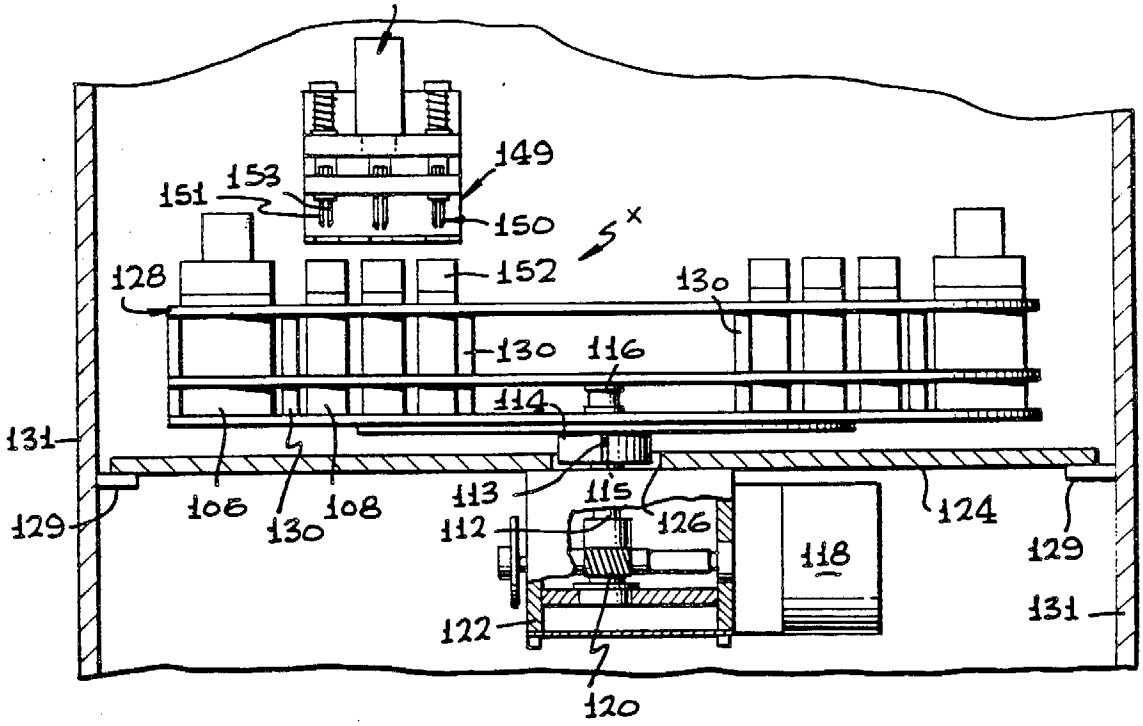

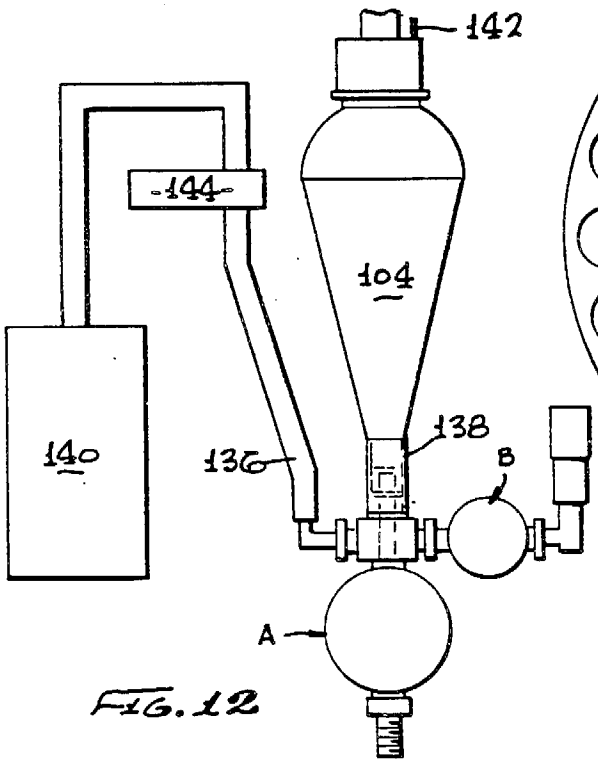

FIG. 12

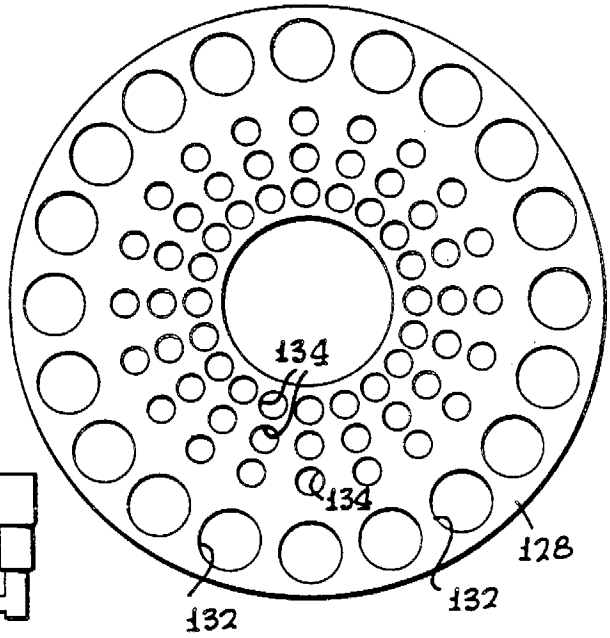

FIG. 13

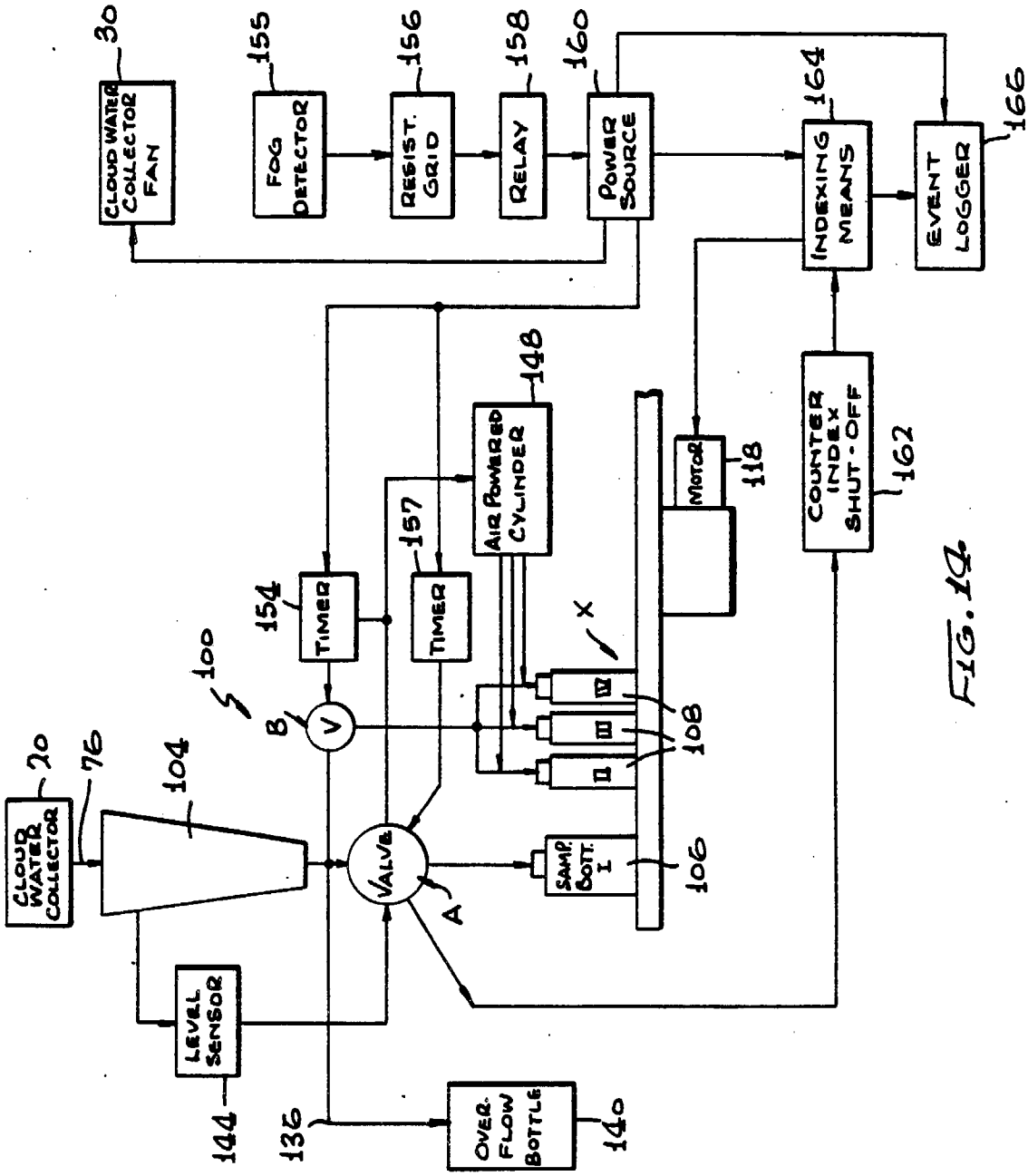
CLOUD WATER COLLECTOR FAN
30
FOG DETECTOR
155
RESIST. GRID
156
RELAY
158
POWER SOURCE
160
INDEXING MEANS
164
EVENT LOGGER
166
AIR POWERED CYLINDER
148
MOTOR
118
COUNTER INDEX SHUT-OFF
162
TIMER
154
TIMER
157
100
B
V
X
IV
III
II
108
CLOUD WATER COLLECTOR
20
76
104
VALVE
A
SAMP. BOTT. I
106
LEVEL SENSOR
144
136
OVER-FLOW BOTTLE
140

FIG. 14

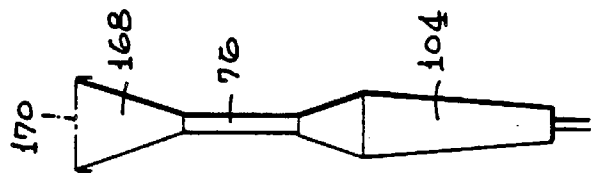
170
168
76
104

FIG. 15

ACTIVE CLOUDWATER COLLECTOR

BACKGROUND OF THE INVENTION

This invention relates to the collection of fog water or cloud water and, more particularly, to the collection of cloud water by a device wherein cloud droplets impact upon Teflon strands and are funneled into a sample bottle.

Under supersaturated conditions in the atmosphere, fog droplets form by activation of condensation nuclei and rapidly grow to diameters of 1 to about 100 microns. Recent reports of extremely high acidities in fogs, and clouds intercepting mountain slopes, have raised concern regarding related environmental consequences. Air quality control agencies in areas exposed to acidic fog have expressed the need to establish networks of sites monitoring the chemical composition of fog on a routine basis.

Various types of fog water collectors have been designed, including use of a filter medium to capture the water on impaction and dripping from large obstacles, such as sails.

U.S. Pat. No. 3,889,532 discloses apparatus for collecting fog water consisting of a slotted rotatable tube. The tube is rotated, and fog droplets are collected by impaction on the tube. Centrifugal force causes the water to flow outward toward the ends of the tube where it is collected in small vials. However, the device of this patent presents safety problems and is not suitable for automation.

SUMMARY OF THE INVENTION

It is an object of the present invention to provide an improved cloud water collector which efficiently collects fog droplets in the 1 to 100 micron diameter range.

Another object of the invention is the provision of a cloud water collector of the above type capable of preserving the size and chemical composition of fog droplets through all stages of collection.

A still further object is to provide a cloud water collector which rapidly collects relatively large amounts of liquid cloud water for wet chemical analysis.

Yet, another object is to provide a cloud water collector which is inexpensive to construct, is reliable and requires minimal maintenance.

Another object is the provision of an efficient cloud water collector which can be automated and including means for automating such collector.

A still further object is to provide an automated sampler, which is particularly useful in combination with the above-noted cloud water collector, or which can be used for collection of rain water samples.

According to the invention, there is provided a cloud water collector comprised of a sampler duct, e.g., in the form of a square box, open at both ends, and having a fan at the back of the duct. The fan draws the cloud through the sampler from the front of the duct, and the droplets in the cloud are impacted on Teflon (polytetrafluoroethylene or a copolymer of tetrafluoroethylene and hexafluoropropylene) strands or filaments which are strung in the form of a screen on a frame. The screen formed of the Teflon strands is inclined at an acute angle, preferably about 35° from vertical, facing the front of the duct.

The droplets in the cloud impacting upon the Teflon strands of the screen are drawn down by both the air drag and by gravity to the bottom of the screen where the water droplets accumulate and are diverted to a sample bottle, and the collected bottle of water is then analyzed chemically.

In preferred practice, the Teflon strand diameter, the spacing of the strands forming the screen, and the angle of the screen have values which provide efficient and rapid collection of fog droplets in the 1 to 100 micron size range while avoiding collection of the sub-micron aerosol particles. Also, in preferred practice, a honeycomb element is provided between the fan and the screen of Teflon strands, to straighten the flow of the sample cloud throuoh the duct and provide uniform flow of the cloud sample across the duct and through the Teflon screen, to improve the performance of the collector.

The cloud water collector of the invention is easily constructed, inexpensive, and operates in a reliable manner.

The cloud water collector of the invention can be modified for automating the device so as to automatically collect successive cloud water samples. The automating means comprises a motor-driven turntable which holds a plurality of sample bottles. The cloud water sample provided by the cloud water collector is discharged into a reservoir having a liquid level sensor. When the reservoir is filled to the predetermined level, the sensor actuates a valve to open same and discharge the sample from the reservoir into one of the bottles on the turntable. The valve closes and the turntable then rotates to index the next bottle beneath the reservoir and the operation is repeated to fill the latter bottle with additional sample cloud water provided by the cloud water collector.

Alternatively, a timer can be employed instead of a liquid level sensor, which actuates a valve to discharge the cloud water sample from the reservoir into the bottle below the reservoir, when a pre-set time interval has elapsed. If desired, a combination of liquid level sensing and timer means can be employed, as described in greater detail below.

The automation device, per se, can also be employed for automatically collecting rain water samples instead of cloud water samples. When so employed, rain water is collected in a funnel and then directed to the reservoir from which it is automatically discharged into the sample bottles in the manner noted above.

BRIEF DESCRIPTION OF THE DRAWINGS

The invention will be more clearly understood by reference to the preferred embodiments set forth hereinafter, taken in conjunction with the accompanying drawings, wherein:

FIG. **1** is a side elevational view of a preferred cloud water collector according to the invention;

FIG. **1***a* is an enlarged elevational view of the front portion of the device of FIG. **1**, showing the inclined screens formed of Teflon strands for collecting cloud water droplets;

FIG. **2** is a front view of the device of FIG. **1**, taken on line **2**—**2** of FIG. **1**, with the Teflon screens removed;

FIG. **3** is a rear view of the device of FIG. **1**, taken on line **3**—**3** of FIG. **1**, with the fan removed;

FIG. **4** is an elevational view of one of the screens of Teflon strands shown in FIG. **1***a*;

FIG. **4***a* is a side view of the Teflon screen of FIG. **4**;

FIG. 5 is a plan view taken on line 5—5 of FIG. 1, showing the trough for cloud water sample collections;

FIG. 6 is a section taken on line 6—6 of FIG. 5;

FIG. 7 is a detail illustrating the means connected to the trough of FIG. 6 for discharging cloud water collected in the trough of FIG. 6, into a sample bottle;

FIG. 8 is an adapter inlet which can be connected to the front of the cloud water collector of FIG. 1, which prevents the larger rain droplets from entering the device;

FIG. 9 is a top view of the adapter inlet of FIG. 8;

FIG. 10 is a front elevation of the automated sampler employed in conjunction with the cloud water collector of FIGS. 1-9;

FIG. 11 is a detailed front elevational view of the carousel assembly for supporting the sample bottles, of FIG. 10;

FIG. 12 is another detail of the sampler device of FIG. 1, showing the collector reservoir and overflow device employed in conjunction therewith;

FIG. 13 is a plan view of the carousel or turntable of FIG. 11;

FIG. 14 is a block diagram of the associated elements for operating the automated sampler of FIG. 10; and

FIG. 15 illustrates use of the automated sampler of FIG. 10 for collecting rain water samples.

DESCRIPTION OF THE PREFERRED EMBODIMENTS

Referring to FIGS. 1, 2 and 3 of the drawings, numeral 20 indicates a cloud water collector according to the invention, comprising an outer housing 21 having a front section 22 and a rear section 24, the front being open at 26 and the back of the collector being open at 28. The housing of collector 20 is in the form of a box having an essentially square cross-section, the rear section 24 of the collector being flared outwardly as indicated at 29 to accommodate a fan or blower 30 in a rear portion 32. The front and rear sections are provided with flanges 25 which are connected by bolts 27.

The outer housing 21 of the cloud water collector is preferably comprised of a clear poly (methyl methacrylate) resin (Plexiglas). Other clear inert plastics can be employed, such as polypropylene or polyethylene. However, the latter two materials tend to degrade in sunlight over a period of time.

Viewing also FIG. 1*a*, a series of three screens 34, each formed of two parallel rows of Teflon strands or filaments, and described in greater detail below, are mounted and inclined at an acute angle in the front section 22 of the collector, adjacent the open front end 26 thereof. A honeycomb element 36 is mounted across substantially the central portion of the collector between the front and rear sections 22 and 24 thereof.

The fan 30 is mounted on a bracket 38 which is suitably bolted at 40 to a support member 42 mounted on the back 28 of the collector.

Now referring to FIGS. 1*a*, 4 and 4*a*, the screens 34 are each formed of a rectangular frame 43 comprised of two stainless steel upper and lower rods 44, preferably Teflon coated, suitably fastened at their ends to opposite side bars 46. Stiffener webs 45 are positioned across frame 43 adjacent the rods 44 at the top and bottom of the frame and are suitably welded at 49 to the opposite side bars 46. The rods 44 are threaded at 47 to received a Teflon strand 48 which is wound around the rods 44 in a vertical direction along the entire width of the screen extending from one side bar 46 to the opposite side bar. It has been found that in order to obtain efficient collection of fog droplets of a size ranging from 1 to 100 microns in diameter, and particularly of droplets in the range of about 5 to about 30 microns, the main portion of fog droplets which impact and collect on the Teflon strands, a preferred diameter of the Teflon strands ranges from about 0.015" to about 0.025", an optimum strand diameter being 0.020".

The spacing between adjacent strands of the filament 48, and hence the spacing between the threads 47 receiving the strands, is preferably between 0.06" and 0.08", optimally about 0.070".

It is preferred to minimize the size or diameter of the Teflon filament while still maintaining it sufficiently large so that it is strong and durable and does not break over a long period of use. The space between adjacent strands mounted on the rods 44 of the frame 43 should be sufficiently large to permit free flow of the cloud water sample through the screen while permitting efficient impaction of fog droplets from the flow of the cloud sample, on the Teflon filaments. Referring to FIG. 1*a*, it will be noted that each of the screens 34 is comprised of two parallel rows 50 of the Teflon strands 48 mqunted on the opposite rods 44.

Referring now to FIGS. 1 and 1*a*, the Teflon screens 34 are mounted at an acute angle, most particularly at an angle of 35° to the direction of the incoming flow of the cloud sample introduced through inlet 26. For this purpose, grooves 52 are provided in the opposite side walls 54 of the front section 22 of the collector, such grooves being inclined at a 35° angle to accommodate the side bars 46 of each of the Teflon screens 34 mounted in parallel inclined relation at such angle in the front section of the collector. It will be seen that in the present embodiment, three collector screens 34 are employed, mounted parallel to each other, and in closely spaced relation within the front section of the collector. The frames 43 of the screens are suitably fastened at 56 and 58 in brackets 60 and 62 mounted respectively in the top 64 and bottom 66 of the front section of the collector.

In the embodiment illustrated in FIGS. 1 and 1*a* employing three Teflon screens 34, since there are two rows of Teflon strands 50 for each screen, there is a total of six rows of Teflon strands in the three screen arrangements shown. In such an arrangement, with Teflon strands of the optimum diameter of 0.020" and a spacing of 0.070", the first row of strands on the first screen 34 facing the inlet 26 samples about 28% of the incoming cloud sample flow, and when all six rows of strands formed by the three screens are included, such six rows sample about 86% of the total air. While it is preferred not to employ more than three Teflon screens 34, only one or two of such screens can be employed if it is desired to slow the collection rate down.

Although the optimum angle of inclination of the screens is 35°, as noted above, the angle of the Teflon screens can range from about 30° to about 40°. Inclining the screens at such angles, particularly the optimum angle of 35°, prevents resuspension into the air flow of fog droplets impacted onto the Teflon filaments. Further, once the droplets are collected on the strands, it is desirable that they be removed from the environment of the sample flow as quickly as possible to prevent evaporation. The above-noted angle of inclination aids in obtaining rapid flow of the droplets down the filaments for collection as quickly as possible. A baffle 67 is provided and suitably connected to the top of the housing

21 and formed of a front downwardly sloping portion 69 which directs the incoming cloud sample downwardly away from the upper structure of the frames 43 including the upper rods 44, and a rear upwardly sloping portion 71, which deflects the air stream passing through screens 34 upwardly across the conduit formed by housing 21.

Referring to FIGS. 5, 6 and 7, a trough 68 is provided across the bottom 66 of the front section 22 of the collector, such trough being inclined downwardly from the opposite side walls 54 of the front portion 22, to the center thereof, as indicated at 70, and terminating in a central discharge outlet 72. A funnel 74 is positioned in the discharge outlet, to which is connected one end of a tube 76, the opposite end of the tube being connected to a sample bottle 78.

It will accordingly be seen that water droplets flowing down the Teflon filaments 48 of the six rows 50 of such strands provided by the three screens 34, will collect in the trough 68 and pass via the funnel 74 and tube 76 into the collection bottle 78.

In operation, the fan 30, which can conveniently operate on 12–14 volt D.C. current, draws a sample cloud through the open front end 26 of the collector and into contact with the Teflon filaments 48 of the screens, causing fog droplets to impact on and flow down the Teflon strands 48 of the screens 34. The velocity of flow can be of the order of about 9 meters per second. Droplets below a certain size pass between the Teflon filaments and are not collected thereon, while larger droplets above a certain size collect on the strands. Droplets in the range of 1 to 100 microns diameter are efficiently collected and, particularly, droplets in the size window of 5 to 30 microns in diameter. While droplets of a size of about 3.8 microns can be collected at 50% efficiency, droplets of the order of 10 microns size and above can be collected at practically 100% efficiency.

The honeycomb element 36 in FIGS. 1 and 3 functions as a flow straightener, that is, it produces uniform flow of the cloud sample across the collector and removes swirl and reduces turbulence created by the fan. Although the honeycomb element can be omitted, the presence of the honeycomb element positioned between the Teflon screens 34 and the fan 30 substantially improves the performance of the device. This arrangement also aids in reducing contamination of the cloud sample and facilitates introduction of a clean, non-contaminated cloud sample into the collector for impingement on the Teflon strands 48.

When the cloud water collector described above is to be employed for sampling during rain, a rain adapter shown in FIGS. 8 and 9 is attached to the front open end 26 of the collector.

The rain adapter indicated at 80 is in the form of a clear plastic member, such as poly (methyl methacrylate) (Lucite), having a downwardly sloping, closed top 82 connected to opposite sides 84 of triangular shape, the lower edges of which terminate in a horizontally positioned, open bottom 86. The inner end of the rain adapter 80 terminates in a square conduit 88 having a flange 90 mounted around its inner end.

The rain adapter 80 can be mounted on the front 26 of the cloud water collector by attaching the flange 90 of the adapter to the flange 92 on the front of the cloud water collector, by suitable fasteners, such as bolts. During the rain, while the air flow sample is drawn in through the open lower end 86 of the adapter, as indicated by the arrow 94, and into the front section of the cloud water collector for impingement on the Teflon screens 34, in the normal manner of operation as noted above, the larger rain droplets impinge on the top 82 of the rain adapter and flow down the top, but such droplets have too much inertia and are unable to be drawn upwardly through the open bottom 86 and into the adapter and the collector, with the air or cloud sample to be collected.

Typical operating parameters for the cloud water collector of the invention described above and shown in the drawings are set forth in the following table:

TABLE

CLOUD WATER COLLECTOR OPERATING PARAMETERS

Strand dia., μm (in.)	510 (0.020)
Strand length, m (ft.)	190 (620.0)
Sampling flow, m3/min. (cfm)	24.5 (870)
# of rows of strand	6
Strand spacing, mm (in.)	1.8 (0.071)
% of air sampled, 1st row	27.9
% of air sampled, total	86.0
Total sampled flow, m3/min	21.1
50% size cut (theor.), μm	3.8
Stokes number (10 μm droplet)	8.4
Inlet velocity, m/s	7.0
Velocity @ strands, m/s (MPH)	8.45 (18.9)
Coll. rate in 0.5 g/m3 fog, 10 μm droplets, ml/min.	9.95
Operating voltage, v.	14.0

The cloud water collector of the invention described above and illustrated in FIGS. 1 to 9 of the drawings can be operated manually so that when a sample bottle of cloud water liquid is filled, it is removed from the apparatus and another bottle is manually connected to the device for collecting another sample, and so on. However, it is often preferred to automate the device so that each sample bottle, when filled with cloud water liquid, is automatically removed from the device and a new bottle arranged in its place to collect the next sample. This permits the cloud water collector to be set up in the field and left to automatically collect the fog water samples, thus providing manpower savings.

Accordingly, there is described below and shown in FIGS. 10 to 14 of the drawings a preferred embodiment of a device which can be employed in conjunction with the cloud water collector described above for automating the collector and obtaining multiple samples of cloud water for chemical analysis.

Referring to FIGS. 10–13 of the drawings, numeral 100 is an automated sampler device, according to the invention, which can be employed in conjunction with the cloud water collector 20 of FIG. 1 for obtaining samples of cloud water collected in collector 20. Preferably, the automated sampler 100 is incorporated in a refrigerator 102 which aids in maintaining the chemical composition of the cloud water samples without change, for example, as a result of evaporation. However, it will be understood that the use of a refrigerator for the automated sampler hereof is not necessary.

When employing the automated sampler 100, the sample collection tube 76 of the cloud water collector, as seen in FIG. 7, is connected directly to a reservoir 104, which is arranged to discharge a predetermined volume of collected cloud water via a valve A sequentially into a plurality of large sample bottles 106, and via a valve B sequentially into a plurality of small sample bottles 108 supported on a turntable or carousel 110,

which is rotated by a shaft **112** connected to a central support block **114** attached to the center of the carousel by the fastener **116**. The shaft **112** and central support block **114** are interconnected by a pair of oppositely disposed pins **113** on the shaft **112**, which are received in oppositely disposed slots **115** in the lower portion of the support block **114**. The shaft **112** and support block **114** are driven by a motor **118** through a worm gear **120** mounted in a centrally positioned frame **122**. The shaft **112** and central support block **114** are received in a central aperture **126** of a support member **124** to maintain the carousel in a substantially central position during operation. The frame **122** is connected to the support member **124** by suitable fasteners (not shown), and hence, the support member supports the frame **122**, motor **118** and carousel **110**. The support member **124** is mounted at opposite ends on outer support blocks **129** attached to opposite side walls **131** of the refrigerator.

A series of large sample bottles **106** is mounted circumferentially adjacent the outer periphery of the carousel in a circular rack **128** supported on the carousel by support pins **130**. The large bottles **106** are each positioned in circular holes **132** provided adjacent the outer periphery of the rack. In the embodiment shown, there are 20 such holes **132** for receiving 20 of the large bottles **106**, e.g., of 60 mls capacity each.

There are also provided in the rack **128** three concentric circles of smaller holes **134** for receiving the small bottles **108**, there being 20 of the small holes **134** in each of the three concentric circles of holes, for receiving 20 of the small bottles **108**, e.g., having a capacity of 8 ml each in the present embodiment.

It will accordingly be seen that at the sample bottle-filling station X, as shown in FIGS. **10** and **11**, there will be one large sample bottle **106** and three oppositely disposed small bottles **108**.

Referring to FIG. **12**, an overflow line **136** is connected to the discharge conduit **138** from the bottom of reservoir **104**, such overflow conduit discharging into an overflow bottle **140**. A vent **142** is provided at the top of the reservoir **104**. A liquid level sensor **144**, in the form of a photoelectric cell, is provided to monitor a predetermined volume of cloud water received in the reservoir **104**.

Now referring to FIGS. **10** and **11**, an auxiliary line **146** is connected to the discharge conduit **138**, a valve B being disposed in the discharge line **146**, for actuation to fill three of the small bottles **108**, simultaneously with actuation of valve A for filling one of the large bottles **106** at the filling station X. An air cylinder powered device **148** is arranged to actuate a sliding assembly **149** carrying three hypodermic needles **150** communicating with line **146**. Each of the needles **150** has a fluid inlet **151** communicating with the line **146** and a vent tube **153**. Each of such needles pierces a septum **152** which tops each of the small bottles **108** when the support assembly **149** is urged downwardly. The air powered assembly is actuated by the opening of valve A, at which time valve B is also opened for filling the three small bottles **108** through the hypodermic needles.

Now referring also to FIG. **14**, showing a block diagram of the automated sampler **100**, it will be noted that a timer **154** is connected to valve B for introducing a predetermined amount of sample liquid from the reservoir **104** into each of the three small sample bottles **108**, simultaneously during the filling of the large bottle **106** via valve A at the filling station X.

The automated sampler **100**, when set up to collect cloud water samples in conjunction with the cloud water collector **20**, operates as follows:

A fog detector indicated at **155**, which is basically a miniature version of the cloud water collector **20**, is actuated, and when fog is present, such fog detector collects a sample amount of the fog water and deposits it onto a resistance grid, indicated at **156**. A circuit (not shown) senses the charge on the resistance grid **156**, due to the presence of the fog water, and trips a relay **158** which supplies power from power source **160** to the various components in the device, as noted below, including fan **30** of the cloud water collector **20**.

Fog water collected in the cloud water collector **20** is discharged via tube **76** into the reservoir **104**. According to one mode of operation, when the liquid sample collected in the reservoir **104** reaches a predetermined volume, as indicated by the level sensor **144**, the sensor actuates the valve A to open same to discharge the liquid sample into the bottle **106** at the fill station X. Simultaneously with the opening of valve A, a timer indicated at **154** opens valve B to discharge liquid from reservoir **104** via hypodermic needles **150** into each of the three small sample bottles **108** at station X. In one example of operation, valve B remains open for about 5 seconds to discharge a total of 15 ml of sample liquid (5 ml per bottle) in the three small 8 ml bottles **108**. During this same period of time, sample liquid flows from reservoir **104** into the large 60 ml sample bottle **106**. The timer **154** then closes valve B. However, valve A remains open to discharge the remainder of the liquid in reservoir into the large bottle **108**. If the pre-set volume of liquid collected in reservoir **104** is 60 ml, then 45 ml of liquid is collected in a total period of 20 seconds in the large 60 ml sample bottle **106**. When the reservoir **104** is emptied, valve A closes to permit the reservoir **104** to again fill with cloud water. When valve A closes, the air powered cylinder is actuated to withdraw the hypodermic needles **150** from the small bottles to the position shown in FIG. **11**.

According to a second mode of operation, a timer **157** is employed in conjunction with valve A, instead of level sensor **144**. In this mode of operation, the timer **157** times the interval for filling the reservoir **104**, say, one hour. This is the "off" interval of the timer **157**. At the end of such time, the timer actuates the valve A, while at the same time, the timer **154** actuates the valve B, to fill the large bottle **106** and the small bottles **108** simultaneously. During this filling operation of about 20 seconds, the timer **157** is in the "on" interval. The timer **157** then switches to the "off" interval again, closing valve A, while timer **154** closes valve B, to permit reservoir **104** to again be filled with sample liquid.

In a third mode of operation employing both the level sensor **144** and the timer **157**, for actuating valve A, if either the time has elapsed as set by timer **157**, for filling the reservoir **104** to a predetermined volume, or the collected volume of liquid as indicated by the level sensor **144** has been achieved, whichever occurs first, valve A will be opened by either the level sensor or the timer **157**, to permit discharge of liquid into the large bottle **106**, while at the same time simultaneously the timer **154** opens valve B to permit discharge of liquid sample into the small bottles **108**, after which valves A and B are closed, as noted above, to permit repeated filling of the reservoir **104**. This third mode of operation is preferred.

After the accumulated liquid has been discharged from the reservoir **104** into the sample bottles at filling station X, and valves A and B have been closed, a counter, indicated at **162**, which is responsive to the closing of valve A, actuates an indexing mechanism **164**, which in turn actuates the motor **118** and worm gear **120** to rotate the carousel a predetermined amount so as to move the filled bottles from the filling station X and to advance the next row comprised of one large bottle **106** and three small bottles **108** into position at the filling station X. The above-described operation for filling the large bottle **106** and the small bottles **108** at fill station X is repeated until all of the 20 large bottles and 60 small bottles on the carousel are filled. At the end of this time, the counter **162** shuts off power to the indexing mechanism **164** and causes diversion of liquid filling the reservoir **104**, through the overflow tube **136** and into the overflow bottle **140**.

An event logger (printer) **166** records the time when sampling begins and when the carousel indexes to a new position.

It will be understood that, if desired, the automated sampler can be used for filling only the large sample bottles **106** and omitting the small sample bottles **108**. Under the circumstances, components for filling the small bottles, including valve B and its associated timer **154**, the auxiliary discharge line **146**, air cylinder **148**, and the hypodermic needle devices **150** can be omitted.

Further, if desired, the above-described mechanism for actuating the automated sampler, including the small fog detector **155**, and its associated resistance grid **156** and relay **158** can be omitted, and the power source at **160** can be turned on manually or by any other means at any desired time.

In addition, the automated sampler **100** can be employed separately, that is, without combining it with the cloud water collector **20**, e.g., for collecting rain water. In the latter case, viewing FIG. **15**, a rain water collecting funnel **168** can be connected to the tube **76** for discharge of a sample of rain water into the liquid reservoir **104**. The automated sampler then functions in the manner described above for collecting multiple samples of the rain water so collected. When not in use for collecting rain water, a cover indicated by dotted lines **170** can be placed over the funnel.

From the foregoing, it is seen that the invention provides an improved device for collecting cloud water or fog water for chemical analysis which operates efficiently and rapidly to collect substantial amounts of liquid water for chemical analysis, and which is reliable, simple to construct and inexpensive. In addition, the cloud water collector can be automated by use in combination with an automated sampler device to collect multiple samples of fog water in the field, with a minimum of attention and labor expense. Further, the automation device can be employed separately for collecting rain water.

Since various additional changes and modifications of the invention will occur to and can be made readily by those skilled in the art without departing from the invention concept, the invention is not to be taken as limited except by the scope of the appended claims.

What is claimed is:

1. A cloudwater collector comprising

a conduit open at opposite ends, including an air inlet at a front end thereof to permit entry of a cloudwater containing air sample into said conduit, and an air outlet at the opposite back end thereof,

a plurality of spaced Teflon strands in said conduit adjacent the front end thereof, said strands being mounted across said conduit at an acute angle facing said inlet,

the diameter of said strands being such that water droplets from a cloudwater sample, of a size range of 1–100 microns are collected on the strands upon impact therewith, said acute angle being such that the impacted droplets flow down said strands and drain into the bottom of said conduit,

a fan at the back end of said conduit adjacent said air outlet for drawing a sample of air containing cloudwater through said inlet into said conduit,

means for reducing turbulence and producing essentially uniform flow of said air sample across said conduit, and

means for collecting a sample of the water droplets from the bottom of said conduit.

2. The cloudwater collector of claim **1**, said Teflon strands being wound in vertical spaced relation on a frame and forming a screen containing two parallel rows of said strands on said frame.

3. The cloudwater collector of claim **2** including a plurality of said screens mounted in spaced parallel relation at said acute angle across said conduit.

4. The cloudwater collector of claim **2**, said Teflon strands and said screen being mounted at an angle of 30°–40° across said conduit facing said inlet.

5. The cloudwater collector of claim **2**, said Teflon strands having a diameter such that water droplets from a cloudwater sample, of a size ranging from 5–30 microns, are efficiently collected on the Teflon strands.

6. The cloudwater collector of claim **2**, said Teflon strands having a diameter ranging from 0.015" to 0.025".

7. The cloudwater collector of claim **1**, said means for reducing turbulence and producing essentially uniform flow of said air sample across said conduit comprising a honeycomb element mounted across said conduit between said Teflon strands and said fan.

8. The cloudwater collector of claim **1**, said means for collecting said water droplet sample comprising a drain in the bottom of said conduit, a funnel connected to said drain, a sample bottle, and tube means communicating said funnel with said sample bottle.

9. The cloudwater collector of claim **1** including a frame for said Teflon strands, said frame having upper and lower threaded rods, said Teflon strands wound on said threaded rods in vertical spaced relation, and forming a screen containing two parallel rows of said strands on said frame, and including a plurality of said screens mounted in spaced parallel relation, said Teflon strands and said screens being mounted at an angle of 35° across said conduit facing said inlet.

10. The cloudwater collector of claim **9**, said Teflon strands having a diameter of about 0.020" and a spacing between strands of about 0.070".

11. The cloudwater collector of claim **10**, said means for reducing turbulence comprising a honeycomb element mounted across said conduit between said Teflon strands and said fan, and said means for collecting said water droplet sample comprising a drain in the bottom of the said conduit, a funnel connected to said drain, a sample bottle, and a tube communicating said funnel with said sample bottle.

12. The cloudwater collector of claim **1** including means for automating the collection of successive cloud water samples, said automating means comprising

a reservoir in fluid communication with said sample collecting means,

turntable means adapted to support a plurality of containers thereon,

means associated with said reservoir for automatically discharging a predetermined volume of cloudwater from said reservoir into a preselected container on said turntable means, and

means to actuate said turntable means to index a successive container to be filled into operative relation with said reservoir when said preselected container has received said predetermined volume of cloudwater.

13. The cloudwater collector of claim 12, said automatic discharge means comprising valve means operable to open when said predetermined volume of cloudwater has been collected to discharge same into said container, said turntable indexing means being actuated when said valve means is closed.

14. The cloudwater collector of claim 12, said automatic discharge means comprising a liquid level sensor for said reservoir and valve means associated with said liquid level sensor, said liquid level sensor actuating said valve means when said reservoir is filled with cloudwater to a predetermined level to discharge the cloudwater from said reservoir into said preselected container.

15. The cloudwater collector of claim 12, said automatic discharge means comprising timer means for timing the flow of cloudwater into said reservoir over a preselected time interval and valve means associated with said timer means, said timer means actuating said valve means after said preselected time interval, to discharge the cloudwater from said reservoir into said preselected container.

16. The cloudwater collector of claim 12, said automatic discharge means comprising a liquid level sensor for said reservoir and valve means associated with said liquid level sensor, said liquid level sensor actuating said valve means when said reservoir is filled with cloudwater to a predetermined level to discharge the cloudwater from said reservoir into said preselected container, and also including timer means for timing the flow of cloudwater into said reservoir over a preselected time interval and valve means associated with said timer means, said timer means actuating said valve means after said preselected time interval, to discharge the cloudwater from said reservoir into said preselected container, said liquid level sensor or said timer means actuating its associated valve means to discharge the cloudwater from said reservoir after said predetermined volume is achieved or said preselected time interval has elapsed, whichever occurs first.

17. The cloudwater collector of claim 12 including means for deactivating said turntable indexing means when all of the containers on said turntable have been filled, and means for thereafter diverting incoming cloudwater from said reservoir to an overflow container.

18. The cloudwater collector of claim 12 including means for actuating said automating means when cloudwater is present, for discharge of sample liquid from the sample collecting means of said cloudwater collector, to said reservoir.

19. The cloudwater collector of claim 12, said means for automatically discharging a predetermined volume of cloudwater from said reservoir including,

a first valve means,

a second valve means,

means for actuating said first valve means when said predetermined volume of cloudwater has been collected in said reservoir to open and fill a first container at a fill station on said turntable,

timer means for actuating said second valve means when said first valve means has been actuated, to open and fill a second smaller container at said fill station on said turntable,

said timer means closing said second valve means after a pre-set time interval, and said means for actuating said first valve means closing same after a longer pre-set time interval, and

means for sensing the closing of said first valve means, to actuate said indexing means to index successive first and second containers for advancement to said fill station.

20. The cloudwater collector of claim 19, said means to actuate said first valve means including a liquid level sensor means to monitor collection of said predetermined volume of cloudwater in said reservoir, and means associated with said liquid level sensor means to actuate said first valve means.

21. The cloudwater collector of claim 19 including a timer means to monitor collection of said predetermined volume of cloudwater in said reservoir, and means associated with said last-mentioned timer means to actuate said first valve means.

22. The cloudwater collector of claim 19 including a rack on said turntable adapted to support a plurality of said first containers in a circle adjacent the outer periphery of said turntable and a plurality of said second smaller containers in a concentric circle adjacent said first containers.

23. The cloudwater collector of claim 1, including means for automating the collection of successive cloudwater samples, said automating means comprising

a reservoir in fluid communication with said sample collecting means,

a carousel,

means supporting said carousel for limited rotation,

a rack on said carousel adapted to support a plurality of first sample bottles in a circle adjacent the outer periphery of said carousel and a plurality of second smaller sample bottles in concentric circles adjacent said circle of first containers,

a fill station on said carousel wherein one of said first bottles and a plurality of said second bottles in said concentric circles are in a row,

a discharge line from said reservoir,

a first valve in said discharge line adapted to discharge liquid from said reservoir into one of said first bottles at said fill station,

a second valve in said discharge line adapted to discharge liquid from said reservoir into the second bottles in said row at said fill station,

a liquid level sensor to monitor collection of a predetermined volume of cloudwater in said reservoir,

means associated with said liquid level sensor to actuate said first valve means when said predetermined volume of cloudwater has been collected in said reservoir to open and fill a first bottle at said fill station,

timer means for actuating said second valve when said first valve has been actuated, to open and fill the second bottles in said row at said fill station, said timer means closing said second valve after a pre-set time interval, and said means for actuating

said first valve closing same after a longer pre-set time interval,

driving means to actuate the carousel to index a successive row of a first bottle and a plurality of second bottles at said fill station,

means for sensing the closing of said first valve to actuate said driving means to index a successive row of bottles at said fill station, said last-mentioned means including a counter for deactivating said driving and indexing means when all of the bottles on said carousel have been filled at said fill station,

an overflow tubing connected to the discharge line from said reservoir, and

an overflow bottle connected to said overflow tube, for receiving liquid from said reservoir after deactivation of said driving and indexing means by said counter.

24. The cloudwater collector of claim **23**, and also including timer means for timing the flow of cloudwater into said reservoir over a preselected time interval to actuate said first valve after said pre-set time interval, to discharge cloudwater from said reservoir into said first bottle at said fill station, said liquid level sensor or said last-mentioned timer means actuating said first valve to discharge the cloudwater from said reservoir after said predetermined volume is achieved or said preselected time interval has elapsed, whichever occurs first.

25. The cloudwater collector of claim **23**, said second smaller bottles having a septum cover thereon, and means for piercing said septum bottles at the fill station for introduction of sample liquid to said bottles when said second valve has been opened.

* * * * *

CHAPTER 2

Instrument to collect fogwater for chemical analysis

Daniel J. Jacob,[a] Jed M. Waldman, Mehrdad Haghi,[b] Michael R. Hoffmann, and Richard C. Flagan[c]

Environmental Engineering Science, W. M. Keck Engineering Laboratories, California Institute of Technology, Pasadena, California 91125

(Received 2 January 1985; accepted for publication 16 February 1985)

An instrument is presented which collects large samples of ambient fogwater by impaction of droplets on a screen. The collection efficiency of the instrument is determined as a function of droplet size, and it is shown that fog droplets in the range 3–100-μm diameter are efficiently collected. No significant evaporation or condensation occurs at any stage of the collection process. Field testing indicates that samples collected are representative of the ambient fogwater. The instrument may easily be automated, and is suitable for use in routine air quality monitoring programs.

Instrument to collect fogwater for chemical analysis

Daniel J. Jacob,[a] Jed M. Waldman, Mehrdad Haghi,[b] Michael R. Hoffmann, and Richard C. Flagan[c]

Environmental Engineering Science, W. M. Keck Engineering Laboratories, California Institute of Technology, Pasadena, California 91125

(Received 2 January 1985; accepted for publication 16 February 1985)

An instrument is presented which collects large samples of ambient fogwater by impaction of droplets on a screen. The collection efficiency of the instrument is determined as a function of droplet size, and it is shown that fog droplets in the range 3–100-μm diameter are efficiently collected. No significant evaporation or condensation occurs at any stage of the collection process. Field testing indicates that samples collected are representative of the ambient fogwater. The instrument may easily be automated, and is suitable for use in routine air quality monitoring programs.

INTRODUCTION

Under supersaturated conditions in the atmosphere, fog drop lets form by activation of condensation nuclei[1] and rapidly grow to sufficiently large diameters (1–100 μm) that the deposition to vegetation canopies is considerably enhanced.[2] Recent reports of extremely high acidities in fogs, and clouds intercepting mountain slopes, have raised concern regarding related environmental consequences.[3] Air quality control agencies in areas exposed to acidic fog have expressed the need to establish networks of sites monitoring the chemical composition of fog on a routine basis. A fogwater sampler to be used in such programs must meet four basic requirements: (1) efficiency collect fog droplets in the 1–100-μm size window while avoiding collection of the submicron nonactivated aerosol, (2) preserve the size and chemical composition of fog droplets through all stages of collection, (3) rapidly collect large amounts of liquid water for wet chemical analysis, (4) be automated, inexpensive to construct, and require minimal maintenance. A recent paper from our group[4] has elaborated on design criteria for fogwater collectors, and reported that none of the currently available instruments is satisfactory in all respects. A rotating arm collector developed in our laboratory[4] has been shown to provide samples representative of the ambient fogwater,[5] but it is not suitable for automation and presents safety problems. We describe herein a collector that we have recently developed explicitly to provide a simple, reliable, and inexpensive instrument for routine monitoring.

I. DESIGN

The instrument (shown in Fig. 1) collects fogwater by inertial impaction of fog droplets on a screen. The screen is made of two layers of 330-μm-diameter Teflon monofilament strung vertically on a frame between two Teflon-coated threaded rods [Fig. 1(c)]. It is placed at an incline ($\theta = 35°$) in a square duct, through which a blower samples ambient fog-laden air at a velocity $U_s = 9$ m s^{-1}. The pressure drop across the screen is 87 Pa. The residence time of impacted droplets on the screen is considerably shortened by placing the screen at an incline instead of vertically, because aerodynamic drag pushes the droplets to the bottom of the screen. Further, inclining the screen at 35° prevents resuspension of impacted droplets into the air flow, which would occur if the screen was placed vertically.[6] Accumulation of water on the screen proceeds by formation of large droplets spaced at intervals along the Teflon strings; these droplets rapidly grow large enough (about 1–2-mm diameter) to flow down. A Teflon funnel drains the fogwater collected at the bottom of the screen into a storage bottle directly below. The instrument is set on a platform surmounted by a wind vane so that the inlet is oriented into the wind at all times. Automation of instrument start up may be provided by a number of methods.

The flow of air through the duct is 22 m^3 min^{-1}, but only a fraction of that air is actually sampled because of the spacing between strings. Based on the dry diameter of the strings, each of the two layers samples 42% of the air flowing through the duct, and the sampling efficiency of the instrument is about $[1 - (0.58)^2] = 66\%$. In practice, accumulation of water on the strings will slightly increase the impaction surface area and, therefore, the amount of air sampled. About 90 ml of sample is collected per hour in a fog of typical liquid water content 0.1 g m^{-3}. This is sufficient for most analytical purposes.

The principle of operation is that inertia prevents droplets approaching the strings from following the curved flow streamlines around the strings. The deviations of droplet trajectories increase with droplet inertia, and droplets above a certain size deviate sufficiently to collect on the strings. The efficiency of this process is characterized by the Stokes number[7] St:

$$\mathrm{St} = \frac{\rho D^2 U_s \cos\theta}{18\mu R}, \tag{1}$$

where ρ is the density of the droplet, D is the droplet diameter, μ is the viscosity of air, and R is the radius of the string. The Reynolds number of the flow through the duct is sufficiently high (10^5), and the Mach number is sufficiently low (0.03), that the collection efficiency can be satisfactorily decribed as solely a function of St and the droplet Reynolds number Re_D.[7,8] Experimental data is available for the collection efficiency of particles on cylinders as a function of these two dimensionless groups.[8] For 1–100-μm-diameter droplets, St ranges from 0.14–1400 and Re_D from 0.5–50.

 0034-6748/85/061291-03$01.30 © 1985 American Institute of Physics

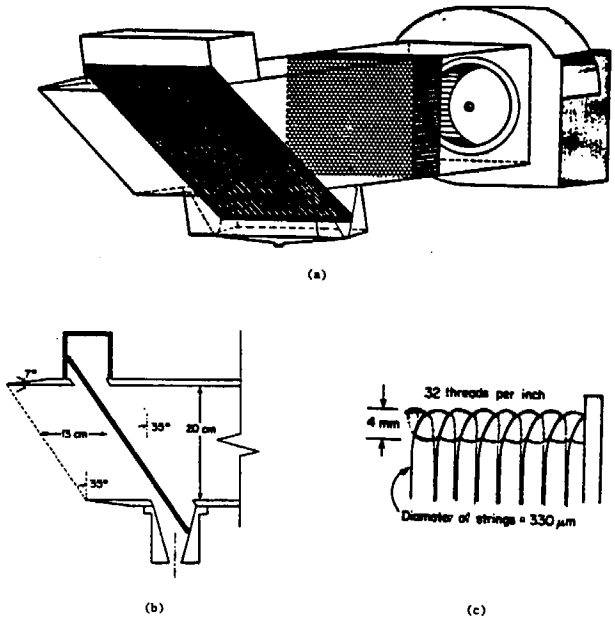

FIG. 1. Screen collector to sample fogwater for chemical analysis. Air is aspirated through a square duct at a rate of 22 m^3 min^{-1} (blower: model 80A, 1/3 HP 115V motor, Central Blower Co., City of Industry, CA). Fog droplets impact on Teflon FEP monofilament (13 mils, Dupont de Nemours Corp.) strung vertically on a brass frame between two Teflon-coated threaded brass rods. Fogwater collected on the strings flows down to a Teflon funnel and a polyethylene bottle directly underneath. (a) Perspective view of the instrument, (b) side view (section), (c) detail of the screen frame.

Because U_s differs from the ambient wind U_a, the flow approaching the inlet is deflected. Large droplets cannot follow the air flow, resulting in an anisokinetic sampling bias at the upper end of the size distribution. To minimize this bias, the instrument must be oriented into the wind at all times. Anisokinetic biases for an inlet oriented into the wind have been documented in detail[9,10] as a function of U_s/U_a and the inlet Stokes number St_i [defined by Eq. (1) when the string radius R is replaced by the half-width of the inlet]. In the special case $U_s = U_a$ (isokinetic sampling), no bias is observed. For $U_s/U_a > 1$ the collection efficiency for large droplets is less than 100% (negative bias), and goes through a St_i-dependent minimum at $U_s/U_a \cong 3$ (maximum deflection of the flow streamlines). At the limit $U_s/U_a \rightarrow \infty$, the flow streamlines are straight and no bias is observed. For $U_s/U_a < 1$, the collection efficiency for large droplets is larger than 100% (positive bias), because the flow is deflected away from the inlet. At very large St_i values, the collection efficiency approaches a limit equal to U_a/U_s.

Sampling may also be biased if the droplets shatter upon high-velocity impact on the strings. Droplet shattering may be expected if the Weber number

$$\mathrm{We} = \frac{\rho D U_c^2}{\sigma} \tag{2}$$

exceeds about 150.[11] U_c is the velocity of the droplet upon impact ($U_c < U_s$), and σ is the surface tension of the droplet–air interface. For a 100-μm-diameter droplet, we find $\mathrm{We} < 110$, below the critical value for droplet shattering. Droplet shattering may be expected for droplets larger than about 140-μm diameter, but this is beyond the usual fog size range.

The collection efficiency of our instrument was determined as a function of droplet size from the data of Refs. 8–10, for various ambient wind velocities and an inlet oriented into the wind (Fig. 2). The impaction Stokes number was calculated by taking R equal to the radius of the dry strings. Droplets in the range 3–100-μm diameter are efficiently collected. Droplets in the size window 10–30-μm diameter, which typically account for over 95% of the total liquid water content in fog,[12] are collected with over 90% efficiency under all sampling conditions. Fog droplets below 3 μm are poorly collected, but represent only a very small fraction of the total suspended liquid water. Collection of submicron aerosol by convective diffusion to the strings is very inefficient: the calculated collection efficiency is 4% for a 0.001-μm-diameter particle, and decreases with increasing particle size.[7] Thus, contamination of fogwater samples due to collection of submicron aerosol is effectively avoided. Anisokinetic sampling biases for very large droplet sizes depend considerably on the ambient wind speed. Wind speeds in radiation fogs are in general less than 2 m s^{-1}, but we have frequently found higher velocities (up to 10 m s^{-1}) in coastal advection fogs. Positive collection biases require ambient wind velocities > 10 m s^{-1}, which could be found in clouds intercepting mountain slopes but are unlikely in other situations.

Perturbation of the ambient relative humidity during the sampling process may change the size of the fog droplets by condensation or evaporation and, therefore, affect chemical concentrations in the sample. Aerodynamic cooling as the droplets are accelerated at the inlet leads to condensation, and aerodynamic heating as the droplets are deceler-

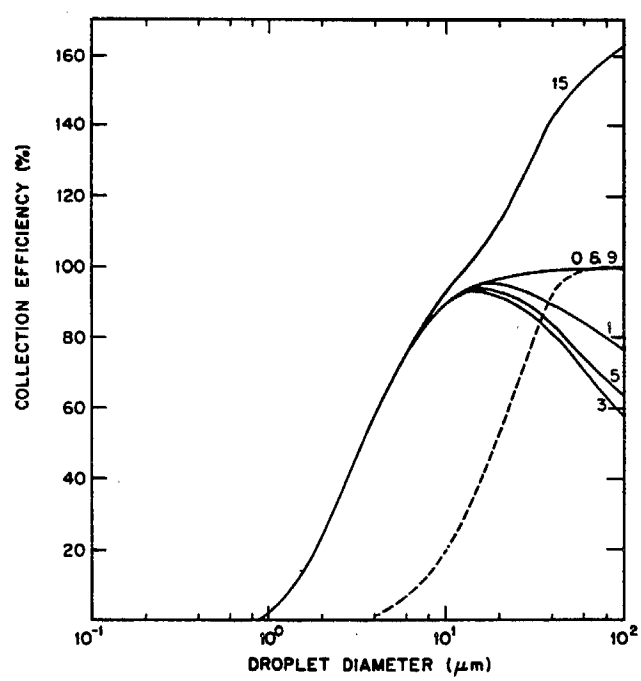

FIG. 2. Collection efficiency vs droplet diameter. Anisokinetic sampling biases are considered for an inlet oriented into the wind and various ambient wind velocities (m s^{-1}) indicated on the curves. No inlet bias occurs for $U_a = 0$ or $U_a = 9$ m s^{-1}. Maximum negative bias occurs for $U_a \cong 3$ m s^{-1}. Collection efficiencies in excess of 100% indicate positive sampling biases ($U_s < U_a$). Dashed line is the experimentally determined collection efficiency of the rotating arm collector. (Ref. 4).

TABLE I. Comparison of fogwater concentrations of samples collected simultaneously with the screen collector (SC) and the rotating arm collector (RAC) set side by side.[a]

	H^+	Na^+	Ca^{2+}	Mg^{2+}	NH_4^+	Cl^-	NO_3^-	SO_4^{2-}
SC/RAC	1.08 ± 0.11	0.71 ± 0.04	0.70 ± 0.10	0.71 ± 0.04	1.14 ± 0.14	0.93 ± 0.10	0.85 ± 0.06	0.99 ± 0.07
	Fe	Pb	Mn	Ni	V	CH_2O	Fogwater Collection rate	
SC/RAC	1.11 ± 0.34	1.12 ± 0.18	0.85 ± 0.28	1.05 ± 0.27	0.99 ± 0.12	1.04 ± 0.08	2.34 ± 0.24	

[a] Comparison of four samples collected on 12 June 1984 at Henninger Flats (Ref. 12).

ated during approach to the strings leads to evaporation. To determine the extent of the resulting droplet size modification, we simultaneously solved the equations for flow field, relative humidity, droplet trajectory, and mass transfer, from equations previously derived.[4] These calculations showed that no significant droplet growth or evaporation occurs for droplets larger than 1-μm diameter. Therefore, droplet sizes are preserved at all stages of approach.

Evaporation on the strings must also be investigated. Aerodynamic heating near the strings leads to a localized subsaturation. Assuming that the compression is adiabatic, the maximum temperature gradient at the surface of the string is

$$\Delta T = \frac{(U_s \cos \theta)^2}{2C_p}, \tag{3}$$

where C_p is the heat capacity of air. We find $\Delta T = 0.03$ K, which corresponds to a decrease in relative humidity of about 0.2%. More important as sources of thermodynamic modification are the fluctuations of the ambient relative humidity in fog: rapid oscillations of up to 1% relative humidity in amplitude have been reported in a radiation fog.[13] Mass transfer calculations for a flow of air at 99% relative past a bank of cylinders[14] indicate an overall rate of evaporation from the screens of 10^{-3} g min^{-1}. This is small compared to the collection rates achieved.

II. FIELD TESTING

The collector was first tested during a stratus cloud sampling program conducted on the mountain slopes above the Los Angeles basin.[12] Collection rates were in the range 0.5–1.5 ml min^{-1}. Four samples were collected simultaneously with the rotating arm collector, and the chemical compositions of the samples were compared (Table I). Concentrations were not significantly different between the two instruments, and usually within the errors previously documented between two rotating arm collectors set side by side.[5]

The similarity of compositions between samples collected by the screen collector and the rotating arm collector is striking, considering that the two instruments have very different collection efficiency vs droplet size characteristics (Fig. 2). A likely explanation is that most of the fogwater mass is present in a narrow droplet size window around 20-μm diameter,[12] and that small fog droplets are not sufficiently different in composition from the bulk fogwater to significantly affect the overall concentration. Small droplets have generally condensed on small nuclei and, therefore, are not systematically more concentrated than the larger droplets. The dependence of fog droplet composition on droplet size is an interesting question which has not been studied to date. Our collector could be conveniently used for such a study; different portions of the droplet size distribution could be sampled by using screens of different string diameters.

ACKNOWLEDGMENTS

Elton F. Daly and Joseph J. Fontana constructed the collector and offered valuable practical suggestions. We thank an anonymous reviewer for valuable comments. This work was funded by the California Air Resources Board.

[a] Present address: Center for Earth and Planetary Physics, Harvard University, Cambridge, Massachusetts.
[b] Present address: Department of Mechanical Engineering, Massachusetts Institute of Technology, Cambridge, Massachusetts.
[c] To whom correspondence should be addressed.

[1] H. R. Pruppacher and J. D. Klett, *Microphysics of Clouds and Precipitation* (Reidel, Dordrecht, 1978), pp. 141, 142, 418–421.
[2] G. M. Lovett, Atmos. Environ. **18**, 361 (1984).
[3] B. Hileman, Environ. Sci. Technol. A **17**, 117 (1983).
[4] D. J. Jacob, R. -F. T. Wang, and R. C. Flagan, Environ. Sci. Technol. **18**, 827 (1984).
[5] S. V. Hering and D. L. Blumenthal, Fog sampler intercomparison study: Final Report to Coordinating Research Council. Available from Coordinating Research Council, 219 Perimeter Center Parkway, Atlanta, GA, 1984.
[6] J. G. Houghton and W. H. Radford, Pap. Phys. Ocean. Met. Mass. Inst. Technol. Woods Hole Ocean. Instn. **6**, 5-31 (1938).
[7] S. K. Friedlander, *Smoke, Dust and Haze* (Wiley, New York, 1977), pp. 50–63 and 95–109.
[8] R. Israel and D. E. Rosner, Aerosol Sci. Technol. **2**, 45 (1983).
[9] P. N. Jasayekara and C. N. Davies, J. Aerosol Sci. **11**, 535 (1980).
[10] C. N. Davies and M. Subari, J. Aerosol Sci. **13**, 59 (1982).
[11] S. A. Self and R. L. Keating, HTGL Report No. 117, Department of Mechanical Engineering, Stanford University, Stanford, CA, 1980.
[12] J. M. Waldman, Ph.D thesis, California Institute of Technology, Pasadena, California, 1985.
[13] H. E. Gerber, J. Atmos. Sci. **38**, 454 (1981).
[14] R. B. Bird, W. E. Stewart, and E. N. Lightfoot, *Transport Phenomena* (Wiley, New York, 1960), p. 646.

CHAPTER 3

A Comparison of Two Cloudwater/Fogwater Collectors: The Rotating Arm Collector and the Caltech Active Strand Collector

by

Jeff Collett, Jr., Bruce Daube, Jr., J. William Munger, and Michael R. Hoffmann*

Environmental Engineering Science
W. M. Keck Laboratories
California Institute of Technology
Pasadena, California 91125

Submitted to

Atmospheric Environment

November 1988

* To Whom Correspondence Should be Addressed

Abstract

A side–by–side comparison of the Rotating Arm Collector (RAC) and the Caltech Active Strand Collector (CASC) was conducted at an elevated coastal site near the eastern end of the Santa Barbara Channel. The CASC was observed to collect cloudwater at rates of up to 8.5 ml min^{-1}. The ratio of cloudwater collection rates was found to be close to the theoretical prediction of 4.2:1 (CASC:RAC) over a wide range of liquid water contents (LWC). At low LWC, however, this ratio climbed rapidly, possibly reflecting a predominance of small droplets under these conditions, coupled with a greater collection efficiency of small droplets by the CASC. The RAC collected cloudwater samples with significantly higher concentrations of Na^+, Ca^{2+}, Mg^{2+}, and Cl^- than were collected by the CASC. These higher concentrations may be due to differences in the chemical composition of large vs. small droplets. No significant differences were observed in concentrations of NO_3^-, SO_4^{2-}, or NH_4^+ in samples collected by the two instruments.

Introduction

The development of the Caltech Active Strand Collector (Daube et al., 1987) led to a need to compare the performance of this collector with the Rotating Arm Collector (Jacob et al., 1984) used in previous studies of fog and cloudwater chemistry in California. Of particular interest were the rate of sample collection by each instrument and the comparability of the chemical composition of the samples collected by the two instruments. In order to make these comparisons we needed a location at which we could sample several fog events with widely varying liquid water contents and chemical compositions. Side–by–side comparison of the collectors under these conditions would provide a good test of the relative performance of the two instruments.

Site Description and Measurement Techniques

- **Sampling Site**

The site selected for the collector comparison was the roof of a one story building located at 475 m, just below the summit of La Jolla Peak. La Jolla Peak is situated 3 km NNE of Pt. Mugu at the eastern end of the Santa Barbara Channel. The collectors were placed approximately 15 m apart with the exhaust from each directed away from the other collector.

This site was selected because of its elevation, its proximity to the ocean, and its location away from major anthropogenic sources. The combination of elevation and proximity to the ocean were expected to result in frequent impaction of coastal stratus moving inland with the nighttime sea breeze during the summer period we planned to sample. The location away from any immediately neighboring anthropogenic sources was expected to provide a variety of cloudwater compositions, these varying with the

mesoscale transport conditions associated with each event. Previous work had suggested that the site might be subjected to pollutant laden air masses originating in the Los Angeles Basin (Shair et al., 1982) or from oil platforms located in the coastal waters to the west (California Air Resources Board, 1982). These types of air masses, if associated with periods of coastal stratus, could result in the presence of highly polluted cloudwater at the site. Alternatively, it was expected that periods of air movement from the southwest (not associated with offshore flow from the South Coast Air Basin) during periods of coastal stratus would result in the presence of much cleaner cloudwater at the site.

- **Measurement Techniques**

Cloudwater samples were collected simultaneously with the Rotating Arm Collector (RAC) and the Caltech Active Strand Collector (CASC) depicted in Figures 1 and 2, respectively. The RAC (Jacob et al.,1984) utilizes a 1.5 HP motor to drive a 63 cm solid stainless steel rod at 1700 rpm. Each end of the rod has a slot milled into its leading edge to collect the impacting fogwater droplets. High density polyethylene (HDPE) bottles mounted on each end of the rod catch the fogwater sample as it is accelerated outward from each slot. Collection rates of up to 2 ml/min have been obtained in the field with this instrument. A scale model calibration of the RAC indicated a 50% lower size cut, based on droplet diameter, of 20 μm for the RAC.

The CASC (Daube et al., 1987) employs a fan to draw air across six angled banks of 510 μm teflon strands at a velocity of 9 m s^{-1}. Cloudwater droplets in the air parcel are collected on the strands by inertial impaction. The collected droplets run down the strands, aided by gravity and aerodynamic drag, through a teflon sample trough into a HDPE collection bottle. This instrument has a theoretical lower size cut of 3.5 μm, based on droplet diameter, and has collected cloudwater at rates of up to 8.5

ml min^{-1} in the field.

The major ions, Cl^-, SO_4^{2-} , and NO_3^- , were measured in our laboratory using a Dionex 2020i ion chromatograph with a Dionex AS–4 column and a bicarbonate–carbonate eluent. Na^+, Ca^{2+}, and Mg^{2+} concentrations were determined using a Varian Techtron AA6 atomic absorption spectrophotometer. NH_4^+ was measured by the phenol–hypochlorite method (Solorzano, 1967) using an Alpkem flow injection analyzer.

Sample Comparison Results

· Collection Rate

The rates of cloudwater collection by the two instruments were compared for 22 periods during which samples were collected simultaneously. The theoretical ratio of collection rates between the two instruments is 4.2:1 (CASC:RAC). This figure is based on the expected air sampling rates of each instrument. In Figure 3 the actual collection rate data from this study are depicted along with this theoretical line. The data are plotted as the ratio of CASC to RAC collection rates vs. CASC collection rate. Most of the data points are scattered closely about the theoretical line. Several points at low CASC collection rate, however, fall well above this line, indicating that under these conditions the performance of the CASC relative to the RAC is much better than expected.

Since the collection rate of the CASC is proportional to the liquid water content (LWC) of the cloud, these particular samples indicate that under low LWC conditions the collection efficiency of the RAC declines to a greater extent than that of the CASC. This may be due to the differing lower sizecuts of the two instruments. Typically low LWC clouds have a greater proportion of liquid water residing in smaller droplets (Best, 1951a). Since the RAC collects only those droplets above 20 μm

efficiently, it may be sampling less than half of the droplet spectrum under these conditions. The 3.5 μm lower size cut of the CASC, however, allows it to sample the bulk of the available liquid water.

- **Chemical Composition**

Of the 22 samples collected simultaneously by the CASC and the RAC, 11 were chosen for a comparison of major ion composition. These 11 samples were collected on three different nights in July and August of 1985. The other 11 samples were relatively small in volume. Since small volume samples are more likely to show signs of contamination than large ones, these samples were not used for this portion of the collector comparison. Trends exhibited by those samples used in the comparison, however, were generally observed in the low volume samples as well.

Seven ions were used for comparison of the samples: NO_3^- , SO_4^{2-} , Cl^-, NH_4^+ , Mg^{2+}, Ca^{2+}, and Na^+. Along with H^+, these ions form the bulk of the ionic composition for all 11 samples. Figures 4 through 10 depict the sample comparison for each ion. Data is plotted as concentration in the CASC sample vs. concentration in the RAC sample. The eleven samples exhibited a wide range of concentrations for each of these ions. Also plotted on each graph is a 1:1 line. If the collected sample pairs were identical in composition, the data points should deviate from this line only due to random errors in analysis.

In the case of NO_3^- , SO_4^{2-} , and NH_4^+ the data points seem fairly well matched with the 1:1 line. Deviation is more evident amongst the Cl^-, Na^+, Mg^{2+}, and Ca^{2+} compositions. In all four cases it appears that the RAC collects these ions preferentially, particularly when the ions are present at higher concentrations.

A statistical analysis was performed to determine whether the deviations suggested above were significant. A linear relationship of the form given by equation 1

$$Y_i = \alpha + \beta X_i + \mu \tag{1}$$

may be hypothesized where Y_i and X_i are the matrices of CASC and RAC concentrations of ion "i", respectively, and "μ" represents the error in the equation. Typically the values of α and β, the intercept and the slope, are estimated using the method of ordinary least squares (OLS). When there are errors in the measurement of both the dependent and independent variables, however, OLS provides a biased estimate of the slope (Johnston, 1984; Maddala, 1977).

Two estimation methods are commonly used to remedy this problem of bias. One requires a fairly accurate knowledge of the magnitudes of the errors. In order to utilize this approach, simultaneous data is needed on side–by side CASC and side–by–side RAC sampling. Since this was not available, the second estimation method was utilized. This method, known as the Instrumental Variable (IV) method (Johnston, 1984), provides a consistent estimate of both the slope and intercept. The method requires a matrix of variables correlated with the X variables but uncorrelated with the errors in the X variables.

The particular method utilized for this comparison has been described in detail by Bartlett (1949), and is a modification of earlier work by Wald (1940). The mean of the coordinates $(\bar{x},\bar{y})$ is used to define one point of the fitted line. To determine the slope, the n data points are divided into three groups which are non–overlapping in either the x or the y direction. The groups should be chosen so that the two extreme groups are as near n/3 as possible. The slope of the fitted line is then defined by the slope of the join of the mean coordinates, $(\bar{x}_1,\bar{y}_1)$ and $(\bar{x}_3,\bar{y}_3)$, for the two extreme groups.

While Bartlett's method provides a consistent estimate for the slope and intercept of the relationship (1) it is not as efficient as OLS. A decrease in efficiency results in an increase in the size of the confidence limits placed on these estimates.

When faced with a situation where there are errors in the independent variables, however, it becomes necessary to sacrifice some efficiency to gain an unbiased estimator. Table 1 lists the results of applying this method to the Na^+, Cl^-, Ca^{2+}, and Mg^{2+} data. The slope and the corresponding 95% confidence limits are given for the CASC vs. RAC comparison for each ion. A slope greater than one indicates preferential collection of that ion by the RAC while a slope less than one indicates that the CASC collects the ion preferentially. A slope of one indicates no preferential collection. The results in Table 1 indicate that at the 95% confidence level the RAC collects Na^+, Cl^-, and Ca^{2+} preferentially. Preferential collection of Mg^{2+} by the RAC is indicated at the 90% confidence level. Data for NH_4^+ , NO_3^- , and SO_4^{2-} indicated no preferential collection of these ions by either collector.

Typically larger condensation nuclei lead to the formation of larger cloud droplets in the lower portions of a cloud not subjected to significant horizontal entrainment of dry air (Best, 1951b, Mason and Chien, 1962, Hudson, 1984). Since sea salt and soil dust are found to reside in the larger end of the aerosol size spectrum (Seinfeld, 1986), the elements found predominantly in these types of particles (e.g. Cl^-, Na^+, Mg^{2+}, and Ca^{2+}) will reside there as well. Therefore, as cloud droplets form on the available aerosol nuclei and grow by condensation, it should be expected that these elements would be found predominantly in the upper end of the droplet size spectrum. In the more mature portions of a cloud this trend may be obscured somewhat as droplet coalescence becomes increasingly important (Mason, 1971).

The fact that the RAC preferentially collected Na^+, Cl^-, Mg^{2+}, and Ca^{2+} is consistent with its lower collection efficiency for small droplets. Since these droplets should come predominantly from condensation on smaller aerosol nuclei, they are likely to contain much lower concentrations of Na^+, Cl^-, Mg^{2+}, and Ca^{2+}. The smaller droplets, collected efficiently by the CASC, act to dilute the concentrations of these four ions in the CASC samples.

In an intercomparison of fogwater collectors conducted at Henninger Flats in (Hering et al., 1987), some of the devices collected samples with higher concentrations of soil dust cations, notably Ca^{2+} and Mg^{2+}, and Na^{+}. Data from a comparison of a Desert Research Institute linear–jet impactor and a RAC exhibited trends very comparable to those seen in the current study for Na^{+}, Ca^{2+}, and Mg^{2+}: preferential collection by the RAC (Hering et al., 1987). A lower size cut of between 2 and 5 μm has been reported for the DRI jet impactor (Katz, 1980), comparable to the lower size cut for the CASC. Some speculation was made about whether the preferential collection by the RAC was due to differences in the lower size cuts of the collectors or due to some other factor. The final conclusion was that this difference was due to intense research activity at the site which probably led to soil dust particles being kicked up. These dense particles would be sampled more efficiently by the RAC than by the DRI jet impactor due to differences in the sampler inlets (Waldman, 1985). No explanation was offered for the preferential collection of Na^{+}, which is primarily derived from sea spray.

In the CASC vs. RAC comparison both samplers were located on a rooftop away from possible sources of soil dust contamination. During sampling periods the rooftop was heavily wetted by deposition from the dense fog, providing further protection from soil dust contamination. There was also very little activity at the site. The combination of these factors in the current study suggests that perhaps the differences seen are due to differences between the collectors in the collection efficiency of small droplets.

During the CASC vs. RAC comparison no significant collection preferences for any ion were exhibited by the CASC. This happened despite the fact that aerosol NO_3^-, SO_4^{2-}, and NH_4^+, resulting primarily from gas–to–particle conversion processes, are found predominantly in the fine particle fraction (Seinfeld, 1986). Since smaller cloud droplets should tend to have smaller condensation nuclei, it might be expected that

these ions would reside mostly in the smaller droplets and therefore be collected preferentially by the CASC. The situation is not so simple, however, since cloudwater concentrations of all three of these ions may be altered by absorption of precursor gas phase species followed by chemical reaction. $NH_3(g)$ can be absorbed by the droplets and protonated to form NH_4^+; $HNO_3(g)$ can be absorbed, followed by deprotonation to yield NO_3^-; $SO_2(g)$ can be absorbed and oxidized to SO_4^{2-}. The first two processes are extremely rapid. The oxidation of S(IV) to S(VI) in cloudwater is also rapid in the presence H_2O_2 or a metal catalyst (Hoffmann and Jacob, 1984). All three of these processes occur throughout the droplet size spectrum making them likely candidates for masking the signature of aerosol NO_3^-, NH_4^+, and SO_4^{2-}.

Summary

A comparison of cloudwater collection characteristics of the Caltech Active Strand Collector (CASC) and the Rotating Arm Collector (RAC) was conducted at an elevated coastal site near the eastern end of the Santa Barbara Channel during the summer of 1985. Of particular interest were the rates of collection and the chemical comparability of the samples obtained using each instrument.

Collection rates as high as 8.5 ml min^{-1} were obtained using the CASC in this study. Collection rates for the RAC have been seen to go as high as 2 ml min^{-1} in past studies. During this intercomparison the ratio of CASC to RAC collection rates was found to be close to the theoretical prediction of 4.2:1 over a wide range of LWC. At low LWC, however, this ratio climbed rapidly. This may be attributable to the differing lower size cuts of the two instruments: since the CASC collects small droplets more efficiently than the RAC, its performance relative to the RAC should increase in thinner fogs and clouds where the mass median droplet diameter decreases.

Concentrations of Na^+, Cl^-, NO_3^- , SO_4^{2-}, NH_4^+, Ca^{2+}, and Mg^{2+} in simultaneous

samples collected by the two instruments were compared. Preferential collection of Na^+, Cl^-, and Ca^{2+} by the RAC was observed to occur with a confidence level greater than 95%. Preferential collection of Mg^{2+} by the RAC was observed to occur with a confidence level greater than 90%. This preferential collection may also be attributable to the differing lower size cuts of the two samplers since these ions, derived primarily from soil dust and sea spray, may be expected to reside primarily in larger cloud droplets which make up a larger fraction of each RAC sample. No significant preferential collection by either collector was observed for NO_3^-, SO_4^{2-}, or NH_4^+.

References

Bartlett, M. S. (1949) Fitting a straight line when both variables are subject to error. *Biometrics* 5, 207–212.

Best, A. C. (1951a) Drop–size distribution in cloud and fog. *Q. Jl. R. met. Soc.* 77, 418.

Best, A. C. (1951b) The size of cloud droplets in layer–type cloud. *Q. Jl. R. met. Soc.* 77, 241.

California Air Resources Board (1982) Air quality aspects of the development of offshore oil and gas resources, a staff report available from the CARB, 1800 15th St., Sacramento, CA.

Daube, B. C., Jr., Flagan, R. C. and Hoffmann, M. R. (1987a) Active cloudwater collector. United States Patent No. 4,697,462.

Hering, S. V., Blumenthal, D. L., Brewer, R. L., Gertler, A., Hoffmann, M., Kadlecek, J. A. and Pettus, K. (1987) Field intercomparison of five types of fogwater collectors. *Environ. Sci. Technol.* 21, 654–663.

Hoffmann, M. R. and Jacob, D. J. (1984) Kinetics and mechanisms of the catalytic oxidation of dissolved sulfur dioxide in aqueous solution: an application to nighttime fogwater chemistry, in Acid Precipitation: SO_2, NO, and NO_x Oxidation Mechanisms: Atmospheric Considerations, J. G. Calvert, ed., Butterworth Publishers, Boston, 101–172.

Hudson, J. G. (1984) Ambient CCN and FCN measurements, in Hygroscopic Aerosols, L. H. Ruhnke and A. Deepak, eds., A. Deepak Publishing, Hampton, VA.

Jacob, D. J., Wang, R. F. T. and Flagan, R. C. (1984) Fogwater collector design and characterization. *Environ. Sci. Technol.* 18, 827–833.

Johnston, J. (1984) Econometric Methods, 3rd Ed., McGraw–Hill, New York.

Katz, U. (1980) A droplet impactor to collect liquid water from laboratory clouds for chemical analysis, in Communications à la VII Conference Internationale sur la Physique des Nuages, Laboratoire Associe de Meteorologie Physique, Aubiere France, 697–700.

Maddala, G. S. (1977) Econometrics, McGraw–Hill, New York.

Mason, B. J. (1971) The Physics of Clouds, 2nd Ed., Oxford University Press, London.

Mason, B. J. and Chien, C. W. (1962) Cloud–droplet growth by condensation in cumulus. Q. *Jl. R. met. Soc.* 88, 133–138.

Seinfeld, J. H. (1986) Atmospheric Chemistry and Physics of Air Pollution, Wiley Interscience, New York.

Shair, F. H., Sasaki, E. J., Carlan, D. E., Cass, G. R., Goodin, W. R., Edinger, J. G. and Schacher, G. E. (1982) Transport and dispersion of airborne pollutants associated with the land breeze–sea breeze system. *Atmos. Environ.* **16**, 2043–2053.

Solorzano, L. (1967) Determination of ammonia in natural waters by the phenol—hypochlorite method. *Limnol. Oceanogr.* **14**, 799–801.

Wald, A. (1940) The fitting of straight lines if both variables are subject to error. *Ann. Math. Stat.* **11**, 284–300.

Waldman, J. M. (1985) Depositional aspects of pollutant behavior in fog, Ph.D. thesis, California Institute of Technology, Pasadena, CA.

Table 1. Slopes Different from One for CASC vs. RAC Sample Ionic Composition Comparison

Ion	*Slope*	*95% Confidence Limits*
Na^+	0.34	(0.18, 0.50)
Cl^-	0.42	(0.22, 0.61)
Ca^{2+}	0.37	(0.08, 0.66)
Mg^{2+}	0.58	(0.14, 1.03)

Figure Captions

Figure 1. Caltech Rotating Arm Collector.

Figure 2. Caltech Active Strand Collector. Air flow is from right to left through the collector as viewed in the figure.

Figure 3. Comparison of CASC and RAC cloudwater collection rates.

Figure 4. Comparison of NO_3^- concentrations in CASC and RAC samples. A line of perfect correlation is included for reference.

Figure 5. Comparison of SO_4^{2-} concentrations in CASC and RAC samples. A line of perfect correlation is included for reference.

Figure 6. Comparison of Cl^- concentrations in CASC and RAC samples. A line of perfect correlation is included for reference.

Figure 7. Comparison of NH_4^+ concentrations in CASC and RAC samples. A line of perfect correlation is included for reference.

Figure 8. Comparison of Mg^{2+} concentrations in CASC and RAC samples. A line of perfect correlation is included for reference.

Figure 9. Comparison of Ca^{2+} concentrations in CASC and RAC samples. A line of perfect correlation is included for reference.

Figure 10. Comparison of Na^+ concentrations in CASC and RAC samples. A line of perfect correlation is included for reference.

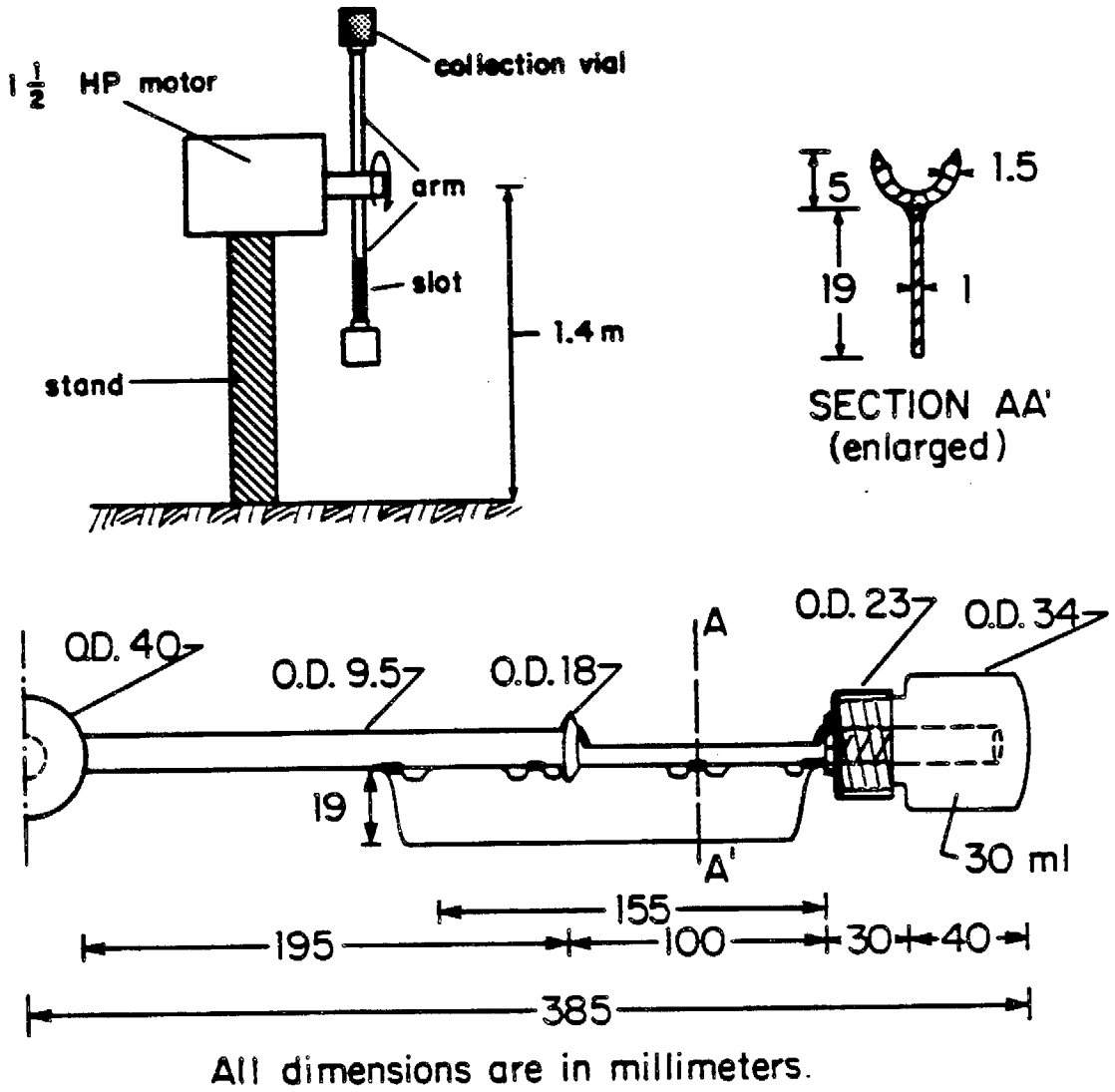

Figure 1. Caltech Rotating Arm Collector.

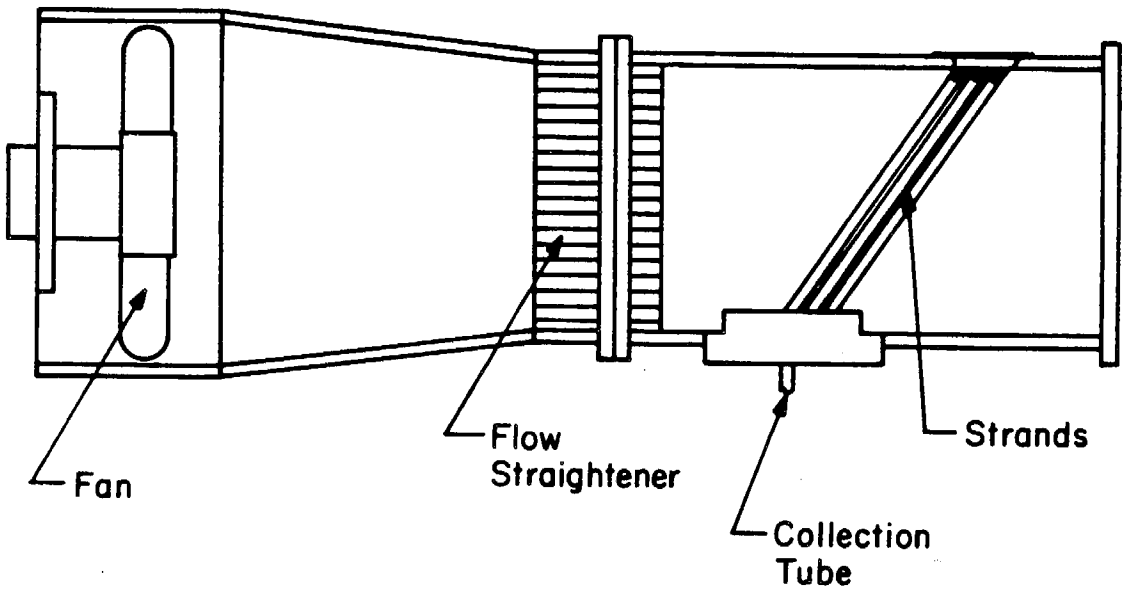

Figure 2. Caltech Active Strand Collector. Air flow is from right to left through the collector as viewed in the figure.

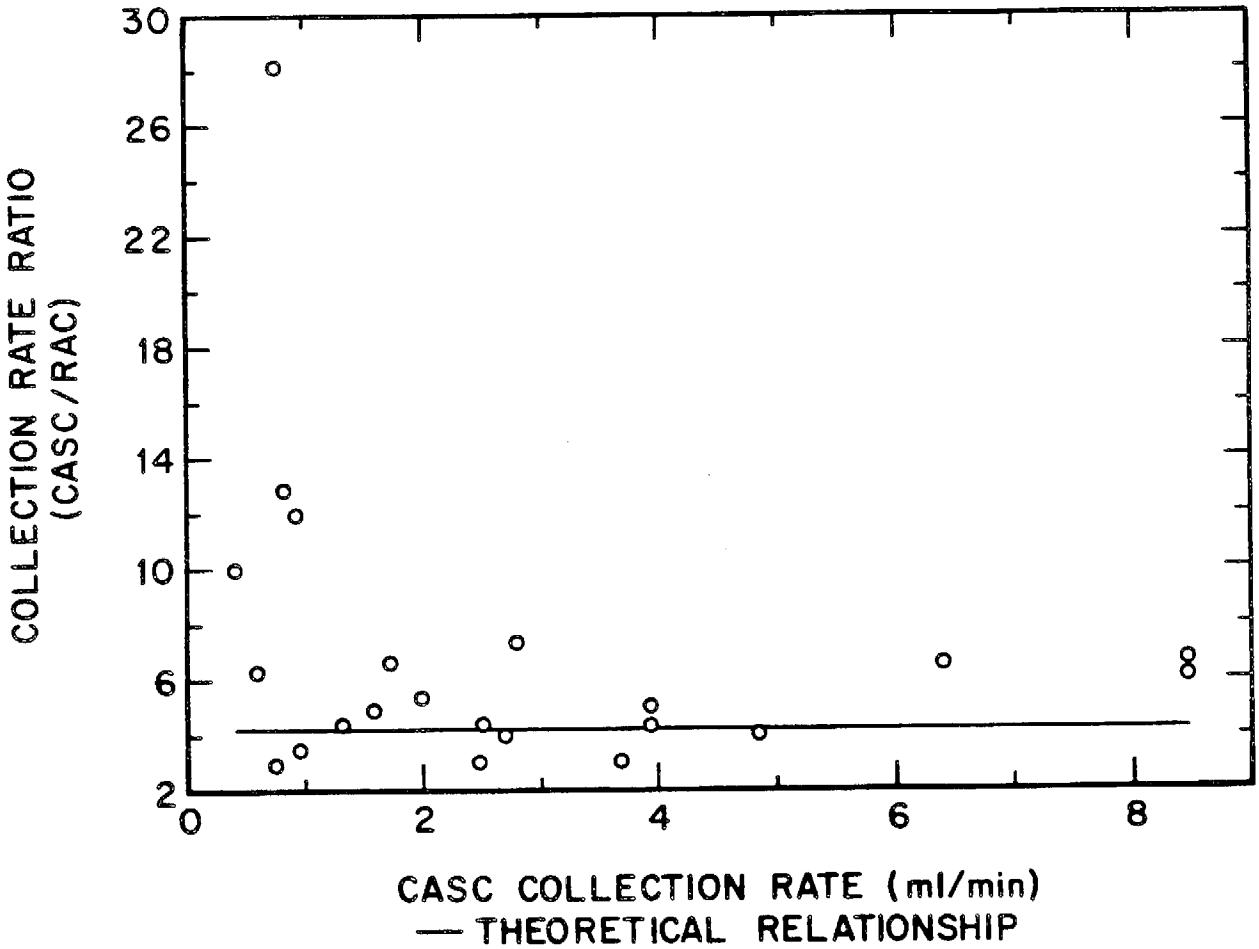

Figure 3. Comparison of CASC and RAC cloudwater collection rates.

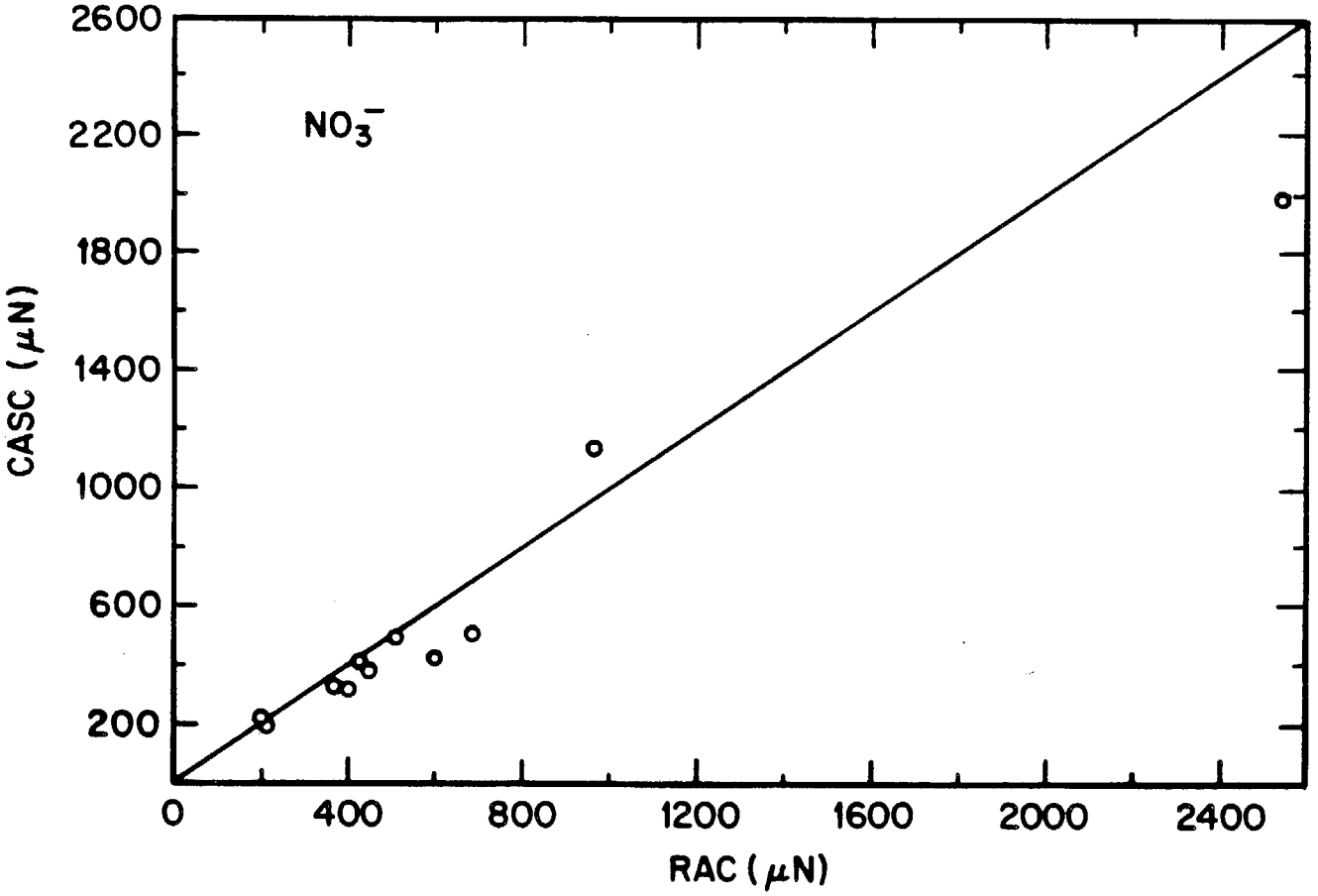

Figure 4. Comparison of NO_3^- concentrations in CASC and RAC samples. A line of perfect correlation is included for reference.

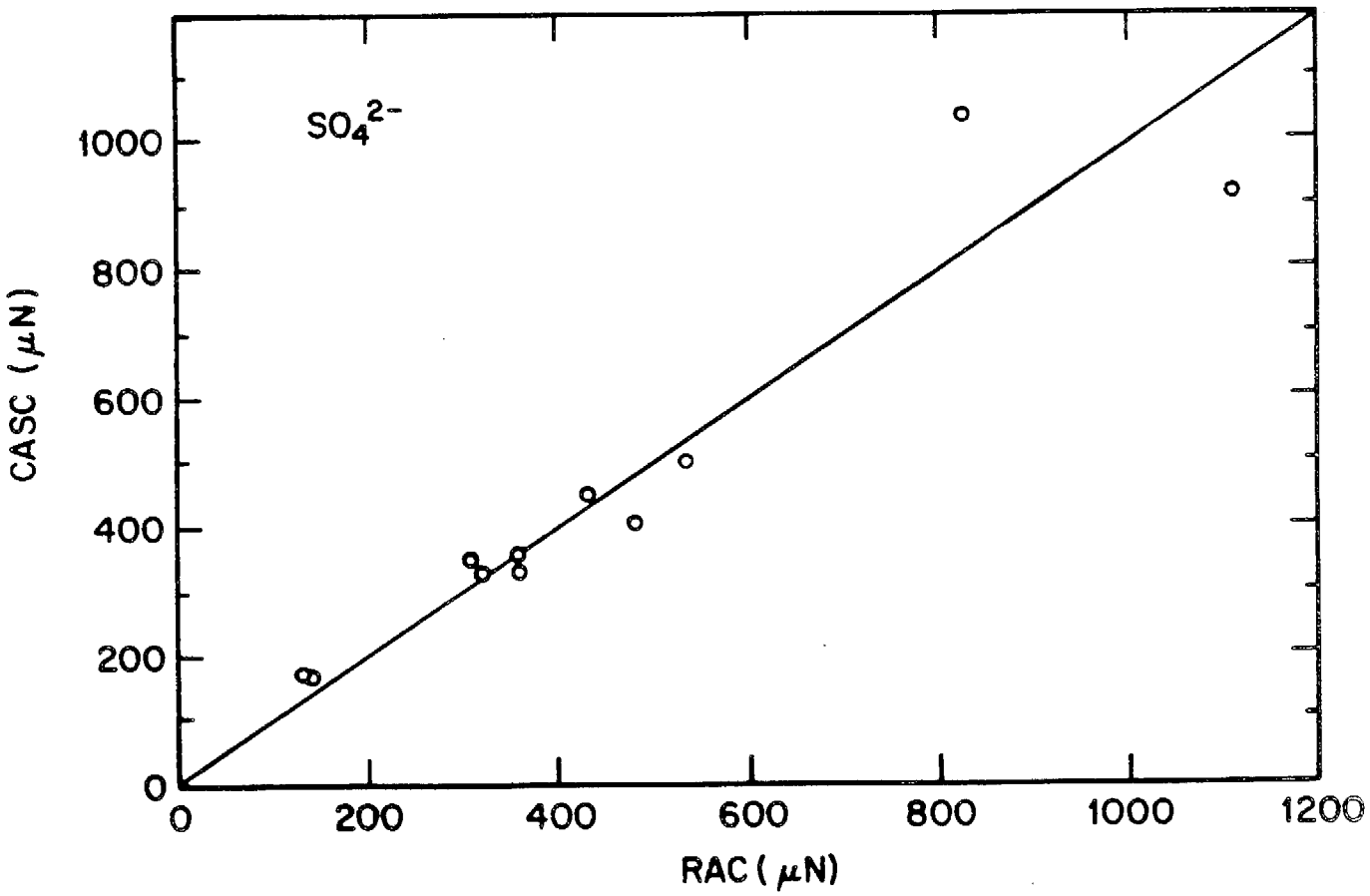

Figure 5. Comparison of SO_4^{2-} concentrations in CASC and RAC samples. A line of perfect correlation is included for reference.

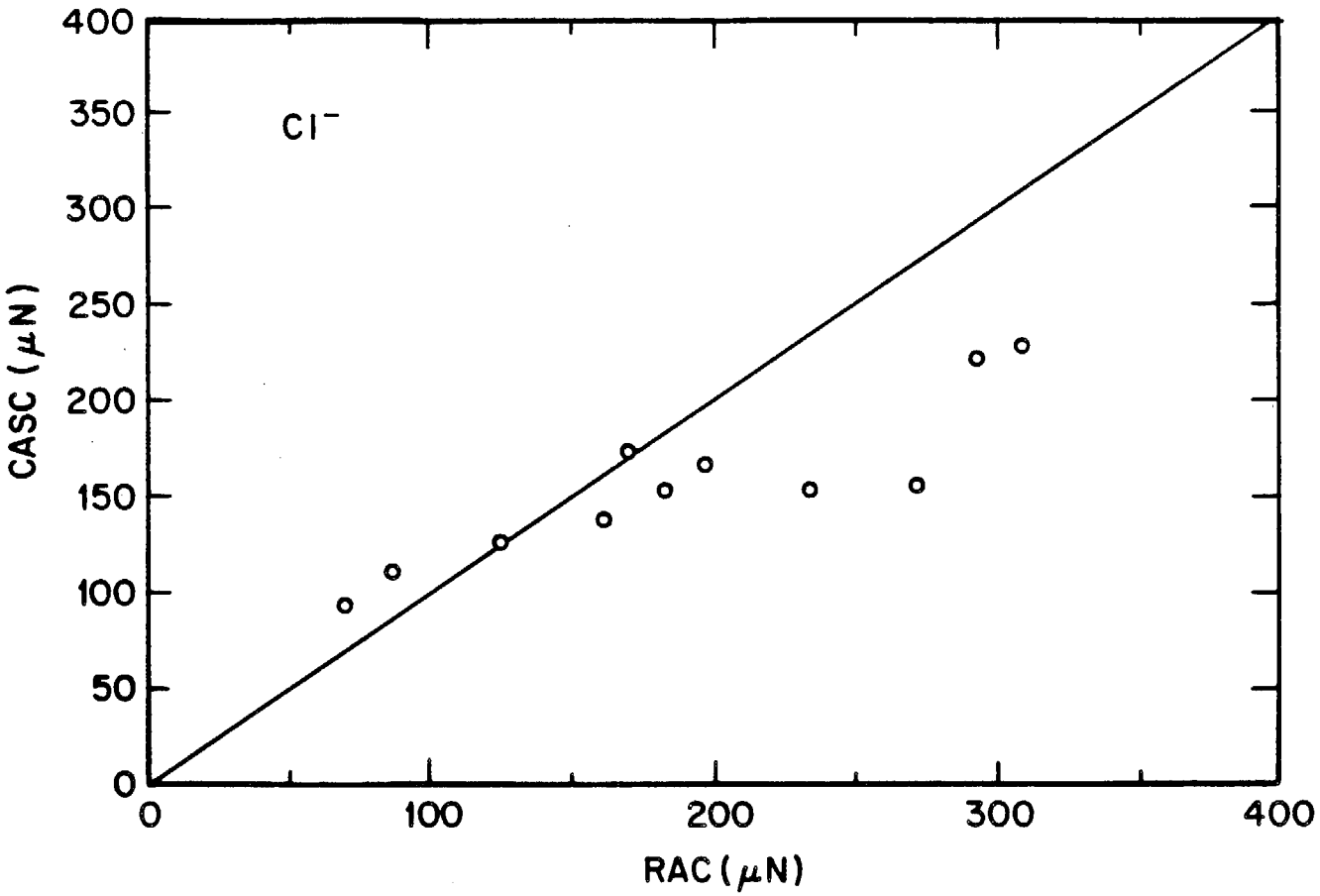

Figure 6. Comparison of Cl^- concentrations in CASC and RAC samples. A line of perfect correlation is included for reference.

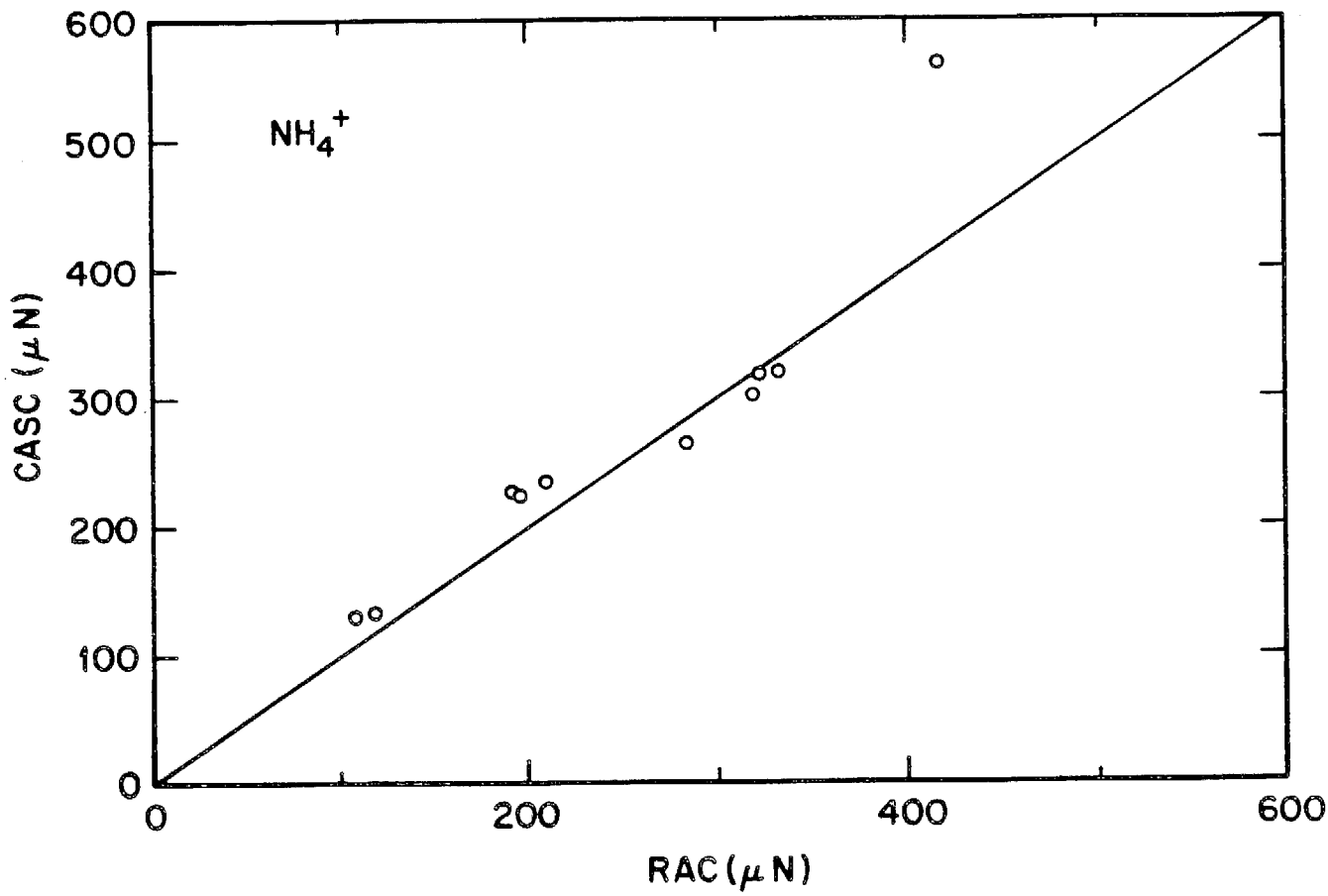

Figure 7. Comparison of NH_4^+ concentrations in CASC and RAC samples. A line of perfect correlation is included for reference.

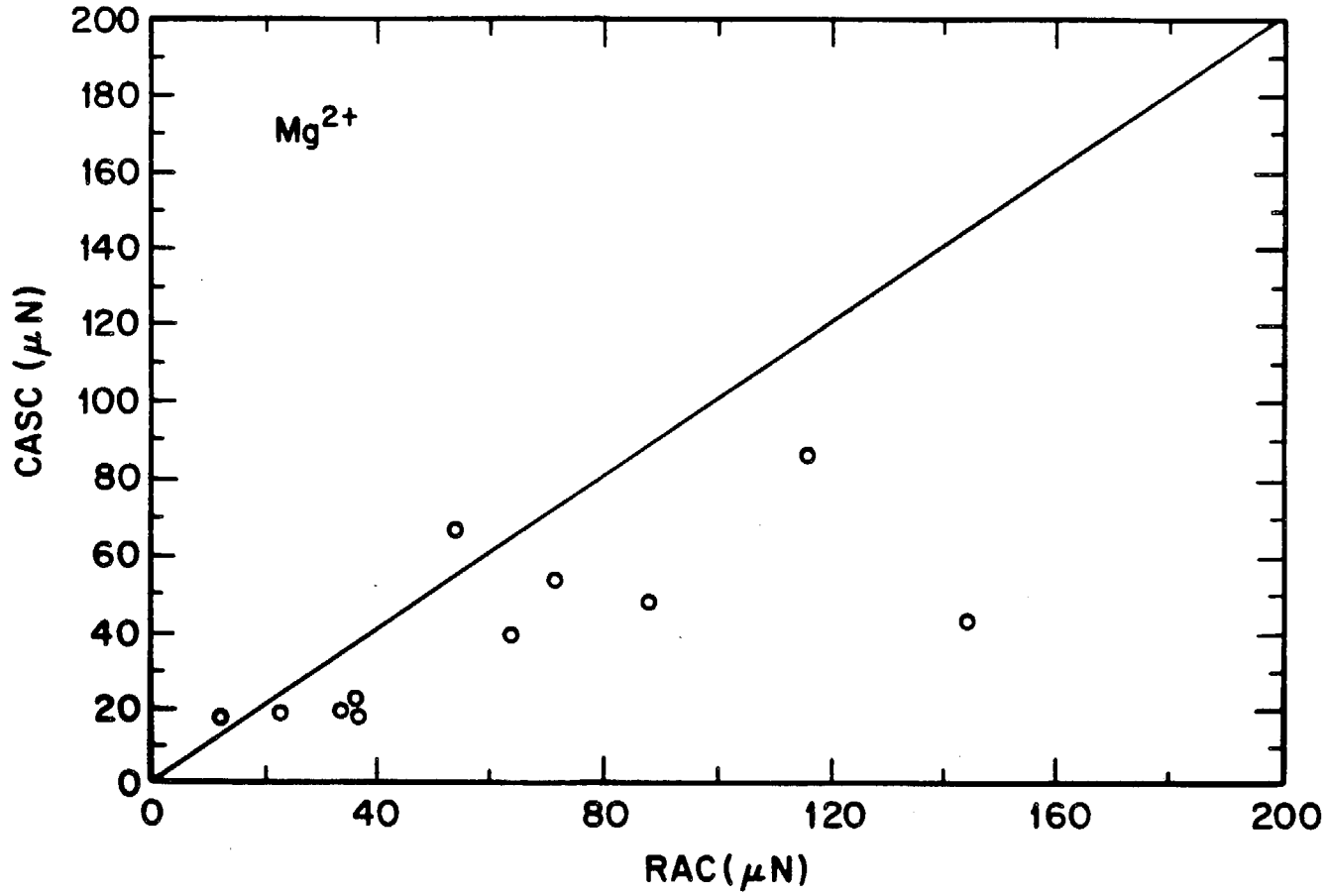

Figure 8. Comparison of Mg^{2+} concentrations in CASC and RAC samples. A line of perfect correlation is included for reference.

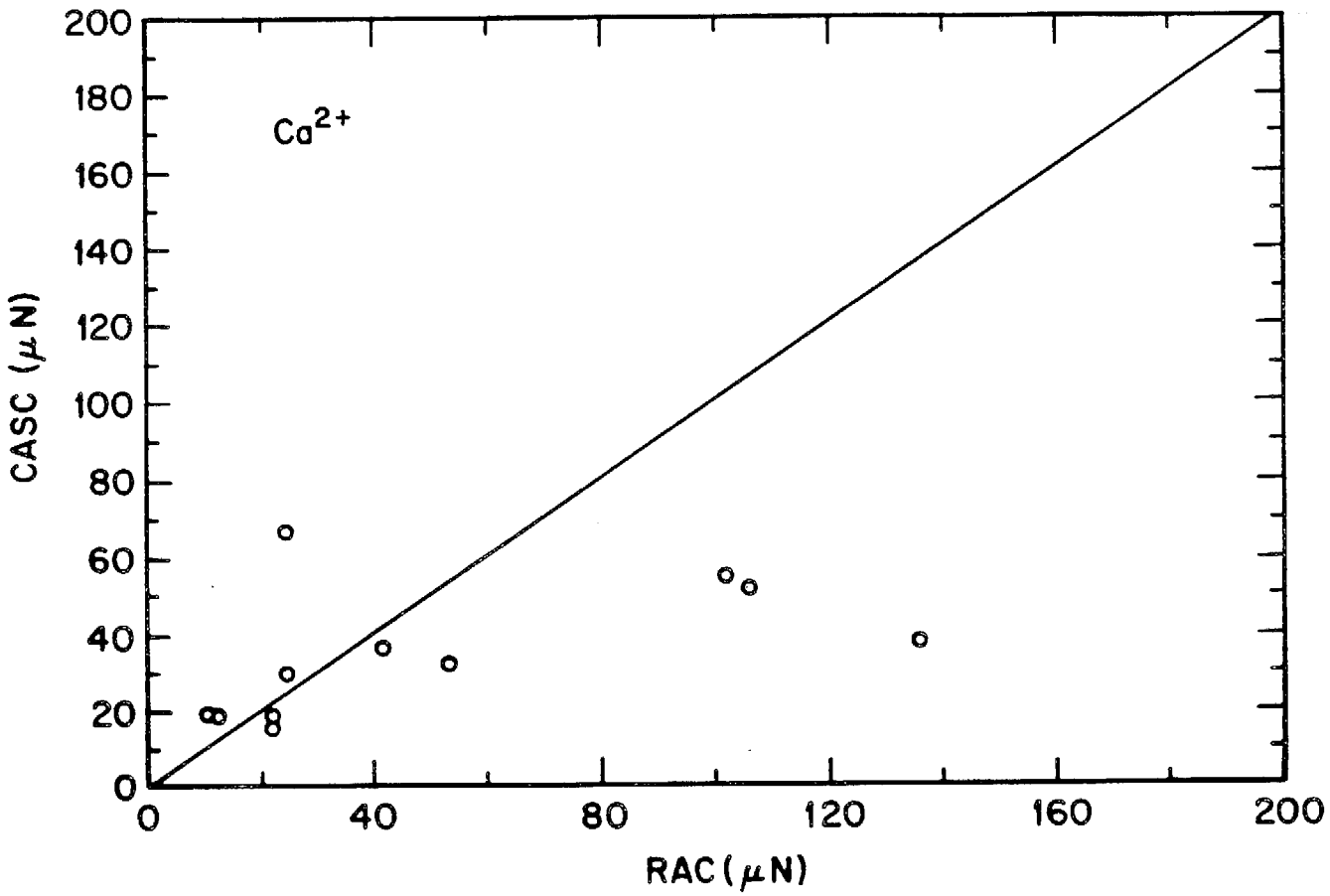

Figure 9. Comparison of Ca^{2+} concentrations in CASC and RAC samples. A line of perfect correlation is included for reference.

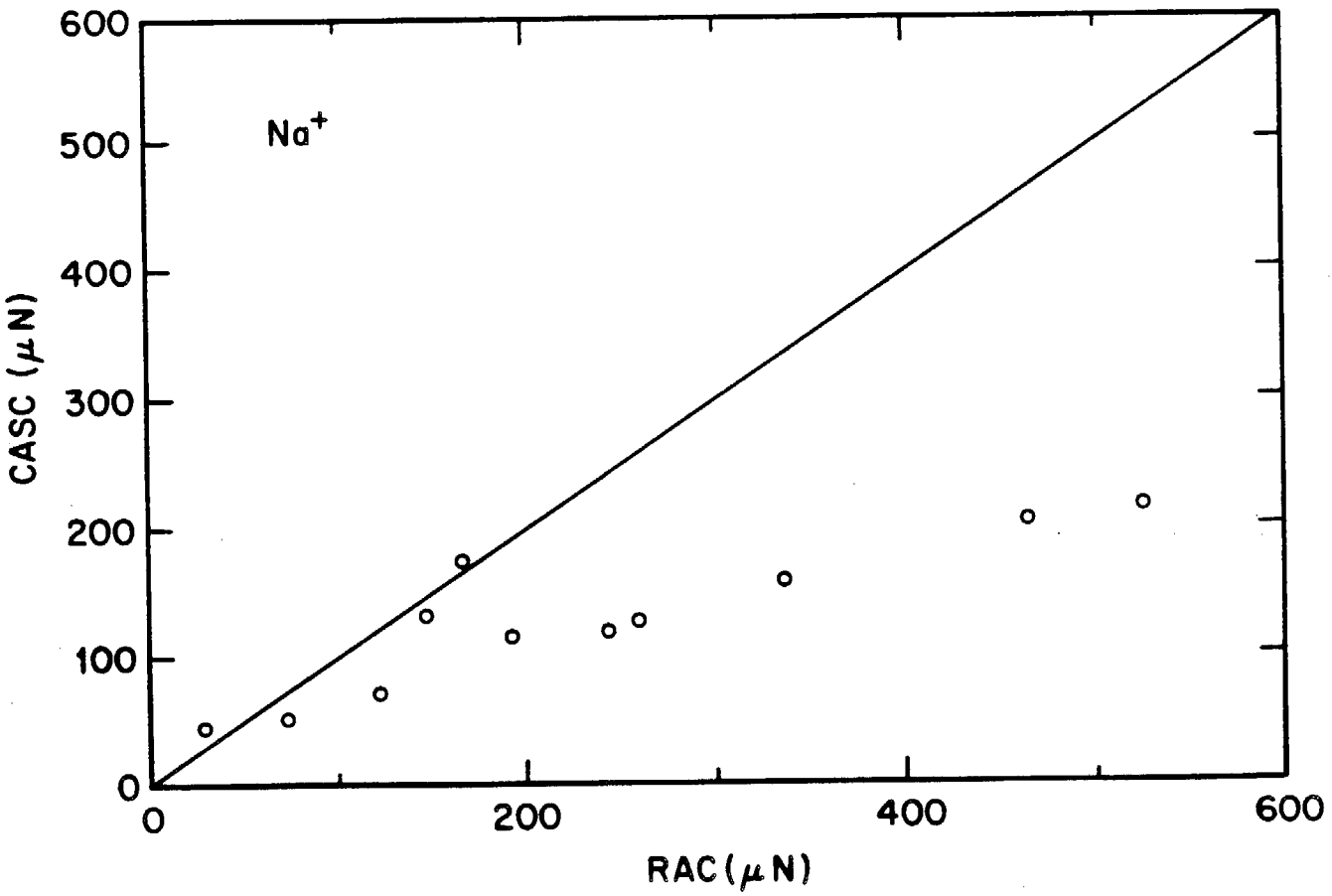

Figure 10. Comparison of Na^+ concentrations in CASC and RAC samples. A line of perfect correlation is included for reference.

CHAPTER 4

JOURNAL OF GEOPHYSICAL RESEARCH, VOL. 91, NO. D1, PAGES 1073–1088, JANUARY 20, 1986

The H_2SO_4-HNO_3-NH_3 System at High Humidities and in Fogs 1. Spatial and Temporal Patterns in the San Joaquin Valley of California

DANIEL J. JACOB,[1] J. WILLIAM MUNGER, JED M. WALDMAN, AND MICHAEL R. HOFFMANN

Environmental Engineering Science, W. M. Keck Engineering Laboratories, California Institute of Techology, Pasadena

A systematic characterization of the atmospheric H_2SO_4-HNO_3-NH_3 system was conducted in the fog water, the aerosol, and the gas phase at a network of sites in the San Joaquin Valley of California. Spatial patterns of concentrations were established that reflect the distribution of SO_2, NO_x, and NH_3 emissions within the valley. The concept of atmospheric alkalinity was introduced to interpret these concentrations in terms of the buffering capacity of the atmosphere with respect to inputs of strong acids. Regions of predominantly acidic and alkaline fog water were identified. Fog water was found to be alkaline in most of the valley, but small changes in emission budgets could lead to widespread acid fog. An extended stagnation episode was studied in detail: progressive accumulation of H_2SO_4-HNO_3-NH_3 species was documented over the course of the episode and interpreted in terms of production and removal mechanisms. Secondary production of strong acids H_2SO_4 and HNO_3 under stagnant conditions resulted in a complete titration of available alkalinity at the sites farthest from NH_3 sources. A steady SO_2 conversion rate of 0.4–1.1% h^{-1} was estimated in the stagnant mixed layer under overcast conditions and was attributed to nonphotochemical heterogeneous processes. Removal of SO_2 was enhanced in fog, compared to nonfoggy conditions. Conversion of NO_x to HNO_3 slowed down during the stagnation episode because of reduced photochemical activity; fog did not appear to enhance conversion of NO_x. Decreases in total HNO_3 concentrations were observed upon acidification of the atmosphere and were attributed to displacement of NO_3^- by H_2SO_4 in the aerosol, followed by rapid deposition of HNO_3(g). The occurrence of fog was associated with general decreases of aerosol concentrations due to enhanced removal by deposition.

JOURNAL OF GEOPHYSICAL RESEARCH, VOL. 91, NO. D1, PAGES 1073–1088, JANUARY 20, 1986

The H_2SO_4-HNO_3-NH_3 System at High Humidities and in Fogs 1. Spatial and Temporal Patterns in the San Joaquin Valley of California

DANIEL J. JACOB,[1] J. WILLIAM MUNGER, JED M. WALDMAN, AND MICHAEL R. HOFFMANN

Environmental Engineering Science, W. M. Keck Engineering Laboratories, California Institute of Techology, Pasadena

A systematic characterization of the atmospheric H_2SO_4-HNO_3-NH_3 system was conducted in the fog water, the aerosol, and the gas phase at a network of sites in the San Joaquin Valley of California. Spatial patterns of concentrations were established that reflect the distribution of SO_2, NO_x, and NH_3 emissions within the valley. The concept of atmospheric alkalinity was introduced to interpret these concentrations in terms of the buffering capacity of the atmosphere with respect to inputs of strong acids. Regions of predominantly acidic and alkaline fog water were identified. Fog water was found to be alkaline in most of the valley, but small changes in emission budgets could lead to widespread acid fog. An extended stagnation episode was studied in detail: progressive accumulation of H_2SO_4-HNO_3-NH_3 species was documented over the course of the episode and interpreted in terms of production and removal mechanisms. Secondary production of strong acids H_2SO_4 and HNO_3 under stagnant conditions resulted in a complete titration of available alkalinity at the sites farthest from NH_3 sources. A steady SO_2 conversion rate of 0.4–1.1% h^{-1} was estimated in the stagnant mixed layer under overcast conditions and was attributed to nonphotochemical heterogeneous processes. Removal of SO_2 was enhanced in fog, compared to nonfoggy conditions. Conversion of NO_x to HNO_3 slowed down during the stagnation episode because of reduced photochemical activity; fog did not appear to enhance conversion of NO_x. Decreases in total HNO_3 concentrations were observed upon acidification of the atmosphere and were attributed to displacement of NO_3^- by H_2SO_4 in the aerosol, followed by rapid deposition of HNO_3(g). The occurrence of fog was associated with general decreases of aerosol concentrations due to enhanced removal by deposition.

INTRODUCTION

Extremely high acidities have been reported in fogs and low stratus clouds collected in southern California [*Munger et al.*, 1983; *Brewer et al.*, 1983; *Waldman et al.*, 1985; *Jacob et al.*, 1984*a*, 1985]. The acidity of these fogs was due to H_2SO_4 and HNO_3, while NH_3 was found to be the main alkaline species titrating the acidity [*Jacob et al.*, 1984*a*]. Therefore one can attempt to model the "acid fog" phenomenon by consideration of acid-base neutralization processes in the H_2SO_4-HNO_3-NH_3 atmospheric system.

Ammonia is released directly to the atmosphere from a variety of sources [*Cass et al.*, 1982], but H_2SO_4 and HNO_3 are mostly produced by atmospheric oxidation of reduced sulfur and nitrogen compounds. Oxidation of SO_2 to H_2SO_4 proceeds in the gas phase [*Calvert and Stockwell*, 1984], in concentrated aerosol [*Kaplan et al.*, 1981; *Crump et al.*, 1983], and in dilute aqueous solutions [*Martin*, 1984]. Oxidation of NO_x to HNO_3 proceeds in the gas phase by the reaction $NO_2 + OH$ and may also proceed heterogeneously following scavenging by aerosol of NO_3 and N_2O_5 produced from the reaction $NO_2 + O_3$ [*Heikes and Thompson*, 1983]. Nitrite is slowly oxidized to NO_3^- in dilute solutions [*Damschen and Martin*, 1983]. Using data available for S(IV) and N(III) oxidation reactions, *Jacob and Hoffmann* [1983] predicted that aqueous phase oxidation of S(IV) in fog droplets could be an important source of H_2SO_4 under polluted conditions; on the other hand, they found that aqueous phase oxidation of N(III) provided only a very small source of HNO_3.

Sulfuric acid is present as an aerosol under usual atmospheric conditions, but HNO_3 and NH_3 have substantial vapor pressures over ammonium nitrate aerosol [*Stelson and Seinfeld*, 1982]. The atmospheric residence times of HNO_3 and NH_3 are strongly dependent on their partitioning between the gas phase and the aerosol. The gaseous species are quickly removed by deposition (1–5 cm s^{-1} for HNO_3(g) over grass [*Huebert*, 1983]). On the other hand, secondary particles formed from H_2SO_4-HNO_3-NH_3-H_2O mixtures are typically in the size range 0.1–1 μm and have low deposition velocities of the order of 0.01–0.1 cm s^{-1} [*Sehmel*, 1980; *Slinn*, 1982]. The occurrence of fog enhances the removal of aerosol species because growth of particles to fog droplet size considerably increases their deposition rates. Fog droplet deposition velocities of 2–7 cm s^{-1} over short grass [*Dollard and Unsworth*, 1983] and 2–4 cm s^{-1} over a dirt surface [*Waldman*, 1986] have been reported.

A general mechanism to account for fog water acidity in polluted atmospheres may therefore include six fundamental processes: (1) emissions of SO_2, NO_x, and NH_3, (2) pollutant transport, (3) secondary production of H_2SO_4 and HNO_3, (4) detailed chemical speciation within the H_2SO_4-HNO_3-NH_3-H_2O system, (5) scavenging by fog droplets, and (6) in-fog aqueous phase oxidation of reduced N and S species.

The San Joaquin Valley of California is an excellent "field laboratory" for the interpretation of fog water composition in terms of the above processes. It is the site of major oil recovery operations, which release large amounts of SO_2 and NO_x. In addition, agricultural and livestock-feeding activities provide important sources of NH_3. Severe stagnation episodes, associated with persistent fog and low-lying stratus clouds, occur frequently during the winter months. These stagnation episodes are caused by persistent temperature inversions based a few hundred meters above the valley floor and below the surrounding mountain ridges [*Holets and Swanson*, 1981]. Tracer studies have documented the lack of ventilation in the valley during these prolonged episodes [*Reible*, 1982]

In a preliminary study at a single site from December 1982 to January 1983, *Jacob et al.* [1984*a*] documented the main

[1]Now at Center for Earth and Planetary Physics, Harvard University, Cambridge, Massachusetts.

Copyright 1986 by the American Geophysical Union.

Paper number 5D0727.
0148-0227/86/005D-0727$05.00

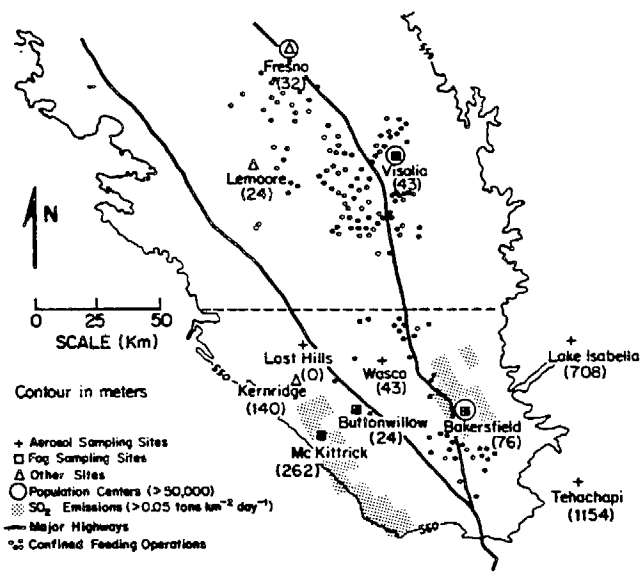

Fig. 1. Sampling sites in the San Joaquin Valley of California. Important emission sources (oil fields, major highways, confined feeding operations) are indicated. The dashed line is the Kern County line, which is the northern boundary of the area referred to in the text as the "southern San Joaquin Valley" (SSJV). Elevations in meters are given for each site, based on a reference elevation at Lost Hills, the lowest site (57 m above mean sea level).

features of aerosol and fog water chemical composition during stagnation episodes in the San Joaquin Valley. The main features observed were as follows: (1) important accumulation of secondary aerosol proceeded under nonfoggy but stagnant conditions, (2) significant pollutant deposition occurred over the course of fog events, (3) SO_2 conversion in fogs did not exceed a few percent per hour, and (4) the fog water *pH* was determined by the availability of NH_3 to neutralize the H_2SO_4 and HNO_3 present.

A more comprehensive study was conducted during January 1984, of which this report presents the main results. Aerosol, fog water, and gas phase concentrations were monitored at a network of sites. Spatial and temporal variations of atmospheric concentrations are established that reflect both the geographical distribution of emission sources and the meteorological conditions. The concept of atmospheric alkalinity is introduced to predict the potential for high-acidity fog events. Pollutant accumulation and removal over the course of a stagnation episode are characterized under both foggy and nonfoggy conditions. The rate of oxidation of SO_2 to H_2SO_4 is estimated. The effect of stagnation on HNO_3 production is discussed. The partitioning of the H_2SO_4-HNO_3-NH_3 system between the gas phase, the aerosol, and the fog water is interpreted in a companion paper in terms of a thermodynamic model [*Jacob et al.*, this issue]. The complete fog water, aerosol, and gas phase data set is given by *Jacob* [1985].

EXPERIMENTAL

The volumetric concentrations of aerosol, HNO_3(g), and NH_3(g) were monitored at eight sites over the period December 31, 1983, to January 14, 1984 (Figure 1). Samples were collected twice daily (0000–0400 and 1200–1600 PST) at the six valley sites and once daily (1000–1600 PST) at the two mountain sites (Tehachapi and Lake Isabella). The sampling stations were located on platforms 15 m above the ground (Wasco and Tehachapi), on the roof of a building or trailer (Bakersfield, Lost Hills, Buttonwillow, McKittrick, and Visalia), or on the ground, 1.5 m above a grassy area (Lake Isabella). Two open-faced 47-mm Gelman Zefluor Teflon filters (1-μm pore size) were operated side by side (10 L min^{-1}) to provide duplicate determinations of the inorganic content of the aerosol. A flat cover 15 cm above the filters prevented collection of large particles by sedimentation. The Stokes number at the filter inlet is 0.05 for a 50-μm-diameter particle, so that even very large fog droplets should be efficiently sampled [*Davies and Subari*, 1982]. Under foggy conditions the determinations of total aerosol NO_3^- and NH_4^+ may be subject to errors because of evaporative losses (see the appendix), and those numbers subject to error were excluded from the data interpretation. A 47-mm Gelman Nylasorb nylon filter collected gaseous nitric acid immediately downstream of one of the Teflon filters, and an oxalic-acid-impregnated glass fiber filter collected gaseous ammonia immediately downstream of the other Teflon filter.

The filters were sealed in petri dishes and kept at 4°C following collection. The Teflon filters were extracted in 10 mL of distilled deionized water (Corning Megapure) for 90 min, using a reciprocating shaker; complete extraction was indicated by insignificant concentrations in repeated extractions. The extracts were analyzed for major ions using standard methods previously described by *Munger et al.* [1983]. The nylon filters were extracted for 90 min, using a reciprocating shaker in a solution 3 m*M* HCO_3^- and 2.4 m*M* CO_3^{2-} (a conventional ion chromatography eluent). Oxalic-acid-impregnated filters were extracted and analyzed following the protocol of *Russell* [1983]. Ion chromatography revealed low levels of S(IV) in the Teflon filter extracts, but these concentrations were small compared to SO_4^{2-}, and their contributions were ignored. Although most of the aerosol sulfur is expected to be present as SO_4^{2-}, some of the measured SO_4^{2-} may have resulted from the oxidation of reduced sulfur species on the filter or in the extract.

Fogs were sampled by event at four sites (Figure 1). Fog water samples were collected with a rotating arm collector [*Jacob et al.*, 1984*b*] for intervals ranging from 30 min to 3 hours. The rotating arm collector has a theoretical sampling rate of 5 m^3 min^{-1} and has been shown to collect fog water samples without evaporation or condensation. Laboratory calibration has indicated a lower size cut (50% collection efficiency) of 20-μm diameter. Because the instrument collects fog droplets by direct impaction and does not require drawing air through an inlet, large fog droplets are efficiently collected. Liquid water content in the fog was determined from the sampling rate of the instrument, assuming that 60% of the total liquid water sampled was actually collected [*Waldman*, 1986].

Fog water samples were preserved and analyzed for major ions and trace metals following the protocol described by *Munger et al.* [1983], with the exception described below. In fog water samples, significant S(IV) concentrations are found during conventional anion analysis by ion chromatography. A possible explanation is the formation of stable but reversible S(IV)-*R*CHO adducts, such as $CH_2(OH)SO_3^-$ [*Munger et al.*, 1984]. The standard ion chromatographic method (Dionex AS-3 column, [3 m*M* HCO_3^- + 2.4 m*M* CO_3^{2-}] eluent, 3 mL min^{-1} flow rate) proposed by *Dionex Corporation* [1981] and used by *Munger et al.* [1983] does not clearly separate S(IV) and NO_3^-. Better separation is achieved with a weaker eluent or with the Dionex AS-4 column, but quantification of S(IV) remains unsatisfactory. To solve this problem, aliquots for anion determination were spiked to 0.09 *M* H_2O_2 several minutes prior to injection and simultaneously made alkaline

by the usual addition of HCO_3^- and CO_3^{2-} to match the eluent; this procedure was found to result in the quantitative oxidation of HSO_3^- and $CH_2(OH)SO_3^-$ standards to SO_4^{2-} and the total suppression of the S(IV) peak in fog water samples. Sulfur(IV) concentrations were separately determined by a pararosaniline colorimetric method on aliquots preserved with buffered (*p*H 4) CH_2O immediately upon sample collection [*Dasgupta et al.*, 1980]. Fog water SO_4^{2-} concentrations were calculated by subtracting the S(IV) concentrations thus obtained from the SO_4^{2-} concentrations determined by ion chromatography. Concentrations of carboxylate ions were determined by ion exclusion chromatography [*Keene et al.*, 1983].

To date there are no standardized sampling procedures for the collection of fog water and aerosol samples for chemical analysis. Therefore it is important to assess the errors associated with our methods. A detailed discussion of sampling biases, artifacts, and standard errors on our data is presented in the appendix.

Hourly average concentrations of SO_2 were measured at Bakersfield by the Getty Oil Company and at McKittrick, Kernridge, and Lost Hills by West Side Operators (WSO). Concentrations of nitrogen oxides, CO, and O_3 were monitored at Kernridge by WSO. Surface winds were measured by WSO (Lost Hills, Kernridge, McKittrick, and Maricopa), Getty Oil Company (Bakersfield), National Weather Service (NWS) (Bakersfield and Fresno), Lemoore Naval Air Force Base, and Kern County Fire Department (Tehachapi). Upper level winds were measured at Edwards Air Force Base, located in the Mojave Desert on the SE side of the Tehachapi Mountains. Mixing heights were measured hourly by WSO at Kernridge with an acoustic sounder. Additional weather data were available from the National Weather Service station at Bakersfield.

To account for the equilibria between gas and aerosol phases, we define S(VI), N(V), and N(−III) to represent the element at the given oxidation state, both in the gas and aerosol phases. Thus N(V) includes HNO_3(g) and NO_3^-, and N(−III) includes NH_3(g) and NH_4^+. We further define [*A*] as the concentration of constituent *A* in fog water (moles per liter of water), and (*A*) as the concentration of *A* in air (moles per cubic meter of air). Concentrations of HNO_3(g) will generally be given in equivalents, for consistency with the units of NO_3^- and NH_4^+ concentrations. "Equivalent" in that sense refers to the proton donor/acceptor capacity of the gas when scavenged by the aerosol. Both HNO_3(g) and NH_3(g) contribute one equivalent per mole; 1 ppb = 43 neq m^{-3} at 5°C.

WEATHER PATTERN AND POLLUTANT TRANSPORT

Figure 2 shows the profile versus time of mixing heights and stratus cloud bases over the valley floor during the sampling program. Two types of mixing height diurnal patterns were observed.

In the first pattern (December 31 to January 1, January 10–12, and January 14), ground-based inversions formed by radiation at night and broke up the following afternoon, leading to mixing heights in excess of 1000 m above ground level (AGL). This pattern was usually associated with clear skies or high cloudiness, but fogs in ground-based inversions were occasional occurrences (for example, at Bakersfield on December 31). Figure 3*a* gives the average wind vectors on the days when this pattern was observed. A net slow NW flow was observed on the valley floor, and upper level winds were NW; this is the usual flow in the area and reflects the circulation around the Pacific High off the California coast. Terrain influences in the southern end of the valley led to convergence of the flow in the SE corner of the valley. Surface winds in the valley frequently shifted in direction, and erratic low winds were typically observed under nighttime stable conditions.

Concentrations of trace gases at Kernridge were lowest on the days when this first pattern was observed (Figure 2) and so were aerosol concentrations [*Jacob*, 1985]. Because net horizontal transport was very slow (Figure 3*a*), it is unlikely that surface winds ventilated the valley by transport over the mountain ridges in the SE corner of the valley. Aerosol concentrations at Tehachapi and Lake Isabella remained much lower than in the valley, which is evidence against such transport. Instead, pollutant removal was due to rapid vertical mixing as the inversion broke up in the afternoon; this vertical mixing diluted the polluted air parcels and allowed their rapid transport by strong upper level NW winds to the surrounding air basins.

A different mixing height pattern was observed on January 2–7; during that period a strong temperature inversion based a few hundred meters above the ground persisted over the valley. This inversion was due to mesoscale subsidence associated with a stationary high-pressure system (Great Basin High) centered over southern Idaho and northern Nevada. Upper level winds at Edwards Air Force Base switched from NW to east during that period (circulation around the Great Basin High), and afternoon winds at Tehachapi were SE. The valley was capped throughout the January 2–7 period by a stratus cloud filling the upper part of the mixed layer (Figure 2); this cloud frequently intercepted the McKittrick site 250 m above the valley floor. On the night of January 4–5 the stratus base lowered sufficiently to cause fog at elevated sites on the valley floor (Kernridge and Bakersfield NWS station), although most of the valley floor remained overcast. On the nights of January 5–6 and 6–7 the stratus base lowered sufficiently to fill the entire mixed layer, as shown in Figure 2, and dense fog was observed throughout the valley. The cloud layer then deepened considerably on January 7–8; mixing heights rose to above 1000 m AGL, and drizzle fell on the valley floor. On January 9 the inversion base dropped again, but upper level winds had switched back to NW. After January 10 the first mixing height pattern (surface inversions at night breaking up in the afternoon) was again observed.

The capping of the valley by a persistent inversion based at a lower altitude than the surrounding mountain ridges obviously restricted ventilation. Concentrations of trace gases at Kernridge (Figure 2) increased over the stagnant January 2–7 period and dropped on January 8, when the mixing height rose above the mountain ridges. Concentrations then increased again on January 9–10 and dropped on January 10.

Winds in the valley during the January 2–7 period are shown in Figure 3*b*. Net horizontal transport was extremely slow. Cross-valley winds were dominant south of Lost Hills; farther north, however, a net flow north out the valley was observed. *Reible* [1982] had previously observed similar flow patterns during stagnation episodes in the valley and found pollutant transport in the southern end of the valley to be extremely complex because of the upslope flow/downslope flow systems associated with the mountain/valley breezes. He concluded from a series of tracer releases that the southern San Joaquin Valley behaved as a stirred tank with a mixing time of 1–2 days, slowly ventilated by the outflow at its northern end. We will try to interpret our data in term of that simple model, and for that purpose we define the "southern San Joaquin Valley" (SSJV) as that portion of the valley south of the Kern County line (see Figure 1).

Figure 3*b* indicates a zone of inflow along the western edge of the SSJV and two possible outflows to the north and to the

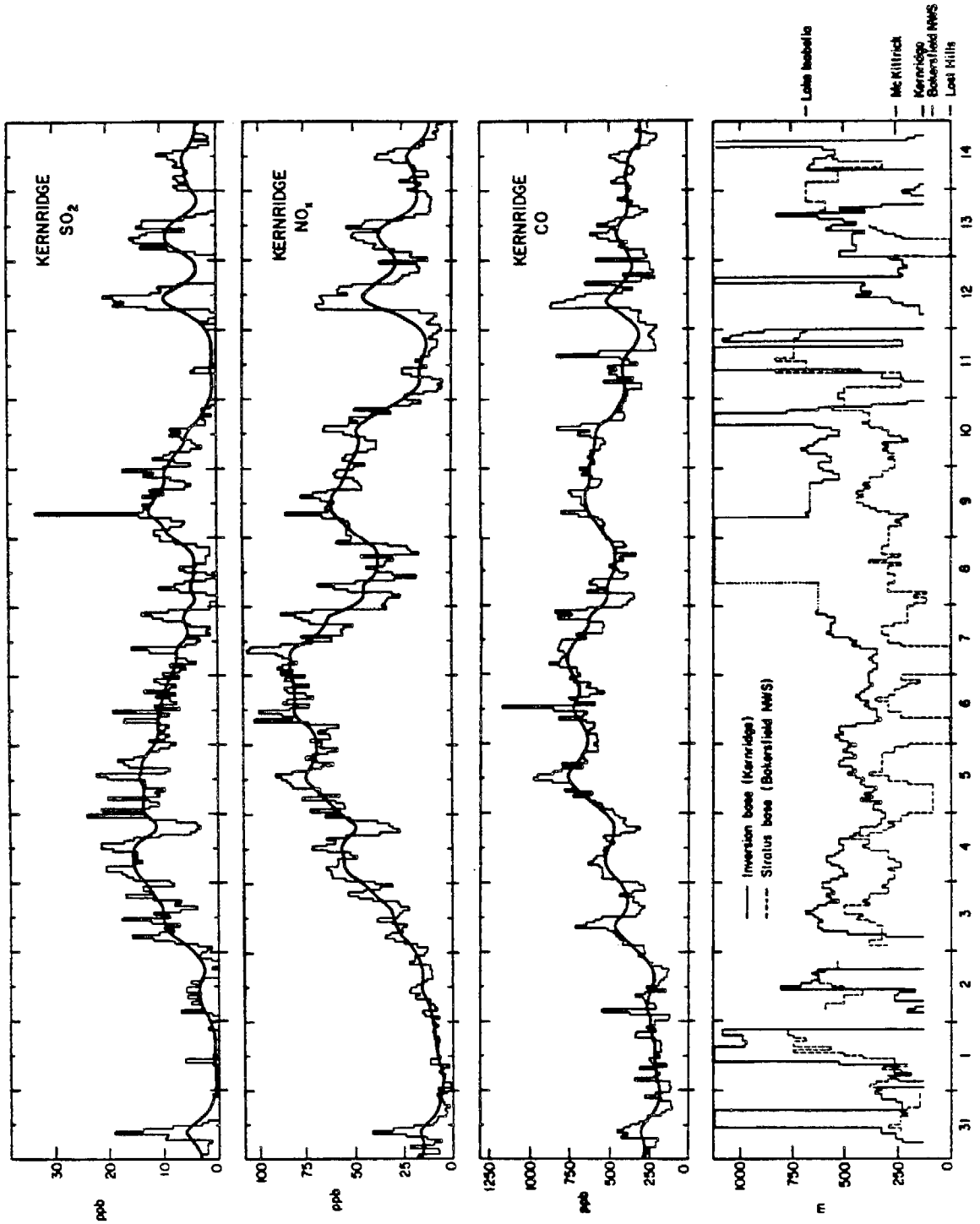

Fig. 2. Concentrations of SO_2, NO_x, and CO at Kernridge: the bold lines were obtained by smoothing the data with a digital filter. Also given are mixing heights (stratus cloud tops) measured at Kernridge and stratus cloud bases measured at the Bakersfield National Weather Service station. The reference altitude is that at Lost Hills, the lowest site on the valley floor. Kernridge hourly mixing height data were missing for January 8–9 (dotted line in the mixing height profile), and mixing heights for that period were interpolated from scattered measurements at Kernridge and cloud top data from pilot reports. Discontinuities in the mixing height profile at the altitude of Kernridge indicate a surface inversion at Kernridge. Discontinuities in the mixing height profile at 1000 m AGL indicate a mixing height in excess of 1000 m AGL.

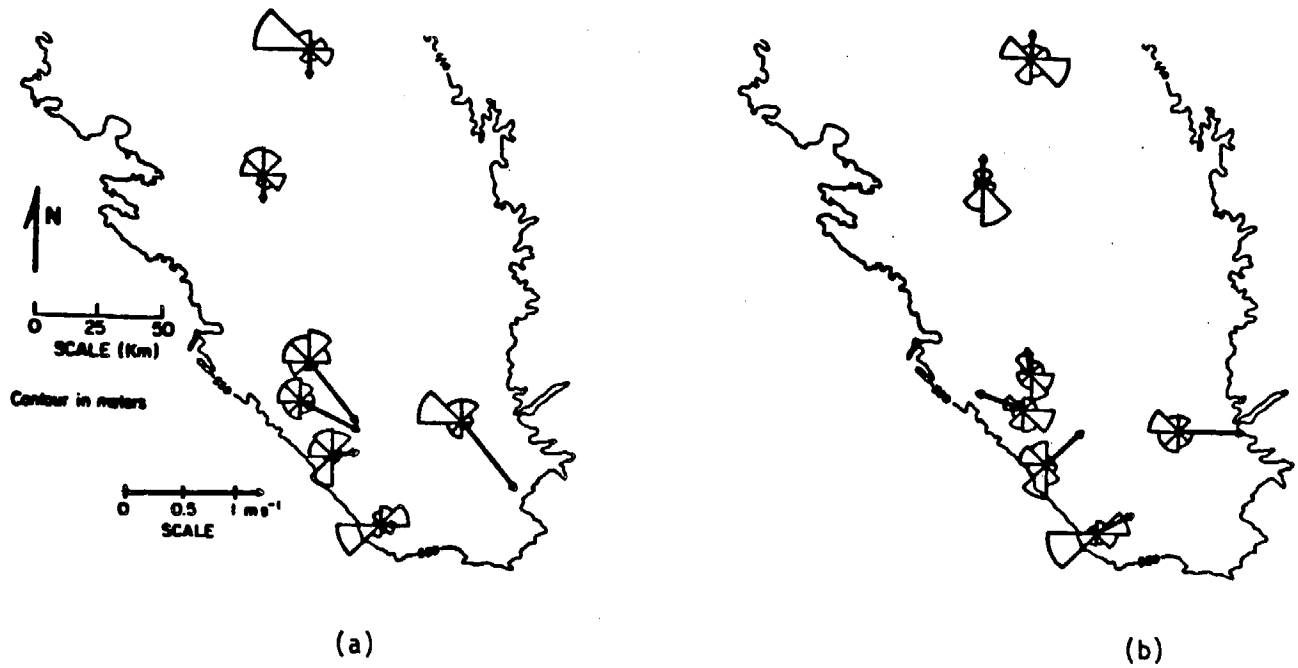

Fig. 3. Flow patterns during the sampling program. The wind roses indicate the frequencies of wind directions. The wind vector is the resultant wind (calculated by averaging the hourly wind vectors). (*a*) Nonstagnant conditions (December 31 to January 1, January 11–12, January 14). (*b*) Stagnant conditions (January 2–7).

east. However, very little transport of boundary layer air is expected over the mountain ridges on the eastern edge of the valley. The inversion did not break down or lift near the slopes: the stratus cloud intercepted the Bakersfield-Tehachapi highway as a well-defined fog layer, and the community of Tehachapi always remained sunny and clear. Further, winds in the SSJV were entirely decoupled from the circulation aloft, as indicated by the upper level winds to the east at Edwards AFB and the SE winds at Tehachapi. Aerosol concentrations remained very low at Tehachapi and Lake Isabella throughout the episode.

Therefore slow transport north out of the valley was the main outflow for SSJV air. Resultant winds at Lemoore, Fresno, and Lost Hills were consistent (Figure 3*b*). Projections of these winds on the valley axis (150°) yielded average speeds of 0.24, 0.26, and 0.22 m s^{-1} at each site, respectively. Since the SSJV is about 100 km long, this flow led to an average residence time of 5 days for an air parcel within the SSJV. The accumulation pattern for CO at Kernridge (Figure 2) suggests approach of a steady state by January 5, which is consistent with a residence time of 5 days.

AVERAGE S(VI), N(V), AND N(−III) CONCENTRATIONS AT EACH SITE

The SSJV is the site of important SO_2, NO_x, and NH_3 emissions (Table 1). The geographical distribution of the main emission sources is shown in Figure 1. Most of the NH_3 is emitted from confined-feeding operations concentrated on the east side of the valley, especially around Bakersfield and Visalia. Another important source of NH_3 is cropland, which occupies most of the land in the valley floor not used for oil recovery operations, and the associated fertilizer use. Emissions of SO_2 and NO_x are concentrated in the east side and west side oil fields of the SSJV; the oil field emissions originate mostly from small boilers, which release their exhausts 10–20 m above the ground and therefore affect the immediate surroundings. Mobile sources (two major highways, off-road farm equipment, and city traffic) also contribute to NO_x emissions.

Spatial patterns of aerosol and fog water concentrations (Tables 2 and 3*a*–3*c*) directly reflected the distribution of emission sources. The ionic content of aerosol in the valley was dominated by SO_4^{2-}, NO_3^-, and NH_4^+, which typically contributed over 90% of the total measured ionic loading. Concentrations of N(−III) were highest at Bakersfield and Visalia, near the large cattle feedlots, and lowest on the west side (Lost Hills and McKittrick). Mountain sites (Lake Isabella and Tehachapi), which have no important local NH_3 sources, had very low N(−III) concentrations.

Concentrations of S(VI) were highest at Bakersfield, which is within the east side oil fields; they were also high at McKittrick, which is within the west side oil fields, and at Buttonwillow, directly downwind of the west side oil fields. Concentrations of S(VI) at Wasco, Lost Hills, and Visalia were lower, reflecting their respective distances from oil recovery operations. Concentrations of S(VI) at the two mountain sites were very low and indicated no observable impact from the valley air.

Because most of the NO_x was emitted from the same sources as SO_2, one would expect the spatial distribution of N(V) concentrations to be similar to that of S(VI). Indeed, N(V) concentrations were highest at Bakersfield; however, N(V) concentrations at McKittrick were low. The lack of NH_3 at McKittrick frequently led to acidic conditions, in which N(V) would be mostly present as HNO_3(g) and therefore quickly removed by deposition. This point will be addressed in more detail below. Concentrations of N(V) were higher at Visalia than would be expected from the spatial distribution of S(VI); Visalia is an important population center, and emissions from mobile sources were probably the dominant source of N(V) precursors at that site.

Fog water concentrations of trace metals were consistent with the above analysis (Table 3*b*). Concentrations of Ni and V, which are almost exclusively associated with residual oil burning [*Cooper and Watson*, 1980], were high at Bakersfield,

TABLE 1. SO_2, NO_x, and NH_3 Emission Inventories for the Southern San Joaquin Valley

Source	Emissions, t d^{-1}
SO_2[a]	
Oil production	
east side	116
west side	69
Agriculture	1
Mobile sources	6
Total emissions	1972
NO_x[b]	
Stationary sources[c]	138
Mobile sources	52
Total emissions	190
NH_3[d]	
Livestock	46
Soil	18
Fertilizer use	10
Domestic	3
Fuel combustion	2
Total emissions	79

See Figure 1 for definition of southern San Joaquin Valley. Area is 7930 km^2.

[a]*Aerovironment, Incorporated* [1984], December 1982 data.

[b]*California Air Resources Board* [1982], 1979 data.

[c]Mostly oil and gas production.

[d]*Jacob* [1985], January 1984 data.

McKittrick, and Buttonwillow and low at Visalia. Concentrations of Pb, which is emitted by automobile exhaust, were high in the population centers (Bakersfield and Visalia) and low at rural sites (McKittrick and Buttonwillow).

Overall, the large differences in S(VI), N(V), and N(−III) concentrations that were observed from one site to another over distances of only a few tens of kilometers show that the composition of the H_2SO_4-HNO_3-NH_3 system at each site was strongly determined by the nature of emission sources in the immediate vicinity. A chemical balance on primary aerosol (based on the work by *Cooper and Watson* [1980]) indicated that all but a negligible fraction of the total S(VI) in the valley was of secondary origin. However, in spite of the time required for oxidation of SO_2 to H_2SO_4, the areas of SO_2 emissions matched the areas of high S(VI) concentrations. This supports our observation that horizontal pollutant transport on the valley floor was very slow. Under such conditions, fog water acidity should be directly determined by the relative abundances of local acidic (SO_2, NO_x) and alkaline (NH_3) emissions. Indeed, Table 3 indicates that fog water acidity differed greatly from site to site, depending on the availability of NH_3 to neutralize S(VI) and N(V); low *p*H values were found at McKittrick and very high *p*H values were found at Visalia. The *p*H of fog samples collected simultaneously at four sites during the widespread January 7 fog event clearly showed this spatial pattern (Figure 4). Acidic fog was consistently observed at McKittrick but never at the other sites.

Acidic fog had frequently been observed at the Bakersfield site during the previous winter [*Jacob et al.*, 1984*a*]. In view of the close balance of acids and bases at that site, small fluctuations in emissions can result in a lack of available base to titrate acid inputs. To predict the vulnerability of an atmosphere to an "acid fog" problem, one must have a quantitative measure of the acid-neutralizing capacity of that atmosphere. To this end we now introduce the concept of atmospheric alkalinity, defined by analogy to the concept of alkalinity used in the aquatic chemistry literature [*Stumm and Morgan*, 1970].

ATMOSPHERIC ALKALINITY

We define fog water alkalinity [ALK] as the deficiency of aqueous phase H^+ with respect to the reference system of "neutralized" fog water species (CAT^{n+}, Cl^-, NO_3^-, SO_4^{2-}, $S(IV)^-$, CO_2, *HA*). CAT^{n+} refers to cations other than H^+, and *HA* refers to undissociated weak acids other than CO_2. In the *p*H range 3–8 the following expression for [ALK] can be used to a good approximation:

$$[\mathrm{ALK}] = \sum [A^-] + [\mathrm{S(IV)}^{2-}] + [\mathrm{HCO_3}^-] + [\mathrm{NH_3(aq)}] + [\mathrm{OH}^-] - [\mathrm{H}^+] \quad (1)$$

The main S(IV) species in the *p*H range 2–7 are expected to be HSO_3^- and stable monovalent S(IV) adducts [*Jacob and Hoffmann*, 1983; *Munger et al.*, 1984; *Boyce and Hoffmann*, 1984]. Therefore the monovalent form of S(IV) is most appropriate for use as reference. If CO_2 was the only weak acid present, fog water at the reference point ([ALK] = 0) would correspond to pure water in equilibrium with atmospheric CO_2, and the corresponding reference *p*H would be about 5.6; because additional weak acids are present, the reference *p*H is lower. At the concentrations of carboxylic acids found in the San Joaquin Valley (Table 2) the reference *p*H is of the order of 4.5. This is still above the threshold at which environmental damage from "acid fog" may be anticipated [*Scherbatskoy and Klein*, 1983; *Granett and Musselman*, 1984; *Hoffmann*, 1984].

Fog water with [ALK] < 0 is said to contain inorganic acidity, and its *p*H is lower than that of the reference system. Such fog water has zero buffer capacity with respect to further inputs of strong acids, which may then lead to extremely acidic conditions. We will use the presence of inorganic acidity as an operational definition of the term "acid fog." Alkaline fog water (defined by [ALK] > 0) has a *p*H higher than that of the reference system and will neutralize acid inputs until exhaustion of the alkalinity. However, [ALK] is not a true measure of the acid-neutralizing capacity of the fog water because it ignores exchanges with the gas phase. In particular, alkaline fog water may support a substantial NH_3 vapor pressure [*Jacob et al.*, this issue], which provides an additional source of acid-neutralizing capacity to the fog water. Further, fog water alkalinity depends on the fraction of the aerosol scavenged in the fog. To use alkalinity as a measure of the acid-neutralizing capacity of the atmosphere with respect to acid fog, we need to introduce a more general concept, atmospheric alkalinity.

The atmospheric alkalinity (ALK) (equivalents per cubic meter of air) is the sum of total aerosol alkalinity and gas phase alkalinity in an atmosphere. That atmosphere may or may not contain fog. The reference system is the same as that used for defining fog water alkalinity; gas phase CO_2 and other weak acids are reference species. The aerosol alkalinity $(\mathrm{ALK})_a$ is given by (1), where fog water concentrations (moles per liter of water) are replaced by total aerosol concentrations (moles per cubic meter of air). The gas phase alkalinity is given by the proton donor and acceptor capacities of water-soluble atmospheric gases with respect to the reference system. Atmospheric alkalinity is a conserved quantity upon fog formation and can therefore be used to predict the potential for acid fog from aerosol and gas phase measurements taken under nonfoggy conditions. Atmospheric alkalinity also gives the amount of strong acids that may be emitted to the atmo-

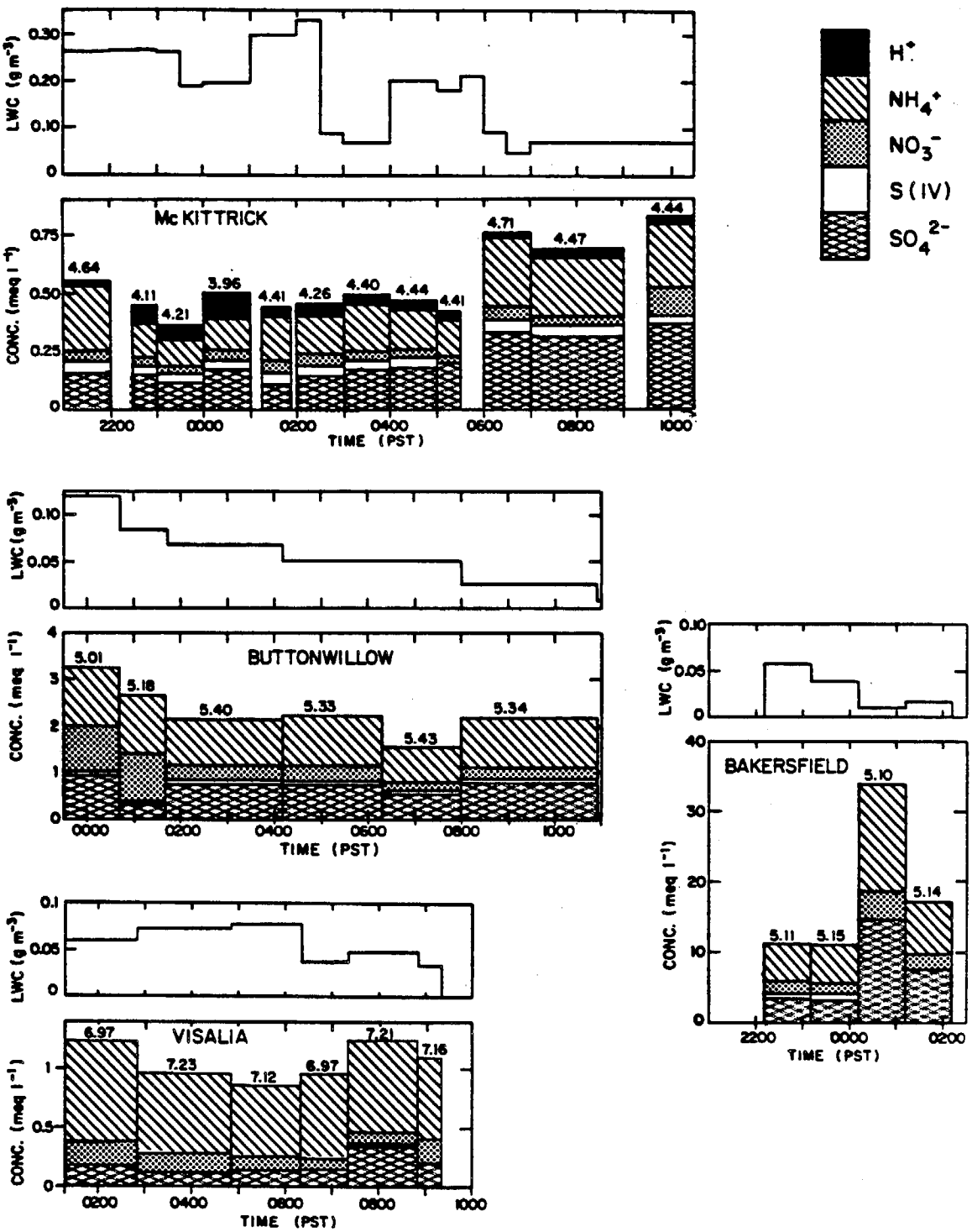

Fig. 4. Fog water composition and liquid water content (LWC) determined simultaneously at four sites during the January 6–7 fog event. The *p*H values are indicated on top of each data bar. Concentrations of S(IV) were not determined in the last two samples at Bakersfield.

sphere before an acid fog problem is to be feared and is thus a useful tool for regulatory purposes.

For the subset of samples analyzed for carboxylic acids we calculated the fog water alkalinity [ALK] as follows:

$$[ALK] = [HCOO^-] + [CH_3COO^-] + [CH_3CH_2COO^-] + [CH_3CH(OH)COO^-] + [HCO_3^-] + [NH_3(aq)] + [OH^-] - [H^+] \quad (2)$$

where $[H^+]$ was directly measured, and the concentrations of alkalinity-contributing species were determined from the fog water concentrations and the equilibrium constants for the acid-base equilibria at 5°C. *Smith and Martell* [1976] and *Martell and Smith* [1977] give K_{a1} values of 1.7×10^{-4} *M*, 1.7×10^{-5} *M*, 1.3×10^{-5} *M*, and 1.3×10^{-4} *M* for HCOOH, CH_3COOH, CH_3CH_2COOH, and $CH_3CH(OH)COOH$, respectively. $K_b = 1.5 \times 10^{-5}$ *M* for NH_3, and $K_w = 2.0 \times 10^{-15}$ M^2 for H_2O dissociation. Concentrations of

TABLE 2. Aerosol, HNO_3(g), and NH_3(g) Data, December 31, 1983 to January 14, 1984

Site	Number of Samples	Na^+	K^+	NH_4^+	Ca^{2+}	Mg^{2+}	Cl^-	NO_3^-	SO_4^{2-}	HNO_3(g)	NH_3(g)	N(V)	N(−III)
Bakersfield	30												
Range		<4–56	<4–19	144–1149	6–75	<4–12	<20–67	85–467	78–855	<4–46	19–483	93–471	209–1204
Mean		15	4	560	35	6	27	276	336	16	146	292	706
Wasco	29												
Range		<4–86	<4–20	74–584	4–43	<4–10	<20–93	23–419	19–312	<4–54	<17–273	54–431	95–648
Mean		12	<4	308	16	<4	22	195	137	19	70	214	378
Lost Hills	25												
Range		<4–48	<4–7	55–553	4–57	<4–11	<20–43	4–310	16–314	<4–174	<17–88	40–414	55–617
Mean		11	<4	223	17	<4	<20	132	108	40	31	172	254
McKittrick	29												
Range		5–70	<4–13	28–424	6–43	<4–10	<20–71	10–246	36–802	<4–164	<17–205	21–347	37–457
Mean		17	<4	224	20	4	21	89	195	34	34	123	258
Buttonwillow[a]	18												
Range		4–51	<4–10	36–663	6–68	<4–11	<20–41	34–400	31–579	<4–37	18–645	77–406	135–1001
Mean		19	<4	306	31	5	23	184	188	12	131	196	437
Visalia[b]	14												
Range		<4–16	<4–7	108–359	6–37	2–5	<20–41	73–318	35–129	<4–15	184–662	73–322	484–869
Mean		7	<4	239	20	<4	<20	175	83	7	450	182	689
Lake Isabella	11												
Range		<4–28	<4–4	<8–32	6–32	<4	<20	<4–23	<4–23	5–36	<17–44	<8–59	<8–44
Mean		10	<4	8	11	<4	<20	9	9	16	19	25	27
Tehachapi	13												
Range		<4–93	<4–140	<8–73	10–126	<4–43	<20–252	<4–50	<4–47	<4–18	<17–74	<8–68	<8–84
Mean		17	12	11	46	8	32	11	17	7	34	18	45

Values are in nanoequivalents per cubic meter. See *Jacob* [1985] for the complete data set.
[a]From January 5 to January 14.
[b]From December 31 to January 7.

HCO_3^- were calculated by assuming equilibrium with $P_{CO2} = 340$ ppm ($H \times K_{a1} = 7.07 \times 10^{-6}$ M^2 atm^{-1} at 5°C). We assumed $[S(IV)^{2-}] = 0$ in all our calculations; free S(IV) is mostly divalent at $pH > 7$, but there is strong evidence that S(IV) in fog water actually combined with aldehydes to form stable adducts [*Munger et al.*, 1984]. These S(IV)-aldehyde adducts remain monovalent over a higher range of pH, up to pH 11.7 for the S(IV)-formaldehyde adduct [*Sørensen and Andersen*, 1970]. Even if S(IV) was actually divalent at $pH > 7$, S(IV) concentrations in fog water at such high pH values were low (Table 3, Visalia), and the contribution of $S(IV)^{2-}$ to the fog water alkalinity would be very small.

Estimating $(ALK)_a$ from the available aerosol data was less straightforward. We assumed that the ions on the right-hand side of (1), possibly plus additional weak acid anions, constituted the aerosol ionic content unaccounted for in our chemical analysis. By a charge balance on the aerosol we obtained:

$$(ALK)_a = (Na^+) + (K^+) + (NH_4^+) + 2(Ca^{2+}) + 2(Mg^{2+}) - (Cl^-) - (NO_3^-) - 2(SO_4^{2-}) \quad (3)$$

Since we have argued that the inorganic acidity in fog is mostly controlled by species in the H_2SO_4-HNO_3-NH_3 system, we will assume that the only gas phase contributors to (ALK) are HNO_3(g) and NH_3(g). A calculation of the ultimate alkalinity of an air parcel should include SO_2(g); however, the contribution of SO_2(g) to (ALK) may be limited by the slow rate of SO_2 scavenging by fog [*Jacob and Hoffmann*, 1983]. For now we ignored the SO_2(g) contribution and calculated the atmospheric alkalinity from the expression:

$$(ALK) = (ALK)_a + (NH_3(g)) - (HNO_3(g)) \quad (4)$$

Average alkalinities at each site are given in Table 4*a*. Because of the possibility of HNO_3 or NH_3 volatilization from aerosol filter samples collected in fog (see appendix), (ALK) and $(ALK)_a$ were calculated only for nonfoggy conditions. (ALK) and $(ALK)_a$ were usually small numbers determined by the difference of two large numbers, so the standard errors were fairly large. The calculation of the fog water alkalinity [ALK] involved subtracting a small number from a large number; the resulting standard errors were small and were not indicated explicitly.

TABLE 3*a*. Liquid Water-Weighted Average For Water Concentrations of Major Ions, December 31, 1983, to January 14, 1984

Site	Number of Samples	pH Range	H^+	Na^+	NH_4^+	Ca^{2+}	Mg^{2+}	Cl^-	NO_3^-	SO_4^{2-}	S(IV), μM	L^a, g m^{-3}
Bakersfield	16	5.10–6.92	2.0	42	3270	169	33	122	819	2070	384	0.057
McKittrick	58	2.68–5.23	93	11	480	39	5	15	250	345	43	0.11
Buttonwillow	7	5.01–6.79	5.6	13	1067	82	10	47	522	760	74	0.050
Visalia	13	5.51–7.23	0.1	6	1080	17	2	115	341	265	12	0.049

Unless otherwise indicated, concentrations are in microequivalents per liter of water. See *Jacob* [1985] for the complete data set.
[a]Average liquid water content, based on the total amount of water collected and the total sampling time.

TABLE 3b. Liquid Water-Weighted Average Fog Water Concentrations of Trace Metals, December 31, 1983, to January 14, 1984

Site	Number of Samples	Fe	Mn	Pb	Cu	Ni	V
Bakersfield	5	438	31	134	19	29	41
McKittrick	42	76	6	27	12	48	91
Buttonwillow	6	142	17	44	82	44	32
Visalia	6	144	7	61	7	11	8

Concentrations are in micrograms per liter of water. See *Jacob* [1985] for the complete data set.

The western edge of the SSJV currently suffers from a general acid fog problem, as shown by the negative average values of (ALK). In the remainder of the valley, (ALK) > 0, and fog water is not usually acidic. However, the average values of (ALK) at Bakersfield and Wasco presently amount to less than 20% of (S(VI) + N(V)) equivalent concentrations. If NH_3 emissions in the SSJV decrease by 20% compared to their current level, for example, because of a decline of the cattle industry or fluctuations in the soil moisture and temperature, a general acid fog situation in the east side of the SSJV will result. The same result will be achieved by a 20% increase in (S(VI) + N(V)) equivalent concentrations due to a rise in SO_2 and NO_x emissions. Fog water alkalinity at Visalia will not be affected by these changes in SSJV emissions, considering the large (ALK)/(S(VI) + N(V)) ratio at that site; therefore there is little risk that an acid fog problem in the SSJV could spread to the northern part of the San Joaquin Valley.

The partitioning of the atmospheric alkalinity between the gas phase and the aerosol is of interest. Scavenging of NH_3(g) to form ammonium salts of weak acids could be a source of important alkalinity in the aerosol or fog water. Indeed, significant alkalinities were found in fog water; however, aerosol collected under nonfoggy conditions was never significantly alkaline. Although the error bars on the determinations of $(ALK)_a$ were large, the absence of positive $(ALK)_a$ values in the presence of large excesses of NH_3(g), as at Visalia, strongly suggests that the alkaline ammonium salts are volatile under nonfoggy conditions. This hypothesis is supported by concurrent sampling of aerosol and fog water at Visalia, where NH_4^+ was in excess of NO_3^- and SO_4^{2-} in the fog water but not in the dried aerosol. Artifact aerosol neutralization should not occur during filter storage (see appendix).

Under nonfoggy acidic conditions the aerosol contained significant inorganic acidity when S(VI) was present in excess of N(−III). This occurred in six of the samples, all at McKittrick. In the remainder of the samples collected under acidic conditions the aerosol was neutralized, and the inorganic acidity was entirely present in the gas phase as HNO_3(g). This observation is in agreement with aerosol equilibrium models [*Bassett and Seinfeld*, 1983]; NH_3(g) is scavenged by acid sulfate aerosol until this aerosol is neutralized as $(NH_4)_2SO_4$. Excess NH_3 may then combine with HNO_3 to add NH_4NO_3 to the aerosol phase, but HNO_3 in excess of NH_3 remains in the gas phase.

TABLE 3c. Liquid Water-Weighted Average Fog Water Concentrations of Carboxylic Acids, December 31, 1983, to January 14, 1984

Site	Number of Samples	Formate	Acetate	Lactate	Propionate
Bakersfield	2	45	155	15	9
McKittrick	26	22	3	2	0
Buttonwillow	2	144	59	3	0
Visalia	6	53	65	7	0

Concentrations are in micromols per liter of water. See *Jacob* [1985] for the complete data set.

TABLE 4a. Average Alkalinities at Each Site

Site	Number of Samples	ALK, neq m^{-3}	ALK_a, neq m^{-3}	ALK_f, μeq L^{-1}	L_w[a], g m^{-3}
Bakersfield	28	111 ± 31	−20 ± 30		
Wasco	27	46 ± 19	−13 ± 18		
Lost Hills	23	−11 ± 16	−2 ± 16		
McKittrick	21	−12 ± 18	−20 ± 17		
Buttonwillow[b]	17	131 ± 31	−14 ± 28		
Visalia[c]	11	441 ± 30	−7 ± 18		
Bakersfield	2			210	0.11
McKittrick				−98	0.11
Buttonwillow[b]				183	0.05
Visalia[c]				220	0.03

ALK is the atmospheric alkalinity, ALK_a is the aerosol alkalinity, ALK_f is the fog water alkalinity. ALK and ALK_a were calculated only for nonfoggy periods. ALK_f was calculated for the subset of samples analyzed for organic acids. Error bounds are the standard errors on the determinations of the means.

[a]Average liquid water content for the subset of fog water samples.

[b]From January 5 to January 14.

[c]From December 31 to January 7.

The contributions of different species to fog water alkalinity are shown in Table 4b. The main contributors to [ALK] at Bakersfield and Buttonwillow were formate and acetate. Formic and acetic acids are efficiently scavenged in fog water at $pH > 5$; they are highly soluble, as indicated by their large Henry's law constants ($H_{HCOOH,298} = 3.7 \times 10^3$ M atm^{-1}, $H_{CH3COOH,298} = 8.8 \times 10^3$ M atm^{-1} [*Weast*, 1984]), and they are mostly dissociated, as indicated by their acidity constants (see above). At Visalia the fog water pH was much higher than at Bakersfield or Buttonwillow, and the contribution from HCO_3^- to [ALK] was correspondingly larger. Carboxylate anions did not provide higher contributions at Visalia than at Bakersfield or Buttonwillow; since carboxylic acids are already efficiently scavenged at pH 5–6, raising the pH higher leads to little additional scavenging.

ACCUMULATION AND REMOVAL OF H_2SO_4-HNO_3-NH_3 SPECIES OVER THE COURSE OF A SEVERE STAGNATION EPISODE

The goal of this section is to interpret the accumulation of S(VI), N(V), and N(−III) species over the course of the January 2–7 severe stagnation episode, in terms of atmospheric production and removal mechanisms. As shown in Figure 5, the stagnation episode was generally associated with high concentrations of S(VI), N(V), and N(−III). The inversion base was roughly stable at $h = 400$ m AGL throughout the episode, and the residence time for air parcels in the SSJV was $\tau_a = 5$ days. Therefore deposition was a more important removal pathway than ventilation for species with deposition velocities > 0.1 cm s^{-1}. The highest concentrations on the SSJV floor (Bakersfield, Wasco, and Lost Hills) were observed on January 5, after 4 days of stagnation under nonfoggy, overcast conditions; low aerosol deposition rates in the absence of fog allowed high levels of pollutant accumulation. Dense, widespread valley fogs on the mornings of January 6 and 7 (Figure 2) were associated with general decreases in aerosol con-

TABLE 4b. Contributions of Different Species to Fog Water Alkalinity

Site	Number of Samples	Free Acidity,[a] μeq L^{-1}	Formate, μeq L^{-1}	Acetate, μeq L^{-1}	Lactate, μeq L^{-1}	Propionate, μeq L^{-1}	HCO_3^-, μeq L^{-1}	NH_3(aq), μeq L^{-1}
Bakersfield	2	−1	45	134	15	9	6	<1
McKittrick	38	−123	22	1	2	<1	<1	<1
Buttonwillow	2	−8	142	44	3	<1	1	<1
Visalia	6	<1	53	65	7	<1	92	2

Contributions calculated from fog water *p*H.
[a]Free acidity = $[H^+] - [OH]$.

centrations, probably due to rapid deposition of fog droplets. *Jacob et al.* [1984*a*] have previously suggested that enhanced aerosol deposition in fogs efficiently limits pollutant accumulation during stagnation episodes, and our data support this hypothesis. Further decreases in atmospheric concentrations were observed on January 7–8, due to the rise of the inversion base (Figure 2) and deposition from drizzle.

As S(VI) and N(V) were produced over the course of the stagnation episode, significant inorganic acidities were observed at Wasco, Lost Hills, and McKittrick. At Bakersfield, sufficient N(−III) was available to totally neutralize acid inputs. Because of the remarkably stable mixing height and the lack of ventilation we can attempt to apply stirred-tank considerations to calculate the rates of H_2SO_4 and HNO_3 production in the SSJV. The residence time τ of a species in a stirred tank is given by the expression:

$$\frac{1}{\tau} = \frac{v}{h} + \frac{1}{\tau_a} + k \qquad (5)$$

where v is the deposition velocity and k is a first-order chemical loss rate. Of special interest is the period January 2–5, ranging from the onset of stagnation to the first widespread valley fog. The SSJV floor (Bakersfield, Wasco, and Lost Hills) remained overcast throughout that period, and roughly constant values of v and k may be expected. We can thus follow the evolution over 4 days of a very well-controlled stagnant atmospheric system.

Production of H_2SO_4

Concentrations of S(VI) increased progressively on the SSJV floor during the nonfoggy January 2–5 period. Concentrations remained very low at Visalia, which is out of the SSJV and far from SO_2 sources. Sulfur dioxide, the main precursor of S(VI) in the SSJV, has a deposition velocity of the order of 1 cm s^{-1} over grass [*Sehmel*, 1980]. A steady state for SO_2 in the SSJV should therefore be approached on a time scale of the order of 1 day after the onset of stagnation, and this appeared to be the case at Kernridge (Figure 2). Measured concentrations of SO_2 at Bakersfield, Kernridge, and Lost Hills during January 3–5 averaged 25, 12, and 3 ppb, respectively; a strong spatial gradient in SO_2 concentrations was maintained because mixing was slow. Modeling of SO_2 transport under stagnant conditions [*Aerovironment, Incorporated*, 1984] indicates that the SO_2 concentration field in the SSJV should be bounded on the lower end at Wasco and Lost Hills and on the upper end at Bakersfield. Therefore we expect steady state SO_2 concentrations in the SSJV mixed layer to range between 3 and 25 ppb. A stirred-tank calculation based on the volume of the SSJV mixed layer and the emission data of Table 1, assuming chemical loss to be slower than deposition ($V_{SO_2} = 1$ cm s^{-1}), gives an average steady state SO_2 concentration of the order of 9 ppb in the SSJV. This is consistent with our observations.

The accumulation pattern of S(VI) on the SSJV floor was consistent with a pseudo first-order conversion rate of SO_2 to S(VI). Concentrations of S(VI) increased relatively steadily during the January 3–5 period, when SO_2 concentrations were approaching steady state. This steady conversion of SO_2 maintained important differences in S(VI) concentrations from site to site within the SSJV. A time lag for S(VI) production was clearly seen at Bakersfield on January 2, attributable to the time required for SO_2 to accumulate after the onset of stagnation. The profiles of S(VI) concentrations in the SSJV did not suggest an approach of steady state by January 5; the residence time of S(VI) aerosol in the SSJV under nonfoggy conditions was thus longer than 3 days, indicating a deposition velocity $v_{S(VI)} < 0.05$ cm s^{-1} (equation (5)). This is in agreement with predicted deposition velocities for particles in the 0.05- to 1-μm size range at low wind velocities [*Sehmel*, 1980]. Over the period January 3–5, S(VI) was produced in the SSJV much faster than it was removed, and we can to a first approximation equate the observed rate of S(VI) accumulation to the rate of SO_2 conversion. The average rates of S(VI) accumulation during January 3–5 were 9 neq m^{-3} h^{-1} at Bakersfield, 3 neq m^{-3} h^{-1} at Wasco, and 3 neq m^{-3} h^{-1} at Lost Hills; from the assumed steady state SO_2 concentration field in the SSJV (range 3–25 ppb, average 9 ppb), we estimate an average SO_2 conversion rate in the range 0.4–1.1% h^{-1}.

Because of the lack of photochemical activity during the stagnation episode (see Figure 6 and discussion below), conversion of SO_2 to H_2SO_4 must have proceeded predominantly in the aerosol and the cloud droplets. A likely pathway is metal-catalyzed autoxidation in the aqueous phase [*Hoffmann and Jacob*, 1984], which does not require photochemically generated oxidants. Considering that a stratus cloud filled a large fraction of the mixed layer during the period of January 3–5, an important question is to determine if the principal site for S(IV) oxidation was the cloud or the haze aerosol below. Concentrations of SO_2 progressively decreased at Kernridge during the foggy January 5–7 period, while concentrations of CO and NOx (which was emitted from the same sources as SO_2) kept on increasing. This is strong evidence that removal of SO_2 from the atmosphere was enhanced in the presence of fog. From Figure 2 the rate of SO_2 scavenging by fog appears to be on the order of 5% h^{-1}. This enhanced scavenging of SO_2 in fog does not necessarily imply enhanced production of S(VI); S(IV) may be stabilized in the aqueous phase by formation of adducts [*Munger et al.*, 1983, 1984] or removed by deposition before being oxidized. We tried to evaluate S(VI) production directly in fog droplets by comparing S(VI) concentrations in successive fog water samples collected at one site, using Ni and V as conservative tracers for sulfur. However, we did not obtain statistically significant rates of SO_2 conversion in fog water (2 ± 6% h^{-1} at Bakersfield, 0 ± 3% h^{-1} at McKittrick [see *Jacob*, 1985]). This failure to find statistically significant rates is probably due to the complex nature of fog droplet growth and transport.

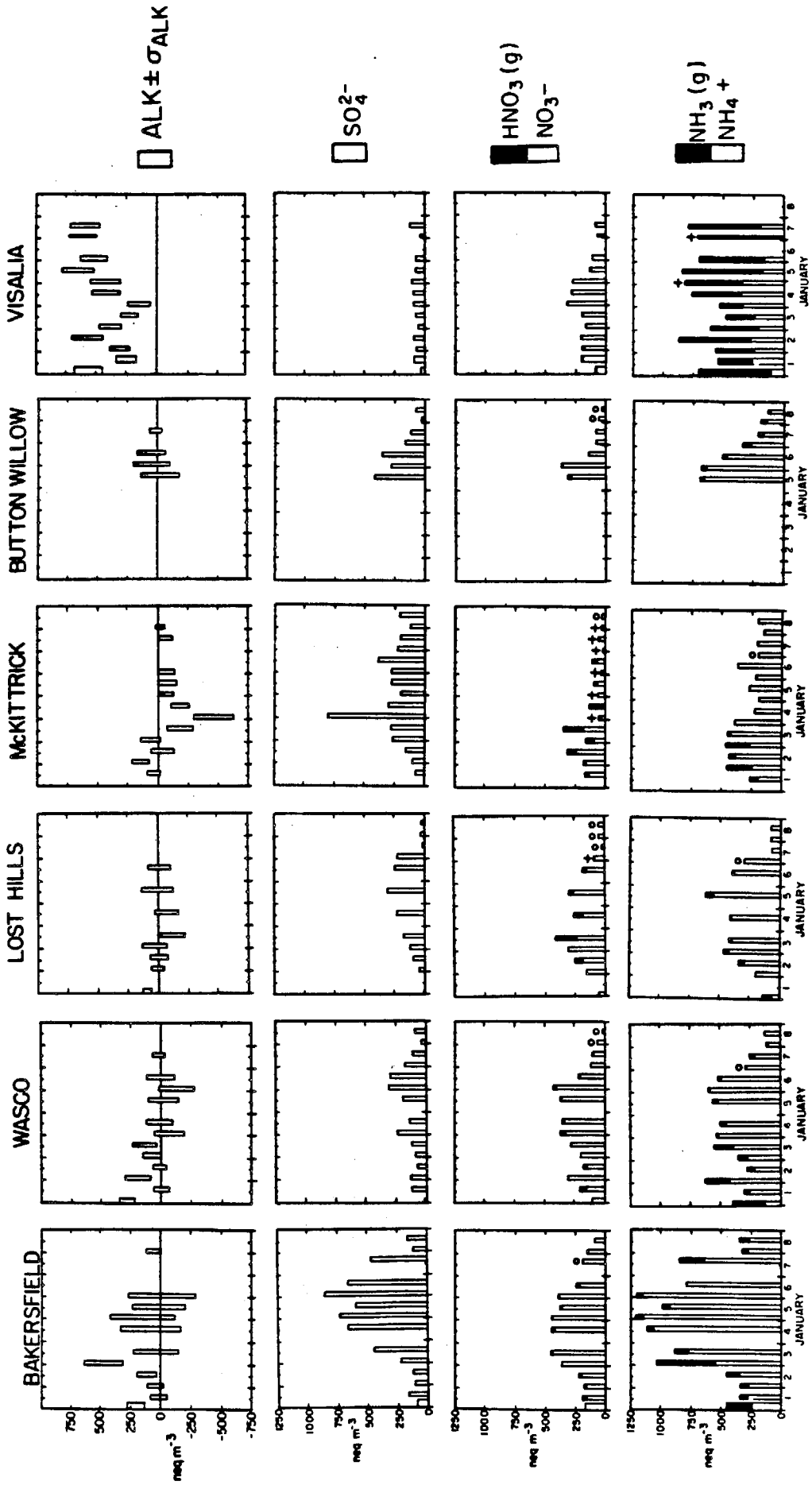

Fig. 5. Aerosol and gas phase concentrations and atmospheric alkalinities at the six valley sites over the period January 1–8. An open circle on top of the data bar indicates that the gas phase species was not measured. A plus sign on top of the data bar indicates that volatilization from the filter in fog could have affected the aerosol measurement (see the appendix).

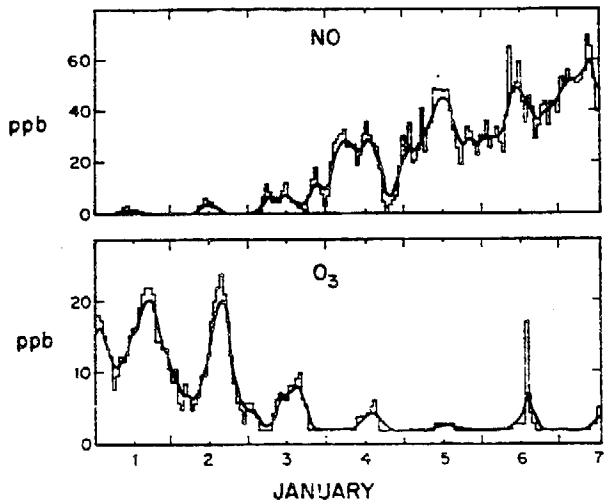

Fig. 6. Concentrations of NO and O_3 at Kernridge. The bold lines were obtained by smoothing the data with a digital filter.

Production of HNO_3

In addition to H_2SO_4, HNO_3 was produced. However, N(V) did not accumulate as steadily as S(VI). Concentrations of N(V) in the SSJV increased rapidly at the onset of stagnation (January 2–3) but did not increase after January 3. Nitrogen oxides accumulated steadily throughout the stagnation episode (Figure 2), showing no indication of loss from chemical conversion. Concentrations of N(V) did not show the large differences from site to site that were observed for S(VI), even though SO_2 and NO_x mostly originated from the same combustion sources.

A logical explanation for these observations is that the rate of HNO_3 production was slow during the stagnation episode because of the widespread and persistent low overcast. Figure 6 shows the NO and O_3 concentration profiles at Kernridge. Ozone levels prior to the onset of stagnation were relatively high, indicating substantial photochemical activity; HNO_3 production by the reaction $NO_2 + OH$ should proceed rapidly under those conditions. Also, O_3 was always present in excess of NO, so that HNO_3 could be produced at night by heterogeneous pathways initiated by the reaction $NO_2 + O_3$ [*Heikes and Thompson*, 1983]. After the onset of stagnation, however, the overcast restricted photochemical activity, and very low O_3 concentrations were observed; OH concentrations were probably very low. Further, since NO progressively accumulated to levels sufficient to titrate O_3 fully, the reaction $NO_2 + O_3$ did not proceed. Therefore little secondary production of HNO_3 would be expected in the SSJV after January 3. Fog did not perceptibly enhance the conversion of NO_x to HNO_3; concentrations of NO_x at Kernridge kept on increasing during the January 5–7 foggy period, similarly to CO, which is not water-soluble. This is consistent with the poor solubilities of NO and NO_2 in water at atmospheric concentrations [*Schwartz and White*, 1981].

The NO_3^- aerosol present after January 3 was therefore mostly aged aerosol, slowly mixing within the SSJV. As mixing proceeded, the differences in NO_3^- concentrations from site to site became progressively weaker. Concentrations of N(V) at Bakersfield and Wasco were similar on January 4–5, even though S(VI) concentrations were much higher at Bakersfield. At Lost Hills and McKittrick, acidification of the atmosphere coincided with a brief increase in HNO_3(g) concentrations, immediately followed by an important drop in total N(V) concentrations. This indicates displacement of NO_3^- by H_2SO_4 in the aerosol, followed by rapid deposition of HNO_3(g). The atmospheric lifetime for HNO_3(g) is thus short (<0.5 days), which implies a large deposition velocity (>1 cm s^{-1}).

Accumulation of NH_3

Almost all of the NH_3 emitted in the SSJV during the stagnation episode was used to neutralize acid inputs. The fate of the resulting (SO_4^{2}, NO_3^-, NH_4^+) aerosol has been discussed above. At Visalia, however, acid inputs were small, and a large fraction of total N(−III) remained in the gas phase as NH_3(g). No accumulation of NH_3(g) was apparent at that site over the course of the episode, and this suggests an atmospheric residence time of <0.5 days for NH_3(g) (deposition velocity of >1 cm s^{-1}). Frequent fog and drizzle after January 5 at Visalia resulted in an important depletion of NH_4^+ aerosol, but NH_3(g) concentrations were unaffected. Ammonia is poorly scavenged at the high *p*H values typical of Visalia fog water [*Jacob et al.*, this issue].

Stirred-Tank Simulation

The above discussions have shown that the profiles of concentrations versus time during a stagnation episode can be successfully interpreted, based on stirred-tank considerations of pollutant accumulation and removal; however, the differences in concentrations from site to site clearly indicate that a stirred-tank model for the SSJV as a whole is not an adequate modeling tool. The major reason is that internal mixing is slow. Nevertheless, the success of the stirred-tank model in interpreting the data at individual sites suggests that one could model the SSJV by subdividing it into a number of cells where the stirred-tank approximation could be properly invoked. Such an exercise is beyond the scope of this paper; however, for the sake of illustrating and summarizing our discussion of field data we will present the results of a stirred-tank calculation applied to the entire SSJV. The accumulation of constituent A in such a model is described by

$$d(A)/dt = E_A + k'(B) - k(A) - \frac{1}{h}\left[(A_g)v_{A_g} + (A_a)v_{A_a} + (A_f)v_{A_f}\right] - (A)/\tau_a \qquad (6)$$

where A_g, A_a, and A_f are the gas phase, aerosol phase, and fog water phase species, respectively, E_A is the emission rate averaged over the volume of the mixed layer (moles per cubic meter per day), and k' is the pseudo first-order rate for conversion of precursor B to A. We simultaneously solved the coupled stirred-tank equations for SO_2, NO_x, S(VI), N(V), and N(−III). The model conditions are given in Table 5 and are for the most part deduced from our discussion of the field data. The emission data are those of Table 1, averaged over the volume of the SSJV mixed layer. We assumed that the aerosol was a neutralized mixture under nonfoggy conditions if N(−III) was in excess of S(VI), and that the formation of NH_4NO_3 aerosol was sufficiently favored to prevent HNO_3 and NH_3 from coexisting in the gas phase under any condition (valid if the atmosphere is sufficiently humid). The simulation was run for 4 days from the beginning of the episode, with a foggy period extending from $t = 2$ days to $t = 3$ days. On the basis of results presented by *Jacob* [1985], *Jacob et al.* [this issue], and *Waldman* [1986] we made the simplifying assumptions that (1) 30% of the aerosol is present in the fog water at any given time, (2) HNO_3(g) is 100% scavenged under all foggy conditions, and (3) NH_3(g) is 100% scavenged

in fog under acid conditions but not scavenged at all under alkaline conditions.

Figure 7 shows the predicted concentration profiles. Aerosol accumulates rapidly under nonfoggy conditions and is partially removed by fog. The main features of the observed concentration profiles are reproduced, in particular, the accumulation patterns for SO_4^{2-} and NO_3^-. The emission rates of Table 1 lead to concentrations of species that are in the range of those observed. Some excess alkalinity as NH_3(g) remains present throughout the episode.

CONCLUSION

A systematic characterization of the H_2SO_4-HNO_3-NH_3 system in the fog water, the aerosol, and the gas phase was conducted at a network of sites in the San Joaquin Valley of California. Spatial patterns of atmospheric concentrations reflected the geographic distribution of oil recovery operations (SO_2, NO_x) and livestock-feeding and agricultural activities (NH_3). The acidity of the fog water was found to be determined by the relative abundances of local acidic (SO_2, NO_x) and alkaline (NH_3) emissions. A region of prevailing acidic conditions was identified on the western edge of the valley, where NH_3 emissions were low. Elsewhere, sufficient NH_3 was available to fully titrate the acidity. In the southern end of the valley, where major oil recovery operations release large amounts of SO_2 and NO_x, a precarious atmospheric balance was found between high concentrations of acids and bases.

The concept of atmospheric alkalinity was introduced as a quantitative measure of the acid-neutralizing capacity of the atmosphere with respect to fog. On the basis of this concept we predicted the regional potentials for high-acidity fog events in the San Joaquin Valley. We concluded that small changes in the activities of the agricultural industry or the oil industry could lead to widespread "acid fog" in the southern end of the valley.

Pollutant concentrations in the valley were strongly affected by the height of the mixed layer and by the occurrence of drizzle or fog. Mixing heights above 1000 m AGL efficiently ventilated the valley. A severe stagnation episode was documented when a temperature inversion based a few hundred meters above the valley floor persisted for 6 days. Progressive accumulation of H_2SO_4-HNO_3-NH_3 species in the mixed layer was observed and interpreted in terms of atmospheric production and removal mechanisms. The accumulation patterns were consistent with very low deposition velocities for secondary (SO_4^{2-}, NO_3^-, NH_4^+) aerosol under nonfoggy conditions (<0.05 cm s^{-1}), and high deposition velocities for HNO_3(g) and NH_3(g) (>1 cm s^{-1}). Decreases in aerosol concentrations were observed following fogs and were attributed to the rapid deposition of fog droplets. Therefore the occurrence of fog was found to effectively limit pollutant accumulation during stagnation episodes.

Secondary production of strong acids under stagnant conditions entirely titrated available alkalinities at the sites farthest from NH_3 emissions. A steady conversion rate of SO_2 to H_2SO_4 was estimated at 0.4–1.1% h^{-1} under overcast stagnant conditions. Conversion of NO_x to HNO_3 was rapid at the beginning of the episode but dropped as the widespread and persistent low overcast reduced photochemical activity. Removal of SO_2 was found to be enhanced in fog, compared to nonfoggy conditions, but NO_x was not scavenged in fog. Acidification of the atmosphere was associated with a brief increase in HNO_3(g) followed by a drop in total N(V) concentrations; this was explained by the displacement of aerosol NO_3^- by H_2SO_4, followed by rapid deposition of HNO_3(g).

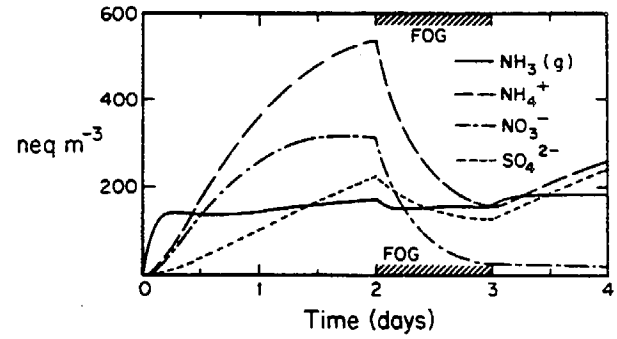

Fig. 7. Stirred-tank simulation of pollutant accumulation in the SSJV over the course of a stagnation episode. The simulation conditions are given in Table 5.

TABLE 5. Parameters for Stirred-Tank Model Simulation

	Deposition velocities, cm s^{-1}
SO_2	1
NO_x	0.1
Nonactivated aerosol	0.05
fog droplets	4
HNO_3(g)	3
NH_3(g)	3
	Conversion rates, % h^{-1}
$SO_2 \rightarrow SO_4^{2-}$, no fog	1
$SO_2 \rightarrow SO_4^{2-}$, fog	5
$NO_x \rightarrow NO_3^-$	10 exp $(-2t)$
	Emission rates, μmol m^{-3} d^{-1}
SO_2	0.95
NO_x	1.3
NH_3	1.4

Residence time of air parcels: 5 days. Mixing height: 400 m AGL; Initial conditions: $(H_2SO_4) = (HNO_3) = (NH_3) = 0$ at $t = 0$; Fog from $t = 2$ to $t = 3$, t is stated in days throughout.

APPENDIX: ERROR ANALYSIS

Fog Water Concentrations

A recent intercomparison study of fog water collectors [*Hering and Blumenthal*, 1985; *Waldman*, 1986] has demonstrated that the California Institute of Technology rotating arm collector provides reproducible and representative samples under both light and heavy fog conditions. The uncertainty on the concentrations of major ions (determined from samples collected with two rotating arm collectors set side by side) was found to be about 15%. Errors due to chemical analysis in the laboratory were about 5% for all analyzed ions. No significant differences in ionic concentrations were found between samples collected concurrently with the rotating arm collector, a jet impactor [*Katz*, 1980], and a screen collector [*Brewer et al.*, 1983], set side by side.

Ionic balances are an indicator of whether all ionic components in the sample have been accounted for in analysis. Ionic

balances in the fog water samples were 0.98 ± 0.18 at Bakersfield ($n = 15$), 1.02 ± 0.09 at McKittrick ($n = 53$), 1.11 ± 0.18 at Buttonwillow ($n = 7$), and 0.60 ± 0.17 at Visalia ($n = 12$). The ionic balances were calculated from the following molar ratio:

Ionic balance

$$= \frac{[Cl^-] + [NO_3^-] + 2[SO_4^{2-}] + [S\ IV]}{[H^+] + [Na^+] + [NH_4^+] + 2[Ca^{2+}] + 2[Mg^{2+}]} \quad (A1)$$

where S(IV) was assumed to be monovalent [*Jacob and Hoffmann*, 1983]. We have argued previously (equation (2)) that this is a good assumption even at high *p*H. The most reliable ionic balances were found at McKittrick, while at Visalia there was a considerable and consistent anion deficiency. Fog water at Visalia had a consistently high *p*H and as a consequence could contain important alkalinity; therefore additional weak acid anions must be considered in an ionic balance. In fog water with low *p*H, such as at McKittrick, weak acids are mostly present in undissociated form and thus (A1) represents a good balance of cations to anions.

The principal ionic contributors to alkalinity in the *p*H range 3–8 are expected to be HCO_3^- and carboxylate ions. Fog water concentrations of four carboxylate ions were determined on a subset of the fog water data set (Table 3). For that subset we calculated the concentrations of the anionic forms of the weak acids from equilibrium at the fog water *p*H and with the acidity constants given in the text. Before inclusion of weak acids the ionic balances were 1.03 ± 0.09 at McKittrick ($n = 25$) and 0.49 ± 0.15 at Visalia ($n = 6$); after inclusion of weak acids the ionic balances were 1.06 ± 0.11 at McKittrick and 0.75 ± 0.15 at Visalia. The McKitrick samples had little alkalinity, and the ionic balance remained close to unity. At Visalia on the other hand, ionic balances were greatly improved. There was still an anion deficiency at Visalia, likely due to undetermined weak acids.

Aerosol, HNO_3(g), and NH_3(g) Concentrations

The filter methods used in this study may lead to two major types of error: (1) N(V) and N(−III) artifacts, and (2) random errors from the sampling process. We will address each in order. An additional source of error could be the neutralization of acidic and alkaline aerosol by absorption of NH_3(g) and HNO_3(g), respectively, during filter storage; however, blank oxalic-acid-impregnated filters and nylon filters were found to remain blank even after extended storage. Therefore aerosol neutralization during storage did not seem to occur.

Stelson and Seinfeld [1982] have shown that an increase in temperature at constant dew point during sampling may volatilize ammonium nitrate collected on Teflon filters and result in artifact HNO_3(g) and NH_3(g). Further, absorption of gaseous nitric acid on the Teflon filter may result in artifact aerosol nitrate [*Spicer and Schumacher*, 1979; *Appel et al.*, 1980]. In an intercomparison study of gaseous nitric acid measurement methods, *Spicer et al.* [1982] found good agreement between the dual-filter method (used here) and other methods. Further, they found that the dual-filter method was accurate in measuring total N(V).

The study of *Spicer et al.* [1982] was conducted under hot, dry conditions. Potential biases are different under the cool, humid conditions found in the San Joaquin Valley. Nighttime samples (0000–0400 PST) were probably unaffected by volatilization because temperatures during the sampling period either remained constant or decreased. During the day, temperature changes were usually small because of the overcast conditions; temperatures recorded hourly at Bakersfield between 1200 and 1600 PST increased on only five of the 15 sampling days and never increased by more than 1°C, except on January 14 (when a 3°C increase was observed). Still, an increase of 1°C in temperature at constant dew point may increase the dissociation constant $K = P_{HNO_3} \times P_{NH_3}$ by a factor of 2 under high-humidity conditions [*Stelson and Seinfeld*, 1982]. The formation of aerosol ammonium nitrate is strongly favored thermodynamically, and aerosol concentrations could not be significantly affected by volatilization; on the other hand, high relative errors may occur in the determination of the gas present at the lowest concentration. Since that concentration was often near or below the detection limit, the error was of little consequence.

Teflon filters run in dense fogs accumulated drops of liquid water at the surface. In those particular cases the filters were dried in the open before being sealed. Nitric acid scavenged in acidic fog volatilizes during drying, leading to an underestimate of total aerosol NO_3^-. No significant NO_3^- loss should occur in nonacidic fog because in that case NO_3^- remains in the aerosol phase as the fog dissipates. Similarly, NH_4^+ aerosol should not volatilize in acidic fog. Volatilization of NH_4^+ from filters collected in alkaline fog depends on the stability of the ammonium salts of weak acids, which appear to be volatile; some volatilization of NH_4^+ was found to occur in a sample collected during fog at Visalia [*Jacob*, 1985].

"Random errors" are of three types: (1) uncertainty in the flow rate through the filter, (2) uncertainty in the efficiency of recovery by extraction, and (3) analytical error. Because the first two sources of error affect the sample as a whole, we expect a correlation to exist between the errors on the different species. To test for these errors, concentrations of SO_4^{2-}, NO_3^-, and NH_4^+ were determined in duplicate for $n = 45$ pairs of filter samples "1" and "2," collected side by side. Concentrations of Cl^- were also determined, but the errors on those concentrations were generally lower than the Cl^- filter blank. The relative differences in the determinations of X for the 45 pairs of duplicate samples were statistically analyzed as follows:

$$D_X = \frac{2(X_2 - X_1)}{X_1 + X_2} \quad (A2)$$

$$\sigma = \left[\frac{\sum (D_X)^2}{n}\right]^{1/2} \quad (A3)$$

Standard deviations σ on the determination of SO_4^{2-}, NO_3^-, and NH_4^+ were 18.6, 18.8, and 19.1%, respectively. These results are comparable to those reported by *Russell and Cass* [1984] for similar measurements. Student "*t*" tests for paired data at the 5% level of significance did not show significant differences between sampling positions 1 and 2 for SO_4^{2-}, NO_3^-, or NH_4^+ at any site, therefore no significant effects from the differences in backup filters were apparent.

We found $D_{SO_4^{2-}}$, $D_{NO_3^-}$, and $D_{NH_4^+}$ to be strongly correlated ($r^2 = 0.71$ between $D_{SO_4^{2-}}$ and $D_{NH_4^+}$, $r^2 = 0.69$ between $D_{NO_3^-}$ and $D_{NH_4^+}$). These correlations must be taken into account in the error analyses of quantities calculated by differences of concentrations, such as (ALK) or gas phase concentrations predicted by thermodynamic models [*Jacob et al.*, this issue]. We resolved σ into its component σ_P, associated with pump operation and filter extraction, and its component $\sigma_{A,X}$, associated with chemical analysis. The error char-

acterized by σ_P may be assumed to be the same for SO_4^{2-}, NO_3^-, and NH_4^+, while the errors due to analysis should be uncorrelated. Because σ is small, we can write as an approximation:

$$\sigma^2 = \sigma_P^2 + \sigma_{A,X}^2 \quad \text{(A4)}$$

By statistical analysis of the differences between NH_4^+, NO_3^-, and SO_4^{2-} concentrations we obtained $\sigma_P = 18.1\%$, $\sigma_{A,SO_4^{2-}} = 4.4\%$, $\sigma_{A,NO_3^-} = 5.1\%$, and $\sigma_{A,NH_4^+} = 6.3\%$. These analytical errors are consistent with our laboratory precision.

No duplicate analyses were made for Na^+, K^+, Ca^{2+}, and Mg^{2+}. Replicate analyses of standards indicate $\sigma_{A,X}^2$ of about 5% for these four ions. Duplicates for $NH_3(g)$ and $HNO_3(g)$ determinations were not collected, but the $\sigma_{A,X}^2$ values should be the same as for NH_4^+ and NO_3^-, respectively. In addition to the analytical error, concentrations of all constituents were assumed to be subject to the same error σ_P. This assumption implies that the variability of the flow rate through the filter is the major contributor to σ_P, which seems justified, since filter extraction efficiencies are better than 95% [*Russell and Cass*, 1984].

The analytical detection limits for a 4-hour sample correspond to 4 neq m^{-3} for NO_3^-, SO_4^{2-}, $HNO_3(g)$, and cations other than NH_4^+, and 8 neq m^{-3} for NH_4^+. Filter blanks for all constituents except Cl^- and $NH_3(g)$ were below these detection limits. Because of substantial filter blanks, effective detection limits for $NH_3(g)$ and Cl^- for a 4-hour sample were 17 neq m^{-3} and 20 neq m^{-3}, respectively.

Acknowledgments. We thank the organizations that provided us with sampling sites: California Air Resources Board, Western Oil and Gas Association, Buttonwillow Park and Recreation, Kern County Fire Department, and U.S. Army Corps of Engineers. We further thank the organizations who provided us with atmospheric data: West Side Operators, California Air Resources Board, National Weather Service, Getty Oil Company, Lemoore Naval Air Station, Tehachapi Fire Station, Edwards Air Force Base, and Kern County Air Pollution Control District. We express our gratitude to D. Buchholz and K. Mayer for their help in the field and to M. Lemons of Getty Oil Company (now Texaco) and the Boy Scouts of Lake Isabella for their contributions to the success of the sampling program. G. R. Cass and A. G. Russell (California Institute of Technology) provided many helpful discussions. This work was funded by the California Air Resources Board (contract A2-048-32). Correspondence should be addressed to M. R. Hoffmann.

REFERENCES

Aerovironment, Incorporated, AVKERN application report, *Rep. AV-FR-83/501R2*, Pasadena, Calif., 1984.

Appel, B. R., S. M. Wall, Y. Tokiwa, and M. Haik, Simultaneous nitric acid, particulate nitrate, and acidity measurements in ambient air, *Atmos. Environ.*, *14*, 549–554, 1980.

Bassett, M. E., and J. H. Seinfeld, Atmospheric equilibrium model of sulfate and nitrate aerosols, *Atmos. Environ.*, *17*, 2237–2252, 1983.

Boyce, S. D., and M. R. Hoffmann, Kinetics and mechanism of the formation of hydroxymethanesulfonic acid at low *p*H, *J. Phys. Chem.*, *88*, 4740–4746, 1984.

Brewer, R. L., E. C. Ellis, R. J. Gordon, and L. S. Shepard, Chemistry of mist and fog from the Los Angeles urban area, *Atmos. Environ.*, *17*, 2267–2271, 1983.

California Air Resources Board, Emission inventory 1979, report, Stationary Source Control Div., Emiss. Invent. Branch, Sacramento, 1982.

Calvert, J. G., and W. R. Stockwell, Mechanism and rates of the gas-phase oxidations of sulfur dioxide and nitrogen oxides in the atmosphere, in *Acid Precipitation: SO_2, NO, and NO_2 Oxidation Mechanisms: Atmospheric Considerations*, edited by J. G. Calvert, pp. 1–62, Butterworth, Woburn, Mass., 1984.

Cass, G. R., S. Gharib, M. Peterson, and J. W. Tilden, The origin of ammonia emissions to the atmosphere in an urban area, *Open File Rep. 82-6*, Environ. Qual. Lab., Calif. Inst. of Technol., Pasadena, 1982.

Cooper, J. A., and J. G. Watson, Jr., Receptor-oriented methods of air particulate source apportionment, *J. Air Pollut. Control Assoc.*, *30*, 1116–1125, 1980.

Crump, J. G., R. C. Flagan, and J. H. Seinfeld, An experimental study of the oxidation of sulfur dioxide in aqueous manganese sulfate aerosols, *Atmos. Environ.*, *17*, 1277–1289, 1983.

Damschen, D. E., and L. R. Martin, Aqueous aerosol oxidation of nitrous acid by O_2, O_3, and H_2O_2, *Atmos. Environ.*, *17*, 2005–2011, 1983.

Dasgupta, P. K., K. DeCesare, and J. C. Ullrey, Determination of atmospheric sulfur dioxide without tetrachlormercurate(II) and the mechanism of the Schiff reaction, *Anal. Chem.*, *52*, 1912–1922, 1980.

Davies, C. N., and M. Subari, Aspiration above wind velocity of aerosols with thin-walled nozzles facing and at right angles to the wind direction, *J. Aerosol Sci.*, *13*, 59–71, 1982.

Dionex Corporation, Determination of anions in acid rain, *Appl. Note 31*, Sunnyvale, Calif., 1981.

Dollard, G. J., and M. H. Unsworth, Field measurements of turbulent fluxes of wind-driven fog drops to a grass surface, *Atmos. Environ.*, *17*, 775–780, 1983.

Granett, A. L., and R. C. Musselman, Simulated acid fog injures lettuce, *Atmos. Environ.*, *18*, 887–891, 1984.

Heikes, B. G., and A. M. Thompson, Effects of heterogeneous processes on NO_3, HONO, and HNO_3 chemistry in the troposphere, *J. Geophys. Res.*, *88*, 10,883–10,896, 1983.

Hering, S. V., and D. L. Blumenthal, Fog sampler intercomparison study: Final report, Coord. Res. Counc., Atlanta, Ga., 1985.

Hoffmann, M. R., Comment on acid fog, *Environ. Sci. Technol.*, *18*, 61–64, 1984.

Hoffmann, M. R., and D. J. Jacob, Kinetics and mechanisms of the catalytic autoxidation of dissolved sulfur dioxide in aqueous solution: An application to nighttime fogwater chemistry, in *Acid Precipitation: SO_2, NO, and NO_2 Oxidation Mechanisms: Atmospheric Considerations*, edited by J. G. Calvert, pp. 101–172, Butterworth, Woburn, Mass., 1984.

Holets, S., and R. N. Swanson, High-inversion fog episodes in central California, *J. Appl. Meteorol.*, *20*, 890–899, 1981.

Huebert, B. J., Measurements of the dry-deposition flux of nitric acid vapor to grasslands and forest, in *Precipitation Scavenging, Dry Deposition, and Resuspension*, vol. 2, edited by H. R. Pruppacher, R. G. Semonin, and W. G. N. Slinn, pp. 785–794, Elsevier North-Holland, New York, 1983.

Jacob, D. J., The origins of inorganic acidity in fogs, Ph.D. thesis, Calif. Inst. of Technol., Pasadena, 1985.

Jacob, D. J., and M. R. Hoffmann, A dynamic model for the production of H^+, NO_3^-, and SO_4^{2-} in urban fog, *J. Geophys. Res.*, *88*, 6611–6621, 1983.

Jacob, D. J., J. M. Waldman, J. W. Munger, and M. R. Hoffmann, A field investigation of physical and chemical mechanisms affecting pollutant concentrations in fog droplets, *Tellus*, *36B*, 272–285, 1984*a*.

Jacob, D. J., R.-F. T. Wang, and R. C. Flagan, Fogwater collector design and characterization, *Environ. Sci. Technol.*, *18*, 827–833, 1984*b*.

Jacob, D. J., J. M. Waldman, J. W. Munger, and M. R. Hoffmann, Chemical composition of fogwater collected along the California coast, *Environ. Sci. Technol.*, *19*, 730–736, 1985.

Jacob, D. J., J. M. Waldman, J. W. Munger, and M. R. Hoffmann, The H_2SO_4-HNO_3-NH_3 system at high humidities and in fogs, 2, Comparison of field data with thermodynamic calculations, *J. Geophys. Res.*, this issue.

Kaplan, D. J., D. M. Himmelblau, and C. Kanaoka, Oxidation of sulfur dioxide in aqueous ammonium sulfate aerosols containing manganese as a catalyst, *Atmos. Environ.*, *15*, 763–773, 1981.

Katz, U., A droplet impactor to collect liquid water from laboratory clouds for chemical analysis, *Conf. Int. Phys. Nuages Commun., 8th*, 697–700, 1980.

Keene, W. C., J. N. Galloway, and J. D. Holden, Jr., Measurement of weak organic acidity in precipitation from remote areas of the world, *J. Geophys. Res.*, *88*, 5122–5130, 1983.

Martell, A. E., and R. M. Smith, *Critical Stability Constants*, vol. 3, Plenum, New York, 1977.

Martin, L. R., Kinetic studies of sulfite oxidation in aqueous solution, in *Acid Precipitation: SO_2, NO, and NO_2 Oxidation Mechanisms: Atmospheric Considerations*, edited by J. G. Calvert, pp. 63–100, Butterworth, Woburn, Mass., 1984.

Munger, J. W., D. J. Jacob, J. M. Waldman, and M. R. Hoffmann, Fogwater chemistry in an urban atmosphere, *J. Geophys. Res.*, *88*, 5109–5121, 1983.

Munger, J. W., D. J. Jacob, and M. R. Hoffmann, The occurrence of bisulfite-aldehyde addition products in fog and cloudwater, *J. Atmos. Chem.*, *1*, 335–350, 1984.

Reible, D. D., Investigations of transport in complex atmospheric flow systems, Ph.D. thesis, Calif. Inst. of Technol., Pasadena, 1982.

Russell, A. G., Analysis of oxalic acid impregnated filters for ammonia determination, *Open File Rep. 83-1*, Environ. Qual. Lab., Calif. Inst. of Technol., Pasadena, 1983.

Russell, A. G., and G. R. Cass, Acquisition of regional air quality model validation data for nitrate, sulfate, ammonium ion and their precursors, *Atmos. Environ.*, *18*, 1815–1827, 1984.

Scherbatskoy, T., and R. M. Klein, Response of spruce and birch foliage to leaching by acidic mists, *J. Environ. Qual.*, *12*, 189–195, 1983.

Schwartz, S. E., and W. H. White, Solubility equilibria of the nitrogen oxides and oxyacids in dilute aqueous solution, *Adv. Environ. Sci. Eng.*, *4*, 1–45, 1981.

Sehmel, G. A., Particle and gas dry deposition: A review, *Atmos. Environ.*, *14*, 983–1011, 1980.

Slinn, W. G. N., Predictions for particle deposition on vegetative canopies, *Atmos. Environ.*, *16*, 1785–1794, 1982.

Smith, R. M., and A. E. Martell, *Critical Stability Constants*, vol. 4, Plenum, New York, 1976.

Sørensen, P. E., and V. S. Andersen, The formaldehyde-hydrogen sulphite system in alkaline aqueous solution: Kinetics, mechanisms, and equilibria, *Acta Chem. Scand.*, *24*, 1301–1306, 1970.

Spicer, C. W., and P. M. Schumacher, Particulate nitrate: Laboratory and field studies of major sampling interferences, *Atmos. Environ.*, *13*, 543–552, 1979.

Spicer, C. W., J. E. Howes, T. A. Bishop, and L. H. Arnold, Nitric acid measurement methods: An intercomparison, *Atmos. Environ.*, *16*, 1487–1500, 1982.

Stelson, A. W., and J. H. Seinfeld, Relative humidity and temperature dependence of the ammonium nitrate dissociation constant, *Atmos. Environ.*, *16*, 983–992, 1982.

Stumm, W., and J. J. Morgan, *Aquatic Chemistry*, pp. 129–132, Wiley-Interscience, New York, 1970.

Waldman, J. M., Depositional aspects of pollutant behavior in fog, Ph.D. thesis, Calif. Inst. of Technol., Pasadena, 1986.

Waldman, J. M., J. W. Munger, D. J. Jacob, and M. R. Hoffmann, Chemical characterization of stratus cloudwater and its role as a vector for pollutant deposition in a Los Angeles pine forest, *Tellus*, *37*, 91–108, 1985.

Weast, R. C. (Ed.), *Handbook of Chemistry and Physics*, 65th ed., Chemical Rubber Company, Cleveland, Ohio, 1984.

D. J. Jacob, Center for Earth and Planetary Physics, Harvard University, Cambridge, MA 02138.

M. R. Hoffmann, J. W. Munger, and J. M. Waldman, Environmental Engineering Science, W. M. Keck Engineering Laboratories, California Institute of Technology, Pasadena, CA 91125.

(Received February 15, 1985;
revised July 25, 1985;
accepted July 31, 1985.)

CHAPTER 5

JOURNAL OF GEOPHYSICAL RESEARCH, VOL. 91, NO. D1, PAGES 1089–1096, JANUARY 20, 1986

The H_2SO_4-HNO_3-NH_3 System at High Humidities and in Fogs 2. Comparison of Field Data With Thermodynamic Calculations

DANIEL J. JACOB,[1] JED M. WALDMAN, J. WILLIAM MUNGER, AND MICHAEL R. HOFFMANN

Environmental Engineering Science, W. M. Keck Engineering Laboratories, California Institute of Technology, Pasadena

Concentrations of HNO_3(g) and NH_3(g) determined in the field were compared to predictions from aerosol equilibrium models. The products of HNO_3(g) and NH_3(g) concentrations measured under cool and humid nonfoggy conditions agreed in magnitude with predictions from a comprehensive thermodynamic model for the atmospheric H_2SO_4-HNO_3-NH_3-H_2O system. Observed concentrations of NH_3(g) in fogs were generally consistent with those predicted at equilibrium with fog water, but important discrepancies were noted in some cases. These discrepancies may be due to fluctuations in fog water composition over the course of sample collection or to the sampling of nonfoggy pockets of air present within the fog. Detectable concentrations of HNO_3(g) (up to 23 neq m^{-3}) were often found in fogs with $pH < 5$ and were attributed to the sampling of nonfoggy air or to the slow rate of HNO_3(g) diffusion to fog droplets. Concentrations of HNO_3(g) in fogs with $pH > 5$ were below the detection limit of 4–8 neq m^{-3}.

JOURNAL OF GEOPHYSICAL RESEARCH, VOL. 91, NO. D1, PAGES 1089–1096, JANUARY 20, 1986

The H_2SO_4-HNO_3-NH_3 System at High Humidities and in Fogs 2. Comparison of Field Data With Thermodynamic Calculations

DANIEL J. JACOB,[1] JED M. WALDMAN, J. WILLIAM MUNGER, AND MICHAEL R. HOFFMANN

Environmental Engineering Science, W. M. Keck Engineering Laboratories, California Institute of Technology, Pasadena

Concentrations of HNO_3(g) and NH_3(g) determined in the field were compared to predictions from aerosol equilibrium models. The products of HNO_3(g) and NH_3(g) concentrations measured under cool and humid nonfoggy conditions agreed in magnitude with predictions from a comprehensive thermodynamic model for the atmospheric H_2SO_4-HNO_3-NH_3-H_2O system. Observed concentrations of NH_3(g) in fogs were generally consistent with those predicted at equilibrium with fog water, but important discrepancies were noted in some cases. These discrepancies may be due to fluctuations in fog water composition over the course of sample collection or to the sampling of nonfoggy pockets of air present within the fog. Detectable concentrations of HNO_3(g) (up to 23 neq m^{-3}) were often found in fogs with $pH < 5$ and were attributed to the sampling of nonfoggy air or to the slow rate of HNO_3(g) diffusion to fog droplets. Concentrations of HNO_3(g) in fogs with $pH > 5$ were below the detection limit of 4–8 neq m^{-3}.

INTRODUCTION

The chemical speciation of the H_2SO_4-HNO_3-NH_3-H_2O system between atmospheric phases has been the subject of much recent interest. Sulfuric acid nucleates with water vapor under usual atmospheric conditions [*Kiang et al.*, 1973], but HNO_3 remains in the gas phase at relative humidities up to about 98% [*Nair et al.*, 1983]. Ammonia is scavenged by acidic sulfate aerosols until eventual neutralization is achieved; however, it has a substantial vapor pressure over ammonium nitrate aerosol. A key question to our understanding of aerosol nitrate formation is the determination of NH_3 and HNO_3 vapor pressures over aerosol formed from H_2SO_4-HNO_3-NH_3 atmospheric mixtures.

A number of thermodynamic models have attempted to answer that question. *Tang* [1980] and *Stelson and Seinfeld* [1982*a*] studied the effect of relative humidity and *p*H on the vapor pressures of HNO_3 and NH_3 over their aqueous solutions. *Stelson and Seinfeld* [1982*b*] determined the dependence on temperature and relative humidity of the ammonium nitrate aerosol dissociation constant $K = P_{HNO_3} \times P_{NH_3}$ and later reported [*Stelson and Seinfeld*, 1982*c*] that addition of H_2SO_4 to the mixture does not lower K greatly unless the H_2SO_4/HNO_3 ratio is very large. *Saxena et al.* [1983] and *Bassett and Seinfeld* [1983, 1984] proposed comprehensive multiphase thermodynamic models for the H_2SO_4-HNO_3-NH_3-H_2O system.

All of the above models are basically consistent one with the other and represent various degrees of sophistication in the treatment of the H_2SO_4-HNO_3-NH_3 system. The Bassett and Seinfeld models offer at present the greatest level of chemical detail. In these models the equilibrium composition is calculated by minimizing the Gibbs free energy of a system composed of the gas phase species H_2SO_4(g), HNO_3(g), and NH_3(g); the aqueous phase species H^+, HSO_4^-, SO_4^{2-}, NO_3^-, and NH_4^+; and the solid phases NH_4HSO_4(s), $(NH_4)_3H(SO_4)_2$(s), $(NH_4)_2SO_4$(s), NH_4NO_3(s), $(NH_4)_2SO_4 \cdot 3NH_4NO_3$(s), and $(NH_4)_2SO_4 \cdot 2NH_4NO_3$(s). The *Bassett and Seinfeld* [1984] model considers in addition the increase in vapor pressure due to the Kelvin effect and thus predicts the size distribution of NO_3^- aerosol from the size distribution of SO_4^{2-} aerosol. The *Bassett and Seinfeld* [1983] model ignores the Kelvin effect, but this is reported to cause only a negligible underestimate of K. In the special case of the HNO_3-NH_3-H_2O system the *Bassett and Seinfeld* [1983] model reduces to the *Stelson and Seinfeld* [1982*b*] model, which uses the same thermodynamic data and ionic strength correction procedures.

The hygroscopic aerosol is an aqueous solution at high humidities, and Table 1 gives the reactions determining the speciation of HNO_3 and NH_3 under those conditions. K decreases rapidly with increasing humidity above the deliquescence point [*Stelson and Seinfeld*, 1982*b*]. Above 100% relative humidity, fog droplets form by activation of condensation nuclei, resulting in a considerable increase of the atmospheric liquid water content and a corresponding enhancement of HNO_3 and NH_3 heterogeneous condensation. Fog droplets are not at stable equilibrium with the surrounding water vapor, and thermodynamic models predicting K as a function of relative humidity cannot be applied; however, HNO_3(g) and NH_3(g) concentrations at equilibrium with the fog water can be directly calculated from measured fog water concentrations. Fog droplets are sufficiently dilute solutions that the Debye-Hückel expression for activity coefficients [*Stumm and Morgan*, 1981] is appropriate.

In fogs the equilibrium partitioning of HNO_3 and NH_3 between the gas phase and the fog water can be determined from the liquid water content, the fog water *p*H, and (R1)–(R3). Liquid water contents in fog range from 0.01–1 g m^{-3}, and fog water *p*H values have been found to range from about 2 to 8 [*Munger et al.*, 1983; *Jacob et al.*, this issue]. Over 99% of total HNO_3 at equilibrium with fog water is scavenged as NO_3^- in this range of conditions (reaction (R1)). No measurable HNO_3(g) should therefore be found at equilibrium in fog, even acidic fog. On the other hand, the equilibrium speciation of NH_3 is strongly dependent on droplet *p*H, liquid water content, and temperature. The fraction F of total NH_3 scavenged by fog is given by:

$$F = \frac{LRTK_2[1 + (K_3[H^+])]}{1 + LRTK_2[1 + (K_3[H^+])]} \quad (1)$$

where the equilibrium constants K_2 and K_3 are the K_{298} values of Table 1 corrected for temperature with the Van't

[1] Now at Center for Earth and Planetary Sciences, Harvard University, Cambridge, Massachusetts.

Copyright 1986 by the American Geophysical Union.

Paper number 5D0728.
0148-0227/86/005D-0728$05.00

TABLE 1. Dissociation and Vapor Pressure Equilibria of HNO_3 and NH_3

Reaction Number	Reaction	K_{298}, kcal mol^{-1}	ΔH_{298}, kcal mol^{-1}	Reference
(R1)	$HNO_3(g) = NO_3^- + H^+$	3.2×10^6 M^2 atm^{-1}	−17.3	*Schwartz and White* [1981]
(R2)	$NH_3(g) = NH_3(aq)$	7.4×10^1 M atm^{-1}	−6.8	*Hales and Drewes* [1979]
(R3)	$NH_3(aq) + H^+ = NH_4^+$	1.7×10^9 M^{-1}	−12.5	*Smith and Martell* [1976]

Hoff equation, L is the liquid water content (cubic meters of water per cubic meter of air), R is the gas constant (8.20568 $\times 10^{-2}$ L atm mol^{-1} K^{-1}), and T is the absolute temperature. Note that in the derivation of (1) the Debye-Hückel activity coefficients cancel each other. F is plotted in Figure 1 as a function of pH under various conditions.

The thermodynamic approaches outlined above provide simple ways for treating aerosol formation and composition in atmospheric chemistry models; therefore it is important to determine the accuracy with which they can describe real atmospheric conditions. The model of *Stelson and Seinfeld* [1982*b*] has been tested with field data in three studies [*Stelson and Seinfeld*, 1982*b*; *Harrison and Pio*, 1983; *Hildemann et al.*, 1984], which all reported that the products of measured $HNO_3(g)$ and $NH_3(g)$ concentrations agreed in magnitude with predicted values of *K. Tanner* [1983] found that the model of *Tang* [1980] adequately predicted concentrations of $HNO_3(g)$ and $NH_3(g)$ over dry aerosol, but he found large discrepancies at high humidities between his field data and the model of *Tang* [1980] for vapor pressures over aqueous aerosol. *Bassett and Seinfeld* [1983] reexamined the data of *Tanner* [1983] in light of their own model and again noted large discrepancies at high humidities between model and observations. No further tests of the *Bassett and Seinfeld* [1983] model have been reported to date.

Measurements of $HNO_3(g)$ and $NH_3(g)$ in fogs or clouds are few. *Daum et al.* [1984] found concentrations of both gases to be below the detection limit of 0.4 ppb (17 neq m^{-3}) in acidic stratus clouds (pH 3.2–4.2). No measurements are available in nonacidic fogs, where NH_3 should have a substantial vapor pressure. *Ayers et al.* [1984] have compared measured ground level $NH_3(g)$ concentrations to those predicted from $[H^+]$ and $[NH_4^+]$ rainwater concentrations and reported large discrepancies between the two.

Over the course of an extensive sampling program in the wintertime atmosphere of the San Joaquin Valley of California [*Jacob et al.*, this issue], we determined $HNO_3(g)$ and $NH_3(g)$ concentrations simultaneously with aerosol and fog water composition. In this paper we compare the concentrations of $HNO_3(g)$ and $NH_3(g)$ determined under nonfoggy conditions to those predicted by the *Bassett and Seinfeld* [1983] model for the H_2SO_4-HNO_3-NH_3-H_2O system. Our data is well suited for such a comparison because the ions SO_4^{2-}, NO_3^-, and NH_4^+ contributed over 90% of the ionic content of the aerosol. In fogs we compare measured concentrations of $HNO_3(g)$ and $NH_3(g)$ to those expected at equilibrium with the fog water concentrations; fog water pH values ranged from 2.9 to 7.6, thus spanning a broad range of predicted $NH_3(g)$-scavenging efficiencies (Figure 1).

Gaseous HNO_3 and NH_3 were determined by dual-filter methods [*Russell and Cass*, 1984]. Aerosol was collected on an open-faced Teflon filter surmounted by a cover to prevent collection of large particles by sedimentation. Fog water was collected with a rotating arm collector [*Jacob et al.*, 1984]. The reader is referred to *Jacob et al.* [this issue] for a description of sampling sites, analytical methods, and a detailed analysis of measurement errors and biases associated with our sampling techniques.

We will generally present $HNO_3(g)$ and $NH_3(g)$ concentrations in units of equivalents per cubic meter, for consistency with the units of NO_3^- and NH_4^+ aerosol concentrations. "Equivalent" in that sense refers to the proton donor or acceptor capacity of the gas when scavenged by the aerosol. Both $HNO_3(g)$ and $NH_3(g)$ contribute one equivalent per mole; 1 ppb = 43 neq m^{-3} at 5°C.

NONFOGGY CONDITIONS

The main site of the San Joaquin Valley sampling program was located in Bakersfield, California. The Bakersfield data are given in Table 2. For comparison with the *Bassett and Seinfeld* [1983] model the aerosol compositions were reduced to model mixtures of SO_4^{2-}, NO_3^-, NH_4^+, and H^+. This was done by assuming concentrations of H^+ and OH^- to satisfy electroneutrality with the measured concentrations of SO_4^{2-}, NO_3^-, and NH_4^+. The presence of other ions in the real aerosol will perturb the thermodynamics, but this perturbation should be small because the ions SO_4^{2-}, NO_3^-, and NH_4^+ contributed over 90% of the total aerosol ionic content [*Jacob et al.*, this issue]. Aerosol concentrations of HCO_3^- and $RCOO^-$ were not determined, but the balances of NH_4^+ to $(NO_3^- + SO_4^{2-})$ in Table 2 show no evidence of excess NH_4^+ attributable to HCO_3^- or $RCOO^-$ ammonium salts. Alkaline ammonium salts appear to be volatile under nonfoggy conditions [*Jacob et al.*, this issue]. Therefore the $(SO_4^{2-}, NO_3^-, NH_4^+, H^+)$ mixture is an adequate model for the ionic content of the Bakersfield aerosol.

We applied the *Bassett and Seinfeld* [1983] model to describe two different partitioning modes for SO_4^{2-} and NO_3^-: (1) SO_4^{2-} and NO_3^- present exclusively in different aerosol phases ("external mixture"), and (2) SO_4^{2-} and NO_3^- al-

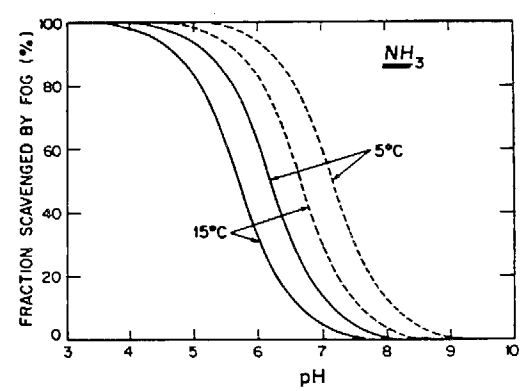

Fig. 1. Fraction of NH_3 scavenged by fog water at equilibrium. All fog droplets are assumed to be at the same pH. Liquid water contents of 0.05 g m^{-3} (solid line) and 0.5 g m^{-3} (dashed line) are considered.

TABLE 2. Bakersfield 1983–1984 Data for Aerosol and Gaseous H_2SO_4-HNO_3-NH_3 Species

Date	Time	NH_4^+	NO_3^-	SO_4^{2-}	NH_3(g)	HNO_3(g)	Temperature, °C	Relative Humidity, %
Dec. 31	0000–0345	573	351	351	19	17	7.8 ± 0.9	96
	1200–1610	669	467	297	158	4	10.8 ± 0.6	93
Jan. 1	0215–0815	242	170	89	212	<4	10.4 ± 0.6	96
	1200–1615	275	161	161	68	35	13.3 ± 0.7	76
Jan. 2	0000–0415	273	168	109	67	14	7.2 ± 1.1	89
	1200–1620	344	201	124	107	25	11.8 ± 0.7	74
Jan. 3	0000–0415	545	370	226	483	<4	9.1 ± 0.8	87
	1200–1615	769	445	445	113	11	9.2 ± 0.6	81
Jan. 4	1200–1700	1057	427	660	55	24	9.9 ± 1.3	80
Jan. 5	0100–0510	1141	442	731	63	6	6.9 ± 0.8	95
	1200–1615	923	362	596	60	19	8.8 ± 0.6	85
Jan. 6	0000–0415	1149	388	855	47	7	7.4 ± 0.6	95
Jan. 8	0000–0405	272	142	118	52	6	6.8 ± 0.6	95
Jan. 9	1420–1825	260	85	219	139	8	7.3 ± 0.6	86
Jan. 10	0000–0415	621	117	570	60	46	6.2 ± 0.6	89
	1200–1615	533	152	417	48	14	6.9 ± 0.8	85
Jan. 11	1200–1615	144	105	78	65	46	9.0 ± 0.7	71
Jan. 12	0000–0415	345	204	149	157	<4	3.0 ± 0.9	91
	1200–1615	331	244	169	334	26	11.2 ± 1.0	66
Jan. 13	0000–0400	486	283	407	208	<4	4.6 ± 0.7	96
	0700–1115	729	349	475	122	6	5.9 ± 0.8	91
	1200–1615	855	437	507	240	14	9.9 ± 1.1	73
	1800–2210	692	402	306	161	10	6.4 ± 0.8	85
Jan. 14	0050–0410	567	423	229	180	5	4.9 ± 1.2	89
	0735–1130	641	423	214	470	6	6.4 ± 1.0	85
	1200–1615	318	263	129	118	43	10.7 ± 1.5	61

Complete aerosol analyses are reported by *Jacob* [1985*a*].
Values are in nanoequivalents per cubic meter unless otherwise indicated; time is local time (PST); and relative humidity is calculated from temperature and dew point.

lowed in the same aerosol phases ("internal mixture"). The actual partitioning will lie somewhere between these two extremes, depending on the aerosol formation processes, the kinetics of coagulation, and the Kelvin effect on HNO_3 vapor pressure [*Bassett and Seinfeld*, 1984]. Since NH_4^+ was always in excess of SO_4^{2-}, the external mixture case was treated by assuming that all SO_4^{2-} was present as $(NH_4)_2SO_4$ and solving the equilibrium problem for the remaining HNO_3 and NH_3 with no SO_4^{2-} present. The internal mixture case was treated by directly solving the equilibrium problem for the H_2SO_4-HNO_3-NH_3-H_2O atmospheric system. The presence of SO_4^{2-} and NO_3^- in the same aqueous phase increases the solubility of HNO_3 and NH_3, compared to an external mixture [*Stelson and Seinfeld*, 1982*c*].

Samples were collected over 4-hour sampling periods, during which temperatures and relative humidities remained stable because of the prevalent low-overcast conditions (Table 2). Temperature and dew point were measured hourly at the National Weather Service (NWS) station 8 km north of the Bakersfield sampling site, and standard deviations for temperature over the 4-hour period were calculated from the hourly temperature record; 0.5°C was added to the standard deviation to account for the sensitivity of the readings. The dew point did not change significantly over the 4-hour sampling periods. A few temperature measurements taken at our sampling site were within 1°C of those taken by NWS. Measurements by the NWS confirm that temperatures and relative humidities at the NWS station are representative of those found at our Bakersfield site (D. Gudgel, Bakersfield NWS, private communication, 1984).

The *Bassett and Seinfeld* [1983] model was run with the computer code provided by *Bassett* [1984]. This code required as input the total (gas plus aerosol) concentrations of H_2SO_4, HNO_3, and NH_3, the temperature, and the relative humidity. To calculate the errors on the predictions from the errors on the measurements, 100 sets of input variables were generated for each data point from a random scheme based on the observed values and standard errors for each of the variables; standard errors on the experimental determinations of concentrations were taken from *Jacob et al.* [this issue]. The expected values and standard errors for the output variables were determined from the outputs for the 100 sets of input variables. Results are shown in Figures 2*a* and 2*b*. The aerosol was predicted to be entirely aqueous except in a few cases (indicated on Figures 2*a* and 2*b*). The standard errors on the predicted values of K were mostly due to errors on the determinations of temperature and relative humidity; they were not affected by errors on H_2SO_4, HNO_3, and NH_3 concentrations in the external mixture assumption and were affected only very weakly in the internal mixture assumption. On the other hand, errors on the concentrations of the individual gases were strongly affected by errors on the determinations of concentrations, especially when a close balance existed between total NH_3 and total acids (HNO_3 + H_2SO_4). In those cases error bars were very large.

The products of partial pressures observed in the field agreed in magnitude with the values of K predicted by the model. However, the model predictions were consistently too low. Predictions with the external mixture assumption were closer to observations than with the internal mixture assumption. The model appeared to give better predictions for individual gases than for K, but this is deceiving. First, the errors on the predicted gas concentrations were large. Second, K was often so small that one of the gases was almost entirely depleted, and the remaining gas was then simply present at its concentration in excess of the neutralized aerosol.

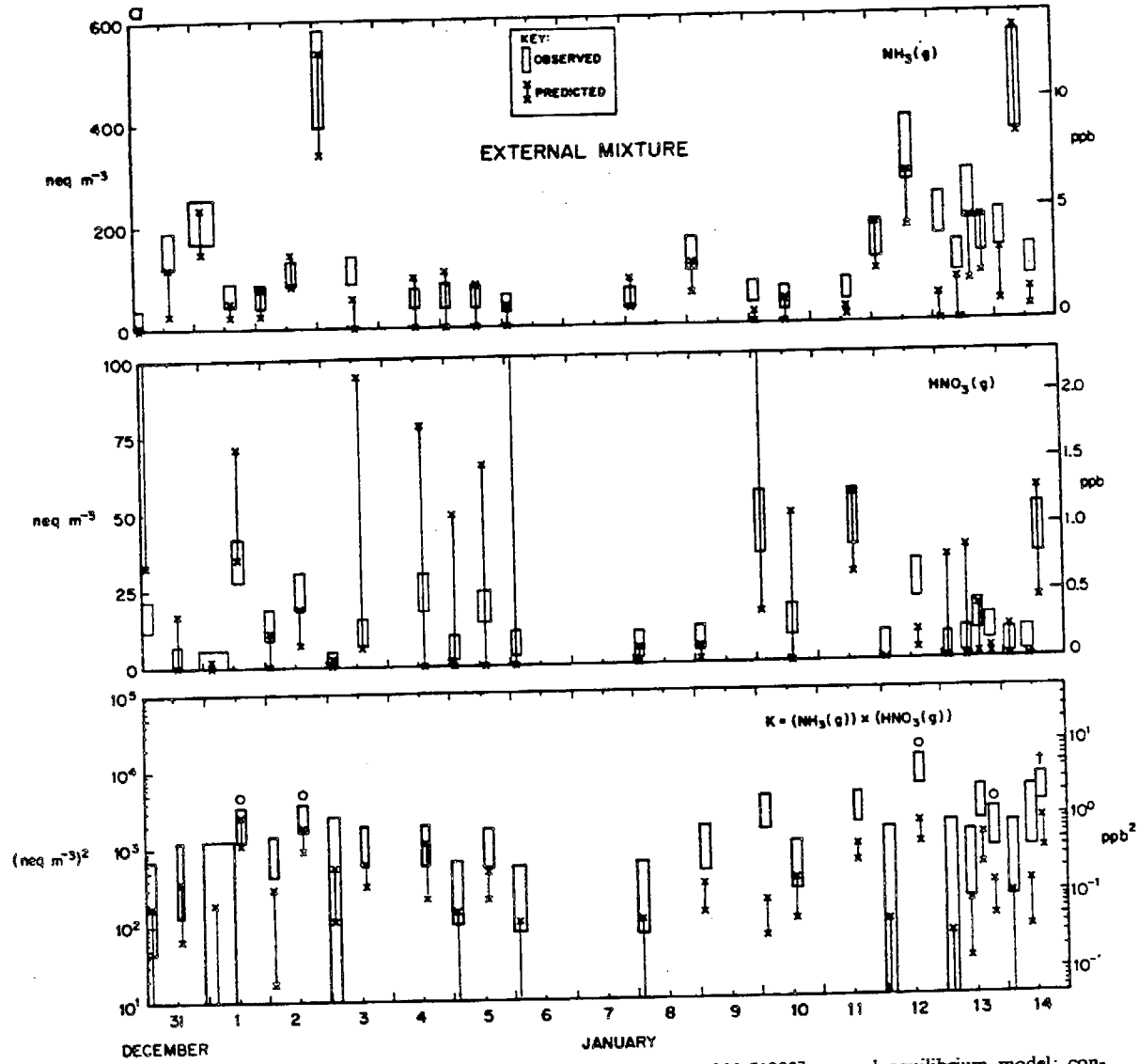

Fig. 2. Comparison of Bakersfield field data to the *Bassett and Seinfeld* [1983] aerosol equilibrium model: concentration products ($HNO_3(g)$) × ($NH_3(g)$), and individual concentrations of $HNO_3(g)$ and $NH_3(g)$. Results are given as error bars extending between the limits (mean $-\sigma$) and (mean $+\sigma$). The aerosol was predicted by the model to be an aqueous solution except when indicated by mixed aqueous-solid (open circle), or solid (dagger). Two limiting cases were considered: (*a*) SO_4^{2-} and NO_3^- present exclusively in different aerosol phases (external mixture assumption) and (*b*) SO_4^{2-} and NO_3^- allowed in the same aerosol phases (internal mixture assumption).

Stelson and Seinfeld [1982*b*] also found that the products of vapor pressures over aqueous aerosol were systematically underpredicted by their model, by factors similar to the ones we observed. *Harrison and Pio* [1983] did not find such a systematic trend, although their determinations may have been subject to large errors because of the considerable fluctuations in temperatures and relative humidities over the course of the sampling periods. Because of the many complicated processes occurring in the atmosphere it is difficult to assess the significance of the model underpredictions. Consideration of droplet curvature would increase the predicted K, but *Bassett and Seinfeld* [1984] found this increase to be negligible. Laboratory data of vapor pressures over concentrated ammonium nitrate solutions should provide a check on the accuracy of the thermodynamic calculations, but they are unavailable at this time.

The dual-filter method is known to be subject to positive interferences, that is, concentrations of $HNO_3(g)$ and $NH_3(g)$ may be overestimated [*Appel et al.*, 1980]. Volatilization of NH_4NO_3 from the Teflon prefilter leads to artifact $HNO_3(g)$ and $NH_3(g)$, but in our case this problem is minimized because temperatures and relative humidities remained stable over the course of the sampling periods (Table 2). Another source of positive interference is the displacement of NO_3^- or NH_4^+ by nonvolatile material collected on the filter, for example, acid sulfates or alkaline carbonates. However, if such dispacement reactions occurred on the filter, this would mean that the atmosphere itself was not at equilibrium; in that case, $HNO_3(g)$ and $NH_3(g)$ atmospheric concentrations could have differed substantially from their equilibrium values.

Indeed, a possible explanation for the discrepancies observed is that the atmosphere was not at chemical equilibrium. The NH_3 observed at Bakersfield originated mostly from local ground level sources [*Jacob et al.*, this issue]; HNO_3 and NH_3 may not have had time to mix sufficiently for equilibrium to be achieved. The incorporation of $HNO_3(g)$ and $NH_3(g)$

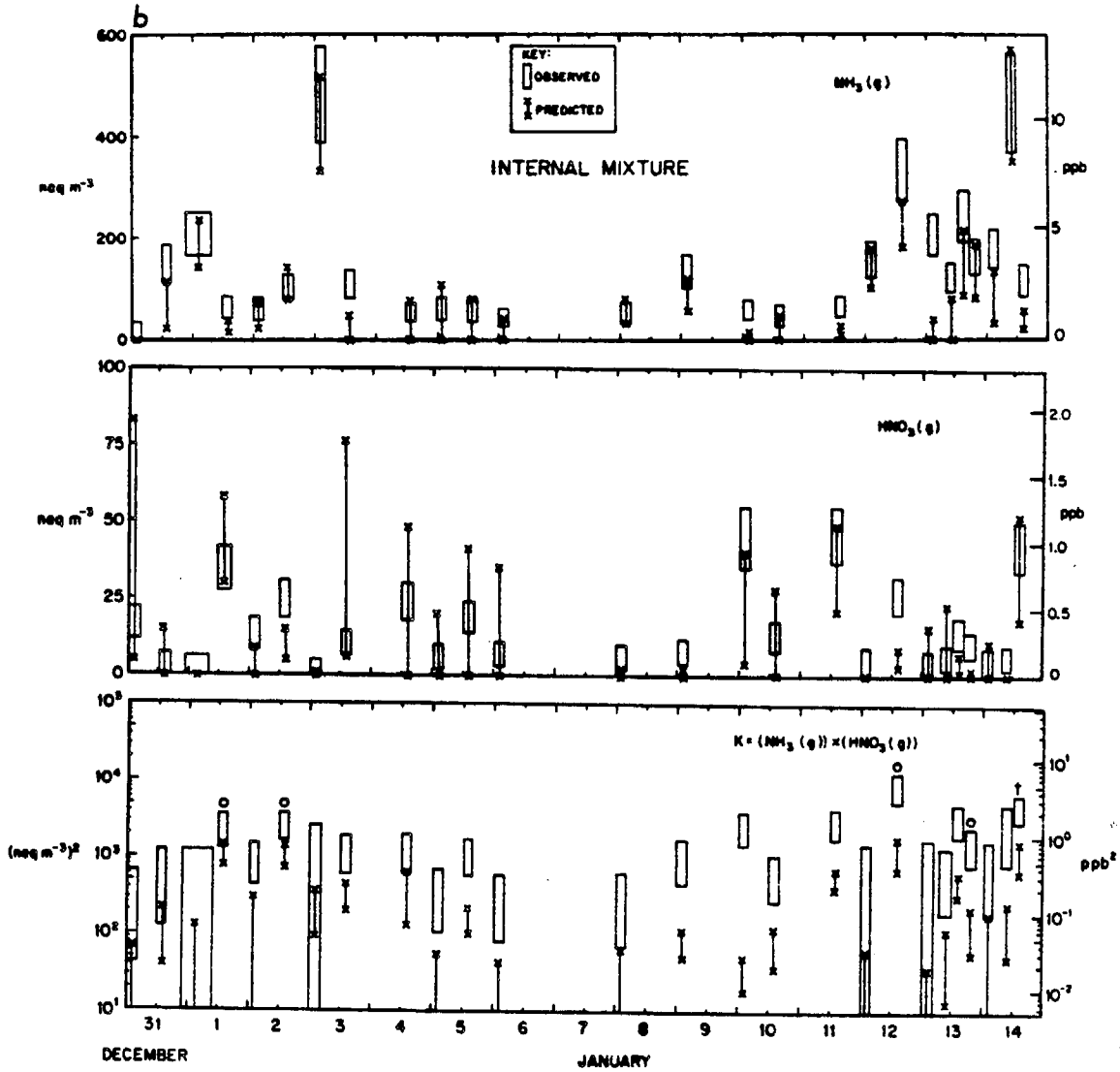

Fig. 2. (continued)

into the aerosol at high humidities proceeds mostly by heterogeneous condensation, which can be a slow process. Based on the calculations of *Fuchs and Sutugin* [1971] over a range of representative conditions, one finds that the diffusion-controlled equilibration time of a gas with low vapor pressure may range from minutes to hours (depending, among other things, on the "sticking coefficient" of the gas molecule on the aerosol).

FOGGY CONDITIONS

Nine concurrent samples of fog water, $HNO_3(g)$, and $NH_3(g)$ were collected during the winter 1983–1984 San Joaquin Valley sampling program at Bakersfield and several other sites, and 19 more samples were collected in a similar program conducted the following winter. All samples were collected during intervals with dense fog throughout. The data are given in Table 3. Concentrations of $NH_3(g)$ at equilibrium with the fog water were calculated from (R2) and (R3):

$$(NH_3(g)) = \frac{1}{RTK_2K_3}[NH_4{}^+]/[H^+] \qquad (2)$$

where $[NH_4{}^+]$ and $[H^+]$ are the fog water concentrations (equivalents per liter of water), and $(NH_3(g))$ is the $NH_3(g)$ concentration (equivalents per liter of air). The standard errors on predicted $(NH_3(g))$ were determined from standard errors of $\pm 1°C$ on temperature and 15% on the determinations of $[NH_4{}^+]$ and $[H^+]$ [*Jacob et al.*, this issue]. Several fog water samples were generally collected over the course of one $NH_3(g)$-sampling period; equilibrium $NH_3(g)$ concentrations were calculated from the fog water concentrations in each individual sample and then time averaged. Results are shown in Table 3 and Figure 3.

The $NH_3(g)$ concentrations calculated from (2) were consistent with observed $NH_3(g)$ concentrations in 22 of the 28 comparisons: they agreed to within a factor of 2 for $NH_3(g)$ concentrations above the detection limit (nine cases) and correctly predicted $NH_3(g)$ concentrations below the detection limit (13 cases). In the remaining six comparisons, however, the agreement was poor. Nonattainment of equilibrium is an unlikely explanation for the observed discrepancies; equilibrium of $NH_3(g)$ with fog water at $pH > 5$ is achieved rapidly because of the relatively low solubility of NH_3 [*Chameides*, 1984]. Also, see discussion by *Jacobs* [1985*b*] and *Chameides* [1985]). However, a major source of error in our calculations is that the fog droplets collected in a fog water sample were not of uniform composition. Fog droplets supporting a

TABLE 3. Concentrations of $HNO_3(g)$ and $NH_3(g)$ in Fogs

Date	Temperature, °C	$HNO_3(g)/NH_3(g)$ Sampling Period, PST	Fog Water Sampling Periods	pH[a]	NH_4^+,[a] μeq L^{-1}	$NH_3(g)$[b] Predicted, neq m^{-3}	$NH_3(g)$ Observed, neq m^{-3}	$HNO_3(g)$ Observed, neq m^{-3}
			Bakersfield					
Jan. 13, 1984	4	0000–0400	0130–0200	6.38	3190	370 ± 86	208	4[c]
			0200–0300	5.92	2800			
			0300–0330	6.72	5920			
			0330–0400	6.74	3300			
Dec. 28, 1984	4	0000–0225	0035–0115	6.80	2680	309 ± 73	363	N/A
			0130–0215	6.20	2780			
Jan. 2, 1985	3.5	2115–0000	2100–2300	6.20	1100	38 ± 15	<25	<6
			2300–0000	5.60	1990			
Jan. 3, 1985	4	0000–0300	0000–0200	5.72	1340	19 ± 7	39	<6
			0200–0305	5.66	1290			
Jan. 3, 1985	2	0300–0700	0305–0500	4.30	781	64 ± 30	262	<4
			0530–0700	6.83	928			
Jan. 3, 1985	1	0700–0930	0700–0830	6.82	1070	161 ± 47	118	<7
			0830–0930	6.51	2900			
Jan. 3–4, 1985	−1	2300–0155	2300–0000	7.08	592	143 ± 42	91	<6
			0000–0100	7.57	379			
			0124–0155	6.76	268			
Jan. 4, 1985	3	2000–2255	2010–2100	6.26	946	22 ± 7	40	<6
			2100–2130	5.16	1340			
			2200–2300	5.46	1440			
Jan. 4–5, 1985	3.5	2310–0205	2300–0000	5.55	1860	11 ± 3	<25	<6
			0000–0100	5.20	1770			
			0100–0200	5.10	1850			
Jan. 5, 1985	2	0400–0805	0400–0500	4.96	1500	7 ± 3	<17	<4
			0500–0600	5.92	1080			
			0600–0700	4.80	1660			
			0700–0800	4.52	720			
Jan. 14, 1985	4.5	0130–0430	0130–0230	6.17	2430	165 ± 45	<25	N/A
			0230–0330	5.56	2390			
			0330–0430	6.72	2170			
Jan. 18, 1985	4	2015–2315	2005–2105	5.85	2400	14 ± 7	<25	9
			2105–2200	4.85	1710			
			2200–2300	4.18	1610			
Jan. 19, 1985	4	0000–0300	0000–0100	3.99	1450	<1	<25	9
			0100–0200	3.86	1450			
			0200–0300	3.67	1590			
Jan. 20, 1985	4	0720–0940	0715–0800	3.06	3130	<1	<29	23
			0800–0845	3.06	3360			
			0845–0930	2.92	3500			
			McKittrick					
Jan. 5, 1984	5	0045–0415	0005–0100	4.02	399	<1	<19	<5
			0100–0200	4.00	347			
			0200–0300	4.02	344			
			0300–0435	4.21	357			
Jan. 6, 1984	5	0000–0410	0035–0100	4.23	241	<1	<16	7
			0100–0200	4.03	294			
			0200–0300	4.22	499			
			0300–0400	4.20	333			
			0400–0500	4.14	345			
Jan. 7, 1984	5	0000–0415	0000–0100	3.96	136	<1	<16	9
			0115–0150	4.41	186			
			0200–0300	4.26	162			
			0300–0400	4.40	204			
			0400–0500	4.44	166			
Jan. 7, 1984	5	1200–1615	1030–1230	4.23	683	<1	<16	11
			1230–1440	4.24	870			
			1440–1540	4.28	740			
			1540–1655	4.12	522			
Jan. 8, 1984	5	0000–0410	2035–0035	4.18	599	1 ± 1	<16	5
			0035–0205	4.50	555			
			0205–0405	5.01	658			
Jan. 10, 1984	5	0045–0445	0010–0120	3.71	845	<1	<17	10
			0120–0525	3.85	351			
			Buttonwillow					
Jan. 7, 1984	6	0100–0500	0040–0140	5.18	1270	10 ± 4	69	4[c]
			0140–0410	5.40	969			
			0410–0620	5.33	1070			
Jan. 3, 1985	4	0000–0220	0000–0215	5.25	2080	11 ± 4	159	<7
Jan. 4, 1985	3	0020–0220	0015–0215	5.73	553	8 ± 3	42	<8
Jan. 4, 1985	1.5	0415–0810	0430–0630	6.14	519	16 ± 6	<17	<4

TABLE 3. (continued)

Date	Temperature, °C	$HNO_3(g)/NH_3(g)$ Sampling Period, PST	Fog Water Sampling Periods	pH[a]	NH_4^+,[a] μeq L^{-1}	$NH_3(g)$[b] Predicted, neq m^{-3}	$NH_3(g)$ Observed, neq m^{-3}	$HNO_3(g)$ Observed, neq m^{-3}
			Buttonwillow (continued)					
Jan. 4, 1985	4	1930–2135	1930–2030	6.55	968	124 ± 33	79	N/A
			2030–2135	6.76	858			
Jan. 5, 1985	2.5	0220–0410	0205–0300	5.70	529	8 ± 2	102	<9
			0300–0400	5.87	483			
Jan. 5, 1985	2	0415–0810	0400–0500	6.16	456	75 ± 21	145	<8
			0500–0615	6.78	683			
			0615–0700	6.89	582			
			0700–0800	6.87	542			
			Visalia					
Jan. 7, 1984	6	0145–0335	0120–0250	6.97	860	355 ± 90	592	<8
			0250–0430	7.23	678			

Measurement errors for $NH_3(g)$ and $HNO_3(g)$ were about 20%. Detection limits depended on filter run time [*Jacob et al.*, this issue]. N/A = not analyzed.

[a]Fog water concentrations. Complete fog water analyses are reported by *Jacob* [1985*a*] for the January 1984 data and by *Waldman* [1986] for the December 1984 to January 1985 data.

[b]Average over time of $NH_3(g)$ concentrations predicted from fog water concentrations and equation (2).

[c]Detection limit.

measurable partial pressure of NH_3 contain alkalinity, and $[H^+]$ will not be conserved upon the mixing of alkalinity-containing droplets of different compositions in the sample. Further, $(NH_3(g))$ is proportional to $1/[H^+]$, a quantity which is not properly averaged by measurement of *p*H in the collected sample. The resulting errors will depend on the extent of nonuniformity in the fog water composition and are difficult to estimate, but they could clearly account for most of the discrepancies. The large variations in *p*H often observed between two consecutive fog water samples (Table 3) are indicative of the variability in fog water composition.

The largest discrepancies were observed for four sampling periods at Buttonwillow when the fog water *p*H was in the range 5–6. In those four cases, equilibrium with fog water considerably underpredicted the observed $NH_3(g)$ concentrations. Fog water at *p*H 5–6 scavenges most of the atmospheric NH_3 (Figure 1) but returns it to the gas phase upon evaporation [*Jacob et al.*, this issue]. An explanation for the large discrepancies that were sometimes observed in this *p*H range is the existence within the fog of pockets of air undersaturated with respect to water vapor [*Gerber*, 1981]. These air pockets would support much larger concentrations of $NH_3(g)$ than the bulk foggy atmosphere and would correspondingly affect the measured $NH_3(g)$ concentration. Further, sampling of undersaturated air may evaporate fog droplets previously collected on the aerosol prefilter and cause artifact $NH_3(g)$.

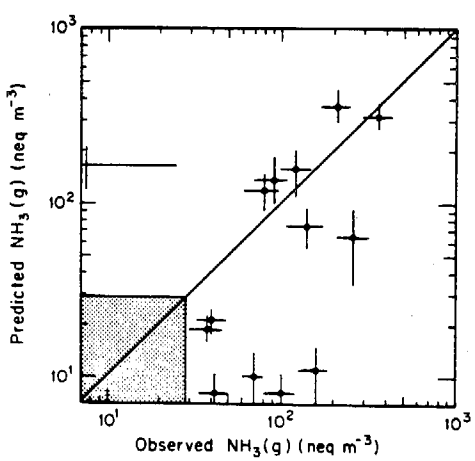

Fig. 3. $NH_3(g)$ concentrations at equilibrium with fog water versus observed $NH_3(g)$ concentrations. Both were below the detection limit for 13 of the points (shaded area). Line represents 1:1 agreement between predictions and observations.

Concentrations of $HNO_3(g)$ in fogs were at or below the detection limit in fogs with *p*H > 5, but detectable $HNO_3(g)$ concentrations (5–23 neq m^{-3}) were found in fogs with lower *p*H. The presence of $HNO_3(g)$ in acidic fog cannot be explained on the basis of equilibrium with fog water. However, the presence of $HNO_3(g)$ can be explained by the substantial vapor pressure of $HNO_3(g)$ over the acid precursor aerosol; undersaturated air pockets within the fog would support $HNO_3(g)$ at equilibrium. An additional explanation is that detectable $HNO_3(g)$ concentrations may subsist for some time in the fog because of the slow rate of $HNO_3(g)$ diffusion to the droplets. *Chameides* [1984] reports that scavenging of $HNO_3(g)$ by diffusion to the fog droplets proceeds on a time scale of a few minutes, but this time may be longer if organic films form at the surface of the droplets [*Gill et al.*, 1983].

CONCLUSION

Concentrations of $HNO_3(g)$ and $NH_3(g)$ were determined in the field under both foggy and nonfoggy conditions, simultaneously with aerosol and fog water composition. Observed concentrations were compared to predictions from thermodynamic models.

Measurements under nonfoggy, cool, and humid conditions (temperatures 3°–13°C, relative humidities 60–100%) were compared to predictions from the *Bassett and Seinfeld* [1983] model for the H_2SO_4-HNO_3-NH_3-H_2O system. The observed products of HNO_3 and NH_3 vapor pressures were of the same magnitude as those predicted by the model; however, the model predictions were consistently too low. The agreement between observations and model was slightly improved by assuming that SO_4^{2-} and NO_3^- were present in different phases (external mixture).

Concentrations of $NH_3(g)$ were below the detection limit of 17–30 neq m^{-3} in fogs with *p*H < 5, and this is consistent with thermodynamic predictions. Substantial $NH_3(g)$ concentrations were observed in fogs with higher *p*H; the observed concentrations were usually within a factor of 2 of those predicted at equilibrium with the fog water, but some

important discrepancies were noted. These discrepancies may be due to fluctuations in fog water composition over the course of sample collection or to the presence of pockets of undersaturated air within the fog.

Concentrations of HNO_3(g) were at or below the detection limit of 4–8 neq m^{-3} in fogs with $pH > 5$, but detectable concentrations (5–23 neq m^{-3}) were often found in fogs with lower pH. Because HNO_3(g) should not be present at equilibrium with fog water, we attribute our observations to the presence of undersaturated air within the fog or to the slow rate of HNO_3(g) diffusion to the fog droplets.

Acknowledgments. A. G. Russell and G. R. Cass (California Institute of Technology) are thanked for many helpful discussions. This work was funded by the California Air Resources Board (A2-048-32). Correspondence should be addressed to Michael R. Hoffmann.

REFERENCES

Appel, B. R., S. M. Wall, Y. Tokiwa, and M. Haik, Simultaneous nitric acid, particulate nitrate, and acidity measurements in ambient air, *Atmos. Environ.*, *14*, 549–554, 1980.

Ayers, G. P., J. L. Gras, A. Adriaansen, and R. W. Gillett, Solubility of ammonia in rainwater, *Tellus*, *36B*, 85–91, 1984.

Bassett, M. E., Mathematical modeling of atmospheric aerosol dynamics and equilibria, Ph.D. thesis, Calif. Inst. of Technol., Pasadena, 1984.

Bassett, M. E., and J. H. Seinfeld, Atmospheric equilibrium model of sulfate and nitrate aerosols, *Atmos. Environ.*, *17*, 2237–2252, 1983.

Bassett, M. E., and J. H. Seinfeld, Atmospheric equilibrium model for sulfate and nitrate aerosols, 2, Particle size analysis, *Atmos. Environ.*, *18*, 1163–1170, 1984.

Chameides, W. L., The photochemistry of a remote marine stratiform cloud, *J. Geophys. Res.*, *89*, 4739–4755, 1984.

Chameides, W. L., Reply, *J. Geophys. Res.*, *90*, 5865–5866, 1985.

Daum, P. H., S. E. Schwartz, and L. Newman, Acidic and related constituents in liquid water stratiform clouds, *J. Geophys. Res.*, *89*, 1447–1458, 1984.

Fuchs, N. A., and A. G. Sutugin, High-dispersed aerosols, in *International Reviews of Aerosol Physics and Chemistry*, vol. 2, edited by G. M. Hidy and J. R. Brock, pp. 1–60, Pergamon, New York, 1971.

Gerber, H. E., Microstructure of a radiation fog, *J. Atmos. Sci.*, *38*, 454–458, 1981.

Gill, P. S., T. E. Graedel, and C. J. Wechsler, Organic films on atmospheric particles, fog droplets, cloud droplets, raindrops, and snowflakes, *Rev. Geophys.*, *21*, 903–920, 1983.

Hales, J. M., and D. R. Drewes, Solubility of ammonia in water at low concentrations, *Atmos. Environ.*, *13*, 1133–1147, 1979.

Harrison, R. M., and C. A. Pio, An investigation of the atmospheric HNO_3-NH_3-NH_4NO_3 equilibrium relationship in a cool, humid climate, *Tellus*, *35B*, 155–159, 1983.

Hildemann, L. M., A. G. Russell, and G. R. Cass, Ammonia and nitric acid concentrations in equilibrium with atmospheric aerosol: Experiment vs. theory, *Atmos. Environ.*, *18*, 1737–1750, 1984.

Jacob, D. J., The origins of inorganic acidity in fogs, Ph.D. thesis, Calif. Inst. of Technol., Pasadena, 1985*a*.

Jacob, D. J., Comment on "The photochemistry of a remote stratiform cloud" by William L. Chameides, *J. Geophys. Res.*, *90*, 5864, 1985*b*.

Jacob, D. J., R.-F. T. Wang, and R. C. Flagan, Fogwater collector design and characterization, *Environ. Sci. Technol.*, *18*, 827–833, 1984.

Jacob, D. J., J. W. Munger, J. M. Waldman, and M. R. Hoffmann, The H_2SO_4-HNO_3-NH_3 system at high humidities and in fogs, 1, Spatial and temporal patterns in the San Joaquin Valley of California, *J. Geophys. Res.*, this issue.

Kiang, C. S., V. A. Mohnen, J. Bricard, and D. Vigla, Heteromolecular nucleation theory applied to gas-to-particle conversion, *Atmos. Environ.*, *7*, 1279–1283, 1973.

Munger, J. W., D. J. Jacob, J. M. Waldman, and M. R. Hoffmann, Fogwater chemistry in an urban atmosphere, *J. Geophys. Res.*, *88*, 5109–5121, 1983.

Nair, P. V. N., P. V. Joshi, U. C. Mishra, and K. G. Vohra, Growth of aqueous solution droplets of HNO_3 and HCl in the atmosphere, *J. Atmos. Sci.*, *40*, 107–115, 1983.

Russell, A. G., and G. R. Cass, Acquisition of regional air quality model validation for nitrate, sulfate, ammonium ion and their precursors, *Atmos. Environ.*, *18*, 1815–1827, 1984.

Saxena, P., C. Seigneur, and T. W. Peterson, Modeling of multiphase atmospheric aerosols, *Atmos. Environ.*, *17*, 1315–1329, 1983.

Schwartz, S. E., and W. H. White, Solubility equilibria of the nitrogen oxides and oxyacids in dilute aqueous solution, *Adv. Environ. Eng. Sci.*, *4*, 1–45, 1981.

Smith, R. M., and A. E. Martell, *Critical Stability Constants*, vol. 4, Plenum, New York, 1976.

Stelson, A. W., and J. H. Seinfeld, Relative humidity and pH dependence of the vapor pressure of ammonium nitrate—nitric acid solutions at 25°C, *Atmos. Environ.*, *16*, 993–1000, 1982*a*.

Stelson, A. W., and J. H. Seinfeld, Relative humidity and temperature dependence of the ammonium nitrate dissociation constant, *Atmos. Environ.*, *16*, 983–992, 1982*b*.

Stelson, A. W., and J. H. Seinfeld, Thermodynamic prediction of the water activity, NH_4NO_3 dissociation constant, density and refractive index for the system NH_4NO_3-$(NH_4)_2SO_4$-H_2O at 25°C, *Atmos. Environ.*, *16*, 2507–2514, 1982*c*.

Stumm, W., and J. J. Morgan, *Aquatic Chemistry*, 2nd ed., p. 134, Wiley-Interscience, New York, 1981.

Tang, I. N., On the equilibrium partial pressures of nitric acid and ammonia in the atmosphere, *Atmos. Environ.*, *14*, 819–828, 1980.

Tanner, R. L., An ambient experimental study of phase equilibrium in the atmospheric system: Aerosol H^+, NH_4^+, SO_4^{2-}, NO_3^-, NH_3(g), HNO_3(g), *Atmos. Environ.*, *16*, 2935–2942, 1983.

Waldman, J. M., Depositional aspects of pollutant behavior in fog, Ph.D. thesis, Calif. Inst. of Technol. Pasadena, 1986.

D. J. Jacob, Center for Earth and Planetary Sciences, Harvard University, Cambridge, MA 02138.

M. R. Hoffmann, J. W. Munger and J. M. Waldman, Environmental Engineering Science, W. M. Keck Engineering Laboratories, California Institute of Technology, Pasadena, CA 91125.

(Received February 15, 1985;
revised July 25, 1985;
accepted July 31, 1985.)

CHAPTER 6

TRANSPORT AND OXIDATION OF SO_2 IN A STAGNANT FOGGY VALLEY

DANIEL J. JACOB
Center for Earth and Planetary Physics, Harvard University, Cambridge, MA 02138, U.S.A.

FREDERICK H. SHAIR
Chemical Engineering, California Institute of Technology, Pasadena, CA 91125, U.S.A.

JED M. WALDMAN,* J. WILLIAM MUNGER and MICHAEL R. HOFFMANN†
Environmental Engineering Science, W. M. Keck Laboratories, California Institute of Technology, Pasadena, CA 91125, U.S.A.

(*First received* 27 *June* 1986 *and in final form* 31 *October* 1986)

Abstract—The fate of SO_2 emitted in the San Joaquin Valley of California under stagnant foggy conditions was determined by the release of an inert tracer and the concurrent monitoring of SO_2 and SO_4^{2-} concentrations. At night, SO_2 was found to be trapped in a dense fog layer below a strong and persistent inversion based a few hundred meters above the valley floor. This lack of ventilation led to the accumulation of SO_2 and SO_4^{2-} over a major SO_2 source region in the valley. The rate of oxidation of SO_2 to SO_4^{2-} in fog was estimated at $3 \pm 2\%\ h^{-1}$. Production of acidity from the oxidation of SO_2 fully titrated the $NH_3(g)$ present before the fog, and led to a progressive drop of the fogwater pH over the course of the night. In the afternoon, the valley was found to be efficiently ventilated by a buoyant upslope flow through the inversion. The tracer data indicated that about 40% of the air transported upslope in the afternoon was returned to the valley in the night-time drainage flow. The fates of SO_2 and SO_4^{2-} in the valley during extended high-inversion episodes appear to depend considerably on the presence of fog or stratus, and on the extent of daytime insolation.

Atmospheric Environment Vol. 21, No. 6, pp. 1305–1314, 1987.
Printed in Great Britain.

0004–6981/87 $3.00 + 0.00
© 1987 Pergamon Journals Ltd.

TRANSPORT AND OXIDATION OF SO_2 IN A STAGNANT FOGGY VALLEY

DANIEL J. JACOB
Center for Earth and Planetary Physics, Harvard University, Cambridge, MA 02138, U.S.A.

FREDERICK H. SHAIR
Chemical Engineering, California Institute of Technology, Pasadena, CA 91125, U.S.A.

JED M. WALDMAN,* J. WILLIAM MUNGER and MICHAEL R. HOFFMANN†
Environmental Engineering Science, W. M. Keck Laboratories, California Institute of Technology, Pasadena, CA 91125, U.S.A.

(*First received* 27 *June* 1986 *and in final form* 31 *October* 1986)

Abstract—The fate of SO_2 emitted in the San Joaquin Valley of California under stagnant foggy conditions was determined by the release of an inert tracer and the concurrent monitoring of SO_2 and SO_4^{2-} concentrations. At night, SO_2 was found to be trapped in a dense fog layer below a strong and persistent inversion based a few hundred meters above the valley floor. This lack of ventilation led to the accumulation of SO_2 and SO_4^{2-} over a major SO_2 source region in the valley. The rate of oxidation of SO_2 to SO_4^{2-} in fog was estimated at $3 \pm 2\% \, h^{-1}$. Production of acidity from the oxidation of SO_2 fully titrated the $NH_3(g)$ present before the fog, and led to a progressive drop of the fogwater pH over the course of the night. In the afternoon, the valley was found to be efficiently ventilated by a buoyant upslope flow through the inversion. The tracer data indicated that about 40% of the air transported upslope in the afternoon was returned to the valley in the night-time drainage flow. The fates of SO_2 and SO_4^{2-} in the valley during extended high-inversion episodes appear to depend considerably on the presence of fog or stratus, and on the extent of daytime insolation.

INTRODUCTION

Sulfur dioxide emitted from the combustion of fossil fuels is oxidized to H_2SO_4 in the atmosphere. The deleterious effects of SO_4^{2-} aerosols on visibility, deposition, and public health are well established (Appel *et al.*, 1985; Gmur *et al.*, 1983; Evans *et al.*, 1984). Atmospheric oxidation of SO_2 can be greatly facilitated by the presence of fog, because SO_2 is absorbed by the fog droplets and is rapidly oxidized in the aqueous phase (Jacob and Hoffmann, 1983; Seigneur and Saxena, 1984). Fogs are usually associated with stagnant weather conditions, which can then lead to very high SO_4^{2-} concentrations in SO_2 source regions. In the Los Angeles basin, for example, it has been observed that days with high SO_4^{2-} concentrations are generally preceded by foggy nights (Zeldin *et al.*, 1976; Cass, 1977).

Sulfate air pollution is a major problem in the San Joaquin Valley of California. The southern end of the valley is the site of important oil recovery by steam injection, and large amounts of SO_2 are emitted about 15 m above ground level by steam generators burning crude oil (Fig. 1). Stagnation high-inversion episodes are frequent in the wintertime, as mesoscale subsidence over the valley due to high pressure aloft produces a strong and persistent temperature inversion based a few hundred meters above the valley floor. Radiative cooling of the moist air trapped below the inversion leads to widespread fog and stratus within the valley. Fog typically forms shortly after sunset, and may not dissipate until the following afternoon. High-inversion episodes persisting for over a week have been documented (Holets and Swanson, 1981).

The ventilation of the valley is severely restricted during high-inversion episodes, because the base of the temperature inversion lies below the mountain ridges surrounding the valley on three sides. Reible (1982) has estimated residence times of the order of 2 days for air parcels in the southern end of the valley under these conditions. Such long residence times, combined with the persistent fog or stratus, favor the oxidation of SO_2 and the subsequent accumulation of SO_4^{2-} aerosol within the valley. In January 1984, our research group conducted an extensive aerosol field study in the San Joaquin Valley during a high-inversion episode with low stratus (Jacob *et al.*, 1986). We observed a steady rise in SO_4^{2-} aerosol concentrations at all valley sites over 4 days of stagnation, and estimated a rate of SO_2 oxidation of 0.4–1.1 % h^{-1} in the overcast mixed layer. We suggested that most of the SO_2 oxidation took place in the stratus cloud which occupied the upper portion of the mixed layer.

* Present address: Dept. of Environmental and Community Medicine, Rutgers Medical School, Piscataway, NJ 08854, U.S.A.

† To whom correspondence should be addressed.

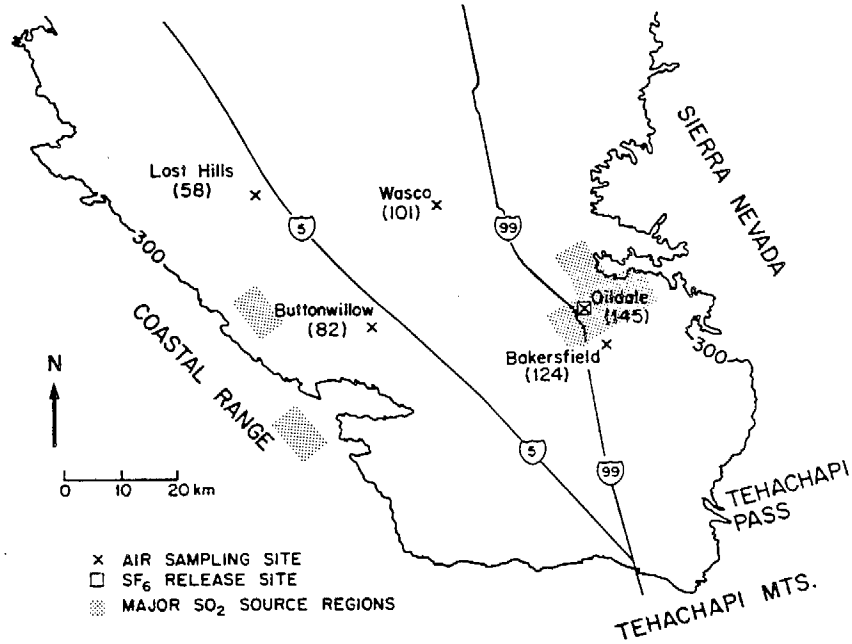

Fig. 1. Sampling sites in the San Joaquin Valley of California. Shaded areas represent major SO_2 source regions (0.3–0.7 tons SO_2 km^{-2} day^{-1}; Aerovironment Inc., 1984). Altitudes are in m MSL. The edge of the valley is defined by the 300 m MSL contour.

A major source of uncertainty in the study of Jacob *et al.* (1986) was the difficulty in characterizing SO_2 transport under stagnant conditions. This transport is very complex because of the frequent wind reversals associated with mountain-valley breezes (Reible, 1982). Transport of SO_2 emitted from the Oildale oil field (Fig. 1) is of particular importance, because that source is responsible for most of the SO_2 emitted in the San Joaquin Valley (Aerovironment Inc., 1984). We present here the results of a study conducted the following year (January, 1985), which was aimed at determining the fate of the Oildale SO_2 plume. The plume was tagged with an inert tracer (SF_6) during a high-inversion stagnation episode, and the tracer was followed in the valley and aloft. We concurrently monitored the concentration of SO_2, the composition of aerosol and fogwater, and the SO_4^{2-} deposition fluxes. From these measurements, we will estimate the rate of SO_2 oxidation in fog.

EXPERIMENTAL

A continuous 23-h release of SF_6 was conducted from Oildale between 1800 LST on 4 January and 1700 LST on 5 January 1985 (LST is local standard time). The SF_6 release rate was 23.4 kg h^{-1}, for a total of 538 kg SF_6 released. Grab samples of air were collected hourly at a number of fixed sites in the southern end of the valley. Networks of automobile traverses were also operated, in which grab samples were collected every mile. Two series of aircraft spirals collected samples at altitudes up to 1220 m MSL. The samples were analyzed by electron capture gas chromatography, which can detect SF_6 concentrations down to 1 ppt. The analytical procedure, and the instrument calibration procedures, have been described by Lamb (1978).

An extensive air sampling network was operated in the San Joaquin Valley during December 1984 and January 1985 (Fig. 1). The complete data sets have been reported by Waldman (1986), along with detailed descriptions of sampling techniques and quality assurance tests. Aerosol samples were collected on open-faced Teflon filters, and fogwater samples were collected with a rotating arm collector (Jacob *et al.*, 1984). The fogwater pH was determined immediately upon sample collection with a Radiometer PHM82 meter and Radiometer GK2320C combination electrode. The analysis of aerosol and fogwater samples followed the protocol of Munger *et al.* (1983), except for fogwater anion analysis which followed the protocol of Jacob *et al.* (1986). The protocol of Jacob *et al.* (1986) makes possible the separate determinations of SO_4^{2-} and S(IV) in the fog sample. Concentrations of NH_3(g) were determined by a dual filter method (Russell, 1983). Concentrations of SO_2 were monitored at Oildale by Texaco. Deposition fluxes of aerosol and fog droplets were measured by Waldman (1986), using polystyrene Petri dish collectors. The fog liquid water content was determined from the collection rate of the rotating arm collector, assuming a collection efficiency of 60% (Jacob *et al.*, 1984). This method has been found to agree fairly well with other liquid water content measurement methods (Waldman, 1986).

Surface winds in the valley were determined at several sites by Texaco and West Side Operators. A tethersonde was launched above Buttonwillow at intervals of 4–8 h, and recorded vertical profiles of temperature, relative humidity, wind speed, and wind direction from 100 to 500 m MSL. Upper air wind data were provided daily by Edwards Air Force Base, located in the Mojave desert on the other side of the Tehachapi mountains. Additional weather data were available from pilot reports and from the National Weather Service station at Oildale.

TRANSPORT OF SF_6 RELEASED FROM OILDALE

1. *Weather pattern*

The SF_6 release was conducted during a typical extended high-inversion episode associated with stationary high pressure over S Idaho and N Nevada (Great Basin High). Strong high pressure was observed over the valley between 1 and 5 January, and produced a persistent subsidence inversion based at 300–400 m MSL. Dense widespread fog filled the mixed layer below the inversion every night; the fog set in shortly after sunset and dissipated late in the following morning, giving way to hazy afternoon sunshine. We show in Fig. 2 some vertical profiles of temperature and relative humidity measured over Buttonwillow during 4–6 January. The inversion was very strong at night and in the morning, but weakened substantially in the afternoon because of solar heating. On the night of 5–6 January no fog was observed in the valley, and the temperature was higher than on the preceding nights; the high pressure had begun to decay. High clouds moved over the valley during that night, and rain began on the afternoon of 6 January. The inversion lifted during the afternoon of 6 January, and unstable conditions prevailed for the next few days.

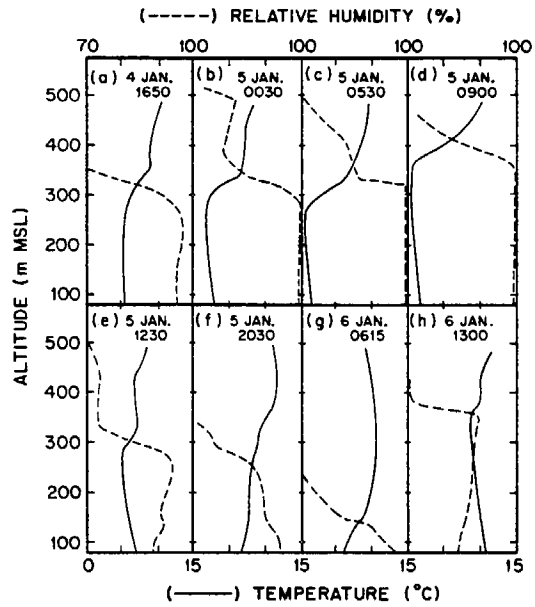

Fig. 2. Vertical profiles of temperature and relative humidity over Buttonwillow. Times are LST.

The Oildale wind data for 4–6 January are summarized in Fig. 3. At night, winds were very weak and frequently shifted in direction. In the daytime, however, a well-defined upslope flow was observed, due to heating of the mountain slopes (Reible, 1982). The upslope flow set in shortly after sunrise, but remained weak until midday. Afternoon insolation of the valley floor following dissipation of the fog strengthened the upslope flow considerably, and wind velocities of 10–20 km h^{-1} were measured at Oildale in the mid-afternoon. Surface winds in the valley were decoupled from the winds aloft; persistent and strong E winds were observed above the inversion, reflecting the circulation around the Great Basin High.

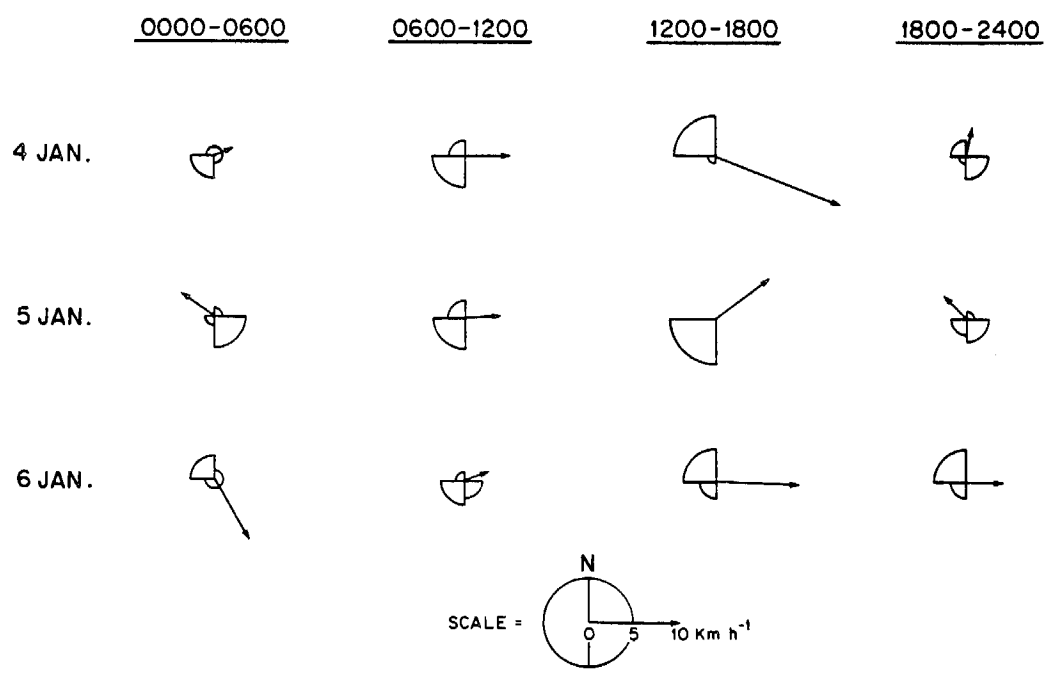

Fig. 3. Surface winds at Oildale. The arrows indicate the mean resultant winds averaged over 6-h periods. The wind roses give the relative frequencies of the different wind directions. Times are LST.

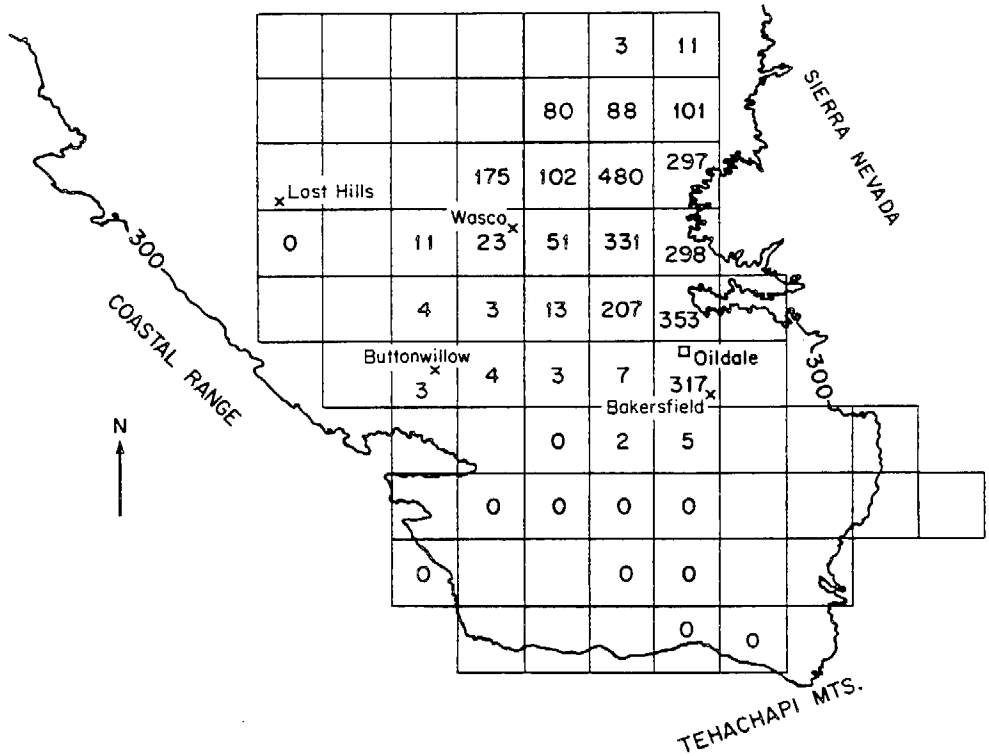

Fig. 4. Surface concentrations of SF_6 (ppt) at 1000–1200 LST on 5 January. The data are averaged over a 10 km × 10 km grid.

2. *Transport of* SF_6

A first network of automobile traverses was operated in the southern end of the valley between 1000 and 1200 LST on 5 January, immediately after the fog had dissipated. The tracer had been released for 16–18 h by that time, and was still being continuously released. The observed concentrations of SF_6, averaged over a 10 km × 10 km grid, are shown in Fig. 4. A mass balance calculation assuming vertical mixing of SF_6 up to the base of the inversion accounted for 91% of the SF_6 released. This demonstrates the lack of ventilation of the valley during the night and morning; almost all of the SF_6 released during the night was trapped within the mixed layer. The SF_6 plume extended about 40 km N of the release site, and spread laterally over about 20 km. This extent of northward transport is consistent with the net weak S–SE winds (2–3 km h^{-1}) observed at Oildale during the night. Concentrations of SF_6 S and W of the release site were very low.

A second network of automobile traverses was operated in the valley during the mid-afternoon of 5 January, but they failed to find the SF_6 plume. The plume had apparently been transported eastward through the inversion by the upslope flow. An aircraft spiral over Oildale at 1530 LST on 5 January indicated the presence of SF_6 within the inversion layer up to at least 1200 m MSL (Fig. 5). The concentration of SF_6 did not decrease progressively with height, as would have been expected from general penetration of SF_6 through the weakened afternoon inversion. Instead, a layer of high SF_6 concentrations was observed at 1200 m MSL, which was also observed in aircraft spirals conducted over other valley sites during the same period. We conclude that SF_6 was transported

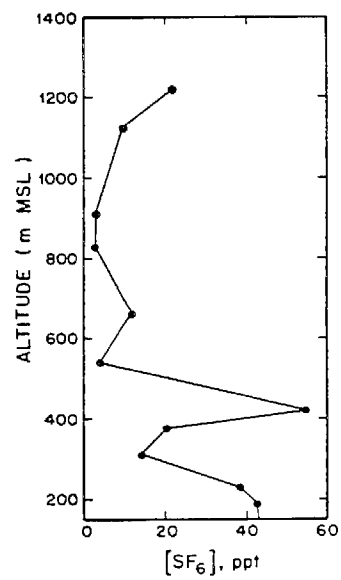

Fig. 5. Vertical profile of SF_6 concentrations over Oildale at 1530 LST on 5 January.

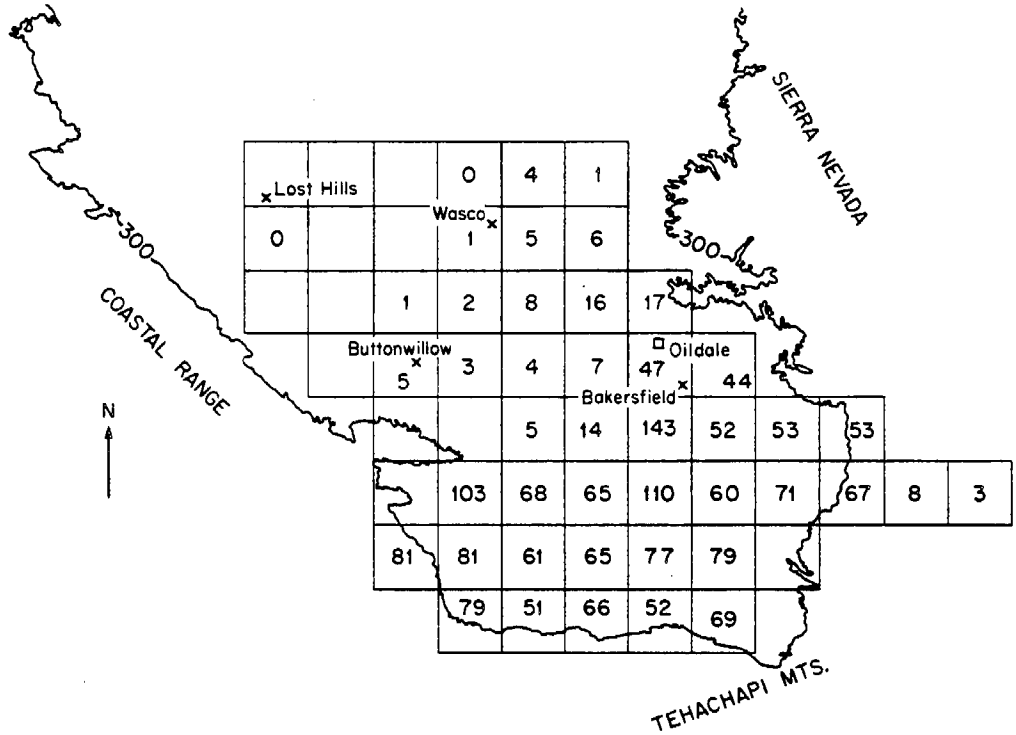

Fig. 6. Surface concentrations of SF_6 (ppt) at 1100–1400 LST on 6 January. The data are averaged over a 10 km × 10 km grid.

upward along the slopes by the buoyant afternoon upslope flow, and was spread out horizontally aloft by the strong upper-level E winds. A rough mass balance, which was based on the aircraft data and dependent on the assumption that SF_6 mixed horizontally aloft over the southern end of the valley, indicated that about 40% of the total SF_6 released was present by mid-afternoon within the inversion layer between 400 and 1200 m MSL. Clearly, the buoyant afternoon upslope flow removed a large fraction of the tracer from the mixed layer below the inversion.

The upslope flow ceased at sunset, and a net weak downslope flow developed in the evening. Winds from the N were observed during the early hours of 6 January, but gave way to weak and inconsistent winds later in the morning (Fig. 3). A network of automobile traverses was operated on 6 January between 1100 and 1400 LST (Fig. 6); high concentrations of SF_6 were found throughout the southern end of the valley. A mass balance calculation from Fig. 6, again assuming vertical mixing up to the base of the inversion, accounted for 37% of the total amount of SF_6 released. Therefore, an important fraction of the SF_6 carried upslope during the afternoon of 5 January was returned to the valley floor in the evening, and was then transported to the southern end of the valley during the night. An aircraft spiral over Oildale at 1220 LST on 6 January (Fig. 7) again showed substantial SF_6 concentrations within the inversion layer.

During the afternoon of 6 January, the upslope flow again transported SF_6 eastward out of the valley. An automobile traverse was conducted in the late afternoon over the Tehachapi pass (1200 m) in the SE end of the valley. Significant SF_6 concentrations (5–20 ppt) were found over the pass and in the Mojave desert on the other side of the mountains. No SF_6 was found to

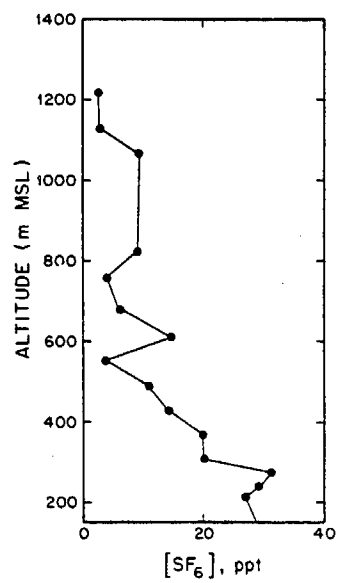

Fig. 7. Vertical profile of SF_6 concentrations over Oildale at 1220 LST on 6 January.

return in the valley on 7 January, probably because of the unstable weather conditions.

TRANSPORT AND OXIDATION OF SO_2

Atmospheric concentrations measured at Oildale during 4–5 January are shown in Fig. 8. Concentrations of SO_2 were very low during the afternoon of 4 January, because of the strong upslope flow carrying SO_2 aloft. After the upslope flow gave way to stagnant conditions in the evening, the SO_2 concentration started to rise and attained a stable value of 40 ppb at midnight. The concentration of SO_2 remained at about 40 ppb from midnight until 1100 LST the following morning, and then dropped rapidly following ventilation of the valley by the upslope flow.

The high night-time SO_2 concentration, combined with the foggy conditions, led to a substantial increase in aerosol SO_4^{2-} concentrations at Oildale. No such increases were observed at Wasco or Buttonwillow, which were both out of the SO_2 plume. Fog set in at Oildale at 2000 LST on 4 January, and persisted until 0900 LST the following morning. The liquid water content of the fog was very stable, and averaged $0.20\ g\,m^{-3}$. Most of the aerosol SO_4^{2-} in the fog was incorporated into fog droplets (Waldman, 1986). The fogwater SO_4^{2-} concentration increased during the early hours of fog, and stabilized after midnight to an average value of $1100\ \mu eq\,\ell^{-1}$. The pH of the fogwater progressively dropped over the course of the night, from 6.26 to 3.75. The acidification of the fogwater resulted in the total depletion of NH_3(g).

The SO_2 sources around Oildale are spread over an area A of about $200\ km^2$ (shaded area in Fig. 1). We assume that this SO_2 source region can be modeled under stagnant conditions as a stirred tank of characteristic length $L = 15$ km and height $h = 130$ m (mixing height over Oildale), slowly ventilated by a steady wind of velocity U. The stable concentrations of SO_2 (40 ppb) and fogwater SO_4^{2-} ($1100\ \mu eq\,\ell^{-1}$) observed at Oildale between 0000 and 0700 LST then correspond to the attainment of a steady state between sources and sinks within the stirred tank. We assume that SO_2 oxidation in fog can be represented by a pseudo first-order rate expression:

$$\frac{d(SO_2)}{dt} = -k(SO_2). \tag{1}$$

The major sinks of SO_4^{2-} within the source region are (1) ventilation (wind velocity U), and (2) fogwater deposition (deposition velocity V_d). The steady-state fogwater SO_4^{2-} concentration in the source region is then given by:

$$\langle [SO_4^{2-}] \rangle = \frac{\frac{2}{WRT} k \langle (SO_2) \rangle + \frac{U}{L}\frac{W_o}{W}[SO_4^{2-}]_0}{\frac{U}{L} + \frac{V_d}{h}} \tag{2}$$

where W is the liquid water content of the fog (v/v), R is the universal gas constant, T is temperature, $\langle (SO_2) \rangle$ is the steady-state SO_2 partial pressure, and the subscript 0 refers to fog upwind from the source region. From Fig. 3, the average wind velocity, U, was between 0000 and 0600 was $4\ km\,h^{-1}$, so that ventilation provided a loss rate of about $27\%\,h^{-1}$. Waldman (1986) measured an average fogwater deposition velocity $V_d = 1\ cm\,s^{-1}$ at Oildale during the night of 4–5 January, corresponding to a deposition rate of $28\%\,h^{-1}$. Therefore, the total rate of SO_4^{2-} removal from the source region (ventilation + deposition) was $55\%\,h^{-1}$. The fogwater composition upwind from the source region can be estimated from fogwater samples collected at Buttonwillow simultaneously with the Oildale samples (Waldman, 1986); these samples contained SO_4^{2-} concentrations averaging $300\ \mu eq\,\ell^{-1}$ for a liquid water content averaging 1.4×10^{-7} v/v. Based on $W = 2.0 \times 10^{-7}$ v/v, $\langle [SO_4^{2-}] \rangle = 1100\ eq\,\ell^{-1}$, $W_0 = 1.4 \times 10^{-7}$ v/v, $[SO_4^{2-}]_0 = 300\ \mu eq\,\ell^{-1}$, and $\langle (SO_2) \rangle = 40$ ppb, we calculate $k = 3\%\,h^{-1}$. An uncertainty of $\pm 2\%\,h^{-1}$ on this value is estimated from the individual uncertainties on the variables in Equation (2).

DISCUSSION

1. SO_2 *oxidation mechanism*

The oxidation of SO_2 to H_2SO_4 can proceed by a number of pathways. Jacob and Hoffmann (1983) and Seigneur and Saxena (1984) have modeled the chemical behavior of night-time fogs in polluted atmospheres, and discussed the relative importances of the major SO_2 oxidation pathways. They predict that SO_2 is rapidly oxidized in the initial stage of a fog by the aqueous-phase reaction of S(IV) with H_2O_2(aq), but that this reaction cannot be sustained because of the depletion of H_2O_2 by SO_2 present in large excess. They find that the main contributor to SO_2 oxidation in the mature stage of the fog is the autoxidation of S(IV) catalyzed by Fe(III) and Mn(II).

These model simulations considered very acidic fogs typical of the Los Angeles coastline (pH 2–4); in our study, however, the fogwater pH remained mostly between 4 and 6, and this can lead to important differences in the rates of SO_2 oxidation. Above pH 4, Fe(III) precipitates, and therefore is not a suitable catalyst for S(IV) autoxidation (Hoffmann and Jacob, 1984). The autoxidation reaction can still be catalyzed by Mn(II), which was present in the Oildale fog samples at concentrations ranging from 0.4 to $0.8\ \mu eq\,\ell^{-1}$ (Waldman, 1986). Assuming a Mn^{2+} concentration of $0.6\ \mu eq\,\ell^{-1}$, an average pH of 5.1, $W = 2.0 \times 10^{-7}$ v/v, and using the rate expression proposed by Hoffmann and Calvert (1985) with the appropriate temperature correction ($T = 278$ K), we estimate that the SO_2 conversion rate by Mn(II)-catalyzed autoxidation was $0.5\%\,h^{-1}$. This reaction appears to be too slow to fully account for the observed rate.

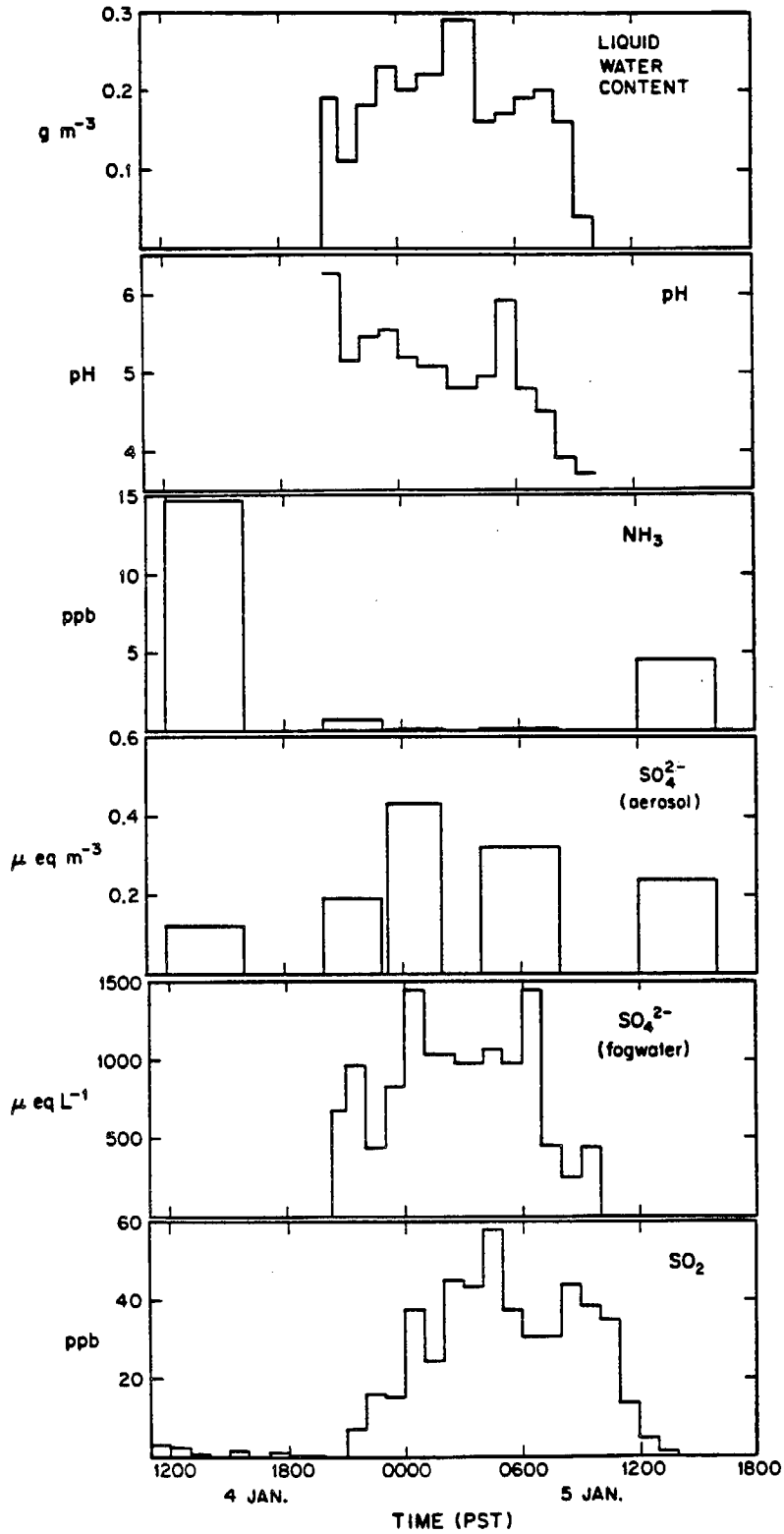

Fig. 8. Atmospheric concentrations measured at Oildale on 4–5 January. Aerosol SO_4^{2-} concentrations are in units of microequivalents m^{-3} of air, and fogwater SO_4^{2-} concentrations are in units of microequivalents per liter of fogwater.

The persistence of a high SO_2 concentration throughout the fog indicates a total depletion of H_2O_2 and organic peroxides, which would otherwise rapidly oxidize SO_2 (Lind *et al.*, 1987); Daum *et al.* (1984) have noted that SO_2 and H_2O_2 appear to be mutually exclusive in clouds. A more important SO_2 oxidation pathway is likely to be the aqueous-phase reaction of S(IV) with O_3 (Hoffmann, 1986), which proceeds rapidly at high pH. Under night-time stagnant conditions in the San Joaquin Valley, O_3 is rapidly depleted in the mixed layer by large excesses of NO (Jacob *et al.*, 1986). However, O_3 concentrations aloft are likely to be higher than at ground level, and O_3 would diffuse to some extent from the inversion layer down into the mixed layer. The O_3 monitoring instrument at Oildale had a detection limit of 10 ppb, and did not measure detectable O_3 concentrations during the night of 4–5 January; however, more sensitive instruments on the west side of the valley reported O_3 concentrations up to 2 ppb. The rate of oxidation of S(IV) by O_3(aq) in fog droplets is limited at high pH by the rate of aqueous-phase diffusion of O_3(aq) within the droplets (Schwartz and Freiberg, 1981; Martin, 1983; Jacob, 1986). If we assume an O_3 concentration of 2 ppb at Oildale, a droplet radius of 10 μm, fogwater pH and W as above, and the kinetic expression of Hoigne *et al.* (1985) with the mass transfer correction of Schwartz and Freiberg (1981), we find an oxidation rate for SO_2 by O_3(aq) of 2% h^{-1} (with $T = 278$ K). This reaction could possibly be an important contributor to S(IV) oxidation in the San Joaquin Valley.

2. *Sulfur budget*

We have shown that the near-totality of SF_6 released between 1800 LST on 4 January and 1100 LST on 5 January (or a period of 17 h) remained trapped within the mixed layer below the inversion. The deposition velocity of SO_2 over grass is about 0.5 cm s^{-1} under stable conditions (Sehmel, 1980); based on $h = 130$ m at Oildale, the SO_2 deposition rate in the valley during the night of 4–5 January was about 14% h^{-1}. In comparison, the SO_2 oxidation rate in fog was previously estimated at 3% h^{-1}. We find from the above loss rates that 33% of the SO_2 released over that 17-h period remained as SO_2 in the mixed layer, 55% was deposited on the valley floor, and the remaining 12% was converted to SO_4^{2-}. Due to the slow rate of SO_4^{2-} production, the maximum SO_4^{2-} concentration in the valley was probably not at Oildale but more likely about 20 km downwind (to the N). Most of the SO_4^{2-} produced was removed to the valley floor by rapid deposition of the fog droplets. The importance of SO_4^{2-} deposition in fogs has been discussed in detail by Waldman (1986).

The fates of SO_2 and SO_4^{2-} determined in the present study differ considerably from those determined in our study of the previous year (Jacob *et al.*, 1986). Jacob *et al.* observed a steady accumulation of SO_2 and SO_4^{2-} over 4 days of stagnation, with no apparent ventilation of the valley and little SO_4^{2-} deposition. In that study, fog did not form on the valley floor; instead, the valley remained overcast as a persistent stratus cloud occupied the upper part of the mixed layer. The overcast limited daytime insolation of the slopes, thereby preventing the upslope flow from ventilating the valley. Further, the deposition of SO_4^{2-} was very slow because of the lack of fog; deposition velocities of haze aerosol particles are over one order of magnitude lower than those of fog droplets (Waldman, 1986). We conclude that the fates of SO_2 and SO_4^{2-} in the San Joaquin Valley during high-inversion episodes depend to a considerable degree on whether or not the valley is insolated, and whether fog or stratus occur. The rate of in-fog SO_2 oxidation estimated in the present study is consistent with the value of 5% h^{-1} estimated in the study of Jacob *et al.* (1986) for SO_2 oxidation in the stratus cloud above the valley floor.

3. *Fogwater and aerosol acidity*

The atmosphere of the San Joaquin Valley usually contains excess alkalinity, due to the presence of important confined cattle feeding operations which discharge large amounts of NH_3 (Jacob *et al.*, 1986). On the afternoon of 4 January, the concentration of NH_3(g) at Oildale was 15 ppb, and the pH of the first fog sample collected that evening was high (pH 6.26). However, the pH dropped progressively over the course of the fog, as the oxidation of SO_2 to H_2SO_4 produced acidity which titrated NH_3(g). By 2300 LST, NH_3(g) was fully titrated, and NH_3(g) concentrations remained below our detection limit of 0.5 ppb until the following afternoon. High concentrations of NH_3(g) were again observed on the afternoon of 5 January, following dissipation of the fog and transport of the acidic aerosol out of the valley.

The decrease in fogwater pH observed after midnight was much slower than that expected from the rate of H_2SO_4 production. The pH drop from 5.5 to 3.75 over 10 h of fog, with $W = 2 \times 10^{-7}$ v/v, is equivalent to the production of 4 neq H^+ m^{-3} h^{-1}; by comparison, oxidation of 40 ppb SO_2 at the rate of 3% h^{-1} produces 100 neq H^+ m^{-3} h^{-1}. It appears that most of the H_2SO_4 produced was neutralized by NH_3, which was continuously being released from ground sources, and therefore that the H_2SO_4 and NH_3 source rates were in close balance.

Jacob *et al.* (1986) had previously reported a similar close balance between high acidic and alkaline emissions in the Southern San Joaquin Valley. Because of the precariousness of the present acid/base balance, relatively small fluctuations in either SO_2 or NH_3 emissions could have important implications for fogwater and aerosol acidity in the San Joaquin Valley. Both SO_2 and NH_3 emissions are currently decreasing in the valley, due to the increasing use of SO_2 scrubbers on steam generators and the decline of the cattle industry. Therefore, it is difficult to forecast whether or not the Southern San Joaquin Valley will be affected by acid fog in the years ahead. The occurrence of acid fog episodes in the valley could have major environmental

implications, in view of the rapidly increasing population and the important agricultural activity. In addition, our data indicate that upslope transport of the acidic aerosol produced in the valley during stagnation episodes affects the National Forests and National Parks on the west side of the Sierra Nevada. Acidic aerosols from the San Joaquin Valley could possibly be a contributing factor to the recent increase in tree necroses observed in Sequoia National Park at elevation 1000–1500 m MSL (California Air Resources Board, private communication, 1986). The possible role of acid fog in provoking pine needle necrosis has been previously discussed by Waldman *et al.* (1984).

CONCLUSIONS

An inert tracer, SF_6, was released from a major SO_2 source region in the San Joaquin Valley of California during an extended high-inversion episode. At night, the near-totality of the tracer was trapped below a strong and persistent subsidence inversion based 200–300 m above the valley floor. In the daytime, however, the upslope flow generated by the insolation of the mountain slopes was sufficiently buoyant to transport the tracer up through the inversion. About 40% of the tracer transported upslope in the afternoon was returned to the valley floor in the evening by the downslope drainage flow.

Considerable accumulation of SO_2 and SO_4^{2-} was observed at night in the stagnant foggy boundary layer. The production of acidity from the oxidation of SO_2 to SO_4^{2-} fully titrated the NH_3(g) present, and led to a progressive decrease of the fogwater pH over the course of the night. A stirred-tank approximation for the SO_2 source region was used to model the night-time sources and sinks of SO_2 and SO_4^{2-}. From that model, the rate of oxidation of SO_2 to SO_4^{2-} in fog was estimated at $3 \pm 2\%\ h^{-1}$. We suggest that SO_2 oxidation proceeded mainly in the fog droplets by reaction of S(IV) with O_2(aq) [catalyzed by Mn(II)] and O_3(aq). In the daytime, the upslope flow efficiently transported SO_2 and SO_4^{2-} out of the valley. By comparing the results of this study to those of a study conducted the previous year, we conclude that the fates of SO_2 and SO_4^{2-} during extended high-inversion episodes in the valley are considerably dependent on the presence of fog or stratus, and on the extent of daytime insolation.

Acknowledgements—We thank D. Gudgel and the Bakersfield National Weather Service office for providing us with the Oildale sampling site and accurate weather forecasts. We also thank D. Anderson from the Bakersfield Texaco office for her helpful co-operation. This research was funded by the California Air Resources Board, Contract No. A4-075-32.

REFERENCES

Aerovironment, Inc. (1984) AVKERN application report, Report AV-FR-83/501R2, Aerovironment, Inc., Pasadena, CA.

Appel B. R., Tokiwa Y., Hsu J., Kothay E. L. and Manh E. (1985) Visibility as related to atmospheric aerosol constituents. *Atmospheric Environment* **19**, 1525–1534.

Cass G. R. (1977) Methods for sulfate air quality management with applications to Los Angeles. Ph.D. thesis, California Institute of Technology, Pasadena, CA.

Daum P. H., Kelly T. J., Schwartz S. E. and Newman L. (1984) Measurements of the chemical composition of stratiform clouds. *Atmospheric Environment* **18**, 2671–2684.

Evans J. S., Posteson P. and Kinny P. L. (1984) Cross-sectional mortality studies and air pollution risk assessment. *Envir. Int.* **10**, 55–83.

Gmur N. F., Evans L. S. and Cunningham E. A. (1983) Effects of ammonium sulfate aerosols on vegetation—II. Mode of entry and responses of vegetation. *Atmospheric Environment* **17**, 715–721.

Hoffmann M. R. (1986) On the kinetics and mechanism of oxidation of aquated sulfur dioxide by ozone. *Atmospheric Environment* **20**, 1145–1154.

Hoffmann M. R. and Calvert J. G. (1985) Chemical transformation modules for Eulerian acid deposition models. Vol. II. The aqueous-phase chemistry. Rep. EPA/600/3-85/017, Envir. Prot. Agency, Research Triangle Park, NC.

Hoffmann M. R. and Jacob D. J. (1984) Kinetics and mechanisms of the catalytic autoxidation of dissolved sulfur dioxide in aqueous solution: an application to night-time fogwater chemistry. In *Acid Precipitation: SO_2, NO, and NO_x Oxidation Mechanisms: Atmospheric Considerations* (edited by Calvert J. G.), pp. 101–172. Butterworth, Boston.

Hoigne J., Bader H., Haag W. R. and Staehelin J. (1985) Rate constants of reactions of ozone with organic and inorganic compounds in water—III. Inorganic compounds and radicals. *Water Res.* **19**, 993–1004.

Holets S. and Swanson R. N. (1981) High-inversion fog episodes in central California. *J. appl. Met.* **20**, 890–899.

Jacob D. J. (1986) The chemistry of OH in remote clouds and its role in the production of formic acid and peroxymonosulfate. *J. geophys. Res.* **91**, 9807–9826.

Jacob D. J. and Hoffmann M. R. (1983) A dynamic model for the production of H^+, NO_3^- and SO_4^{2-} in urban fog. *J. geophys. Res.* **88**, 6611–6621.

Jacob D. J., Munger J. W., Waldman J. M. and Hoffmann M. R. (1986) The H_2SO_4–HNO_3–NH_3 system at high humidities and in fogs—I. Spatial and temporal patterns in the San Joaquin Valley of California. *J. geophys. Res.* **91**, 1073–1088.

Jacob D. J., Wang R.-F. T. and Flagan R. C. (1984) Fogwater collector design and characterization. *Envir. Sci. Technol.* **18**, 827–833.

Lamb B. K. (1978) Development and application of dual atmospheric tracer techniques for the characterization of pollutant transport and dispersion. Ph.D. thesis, California Institute of Technology, Pasadena, CA.

Lind J., Lazrus A. L. and Kok G. L. (1987) Aqueous-phase oxidation of S(IV) by hydrogen peroxide, methyl hydroperoxide, and peroxyacetic acid. *J. geophys. Res.* (in press).

Martin L. R. (1983) Measurements of sulfate production in natural clouds (Discussion). *Atmospheric Environment* **17**, 1603–1604.

Munger J. W., Jacob D. J., Waldman J. M. and Hoffmann M. R. (1983) Fogwater chemistry in an urban atmosphere. *J. geophys. Res.* **88**, 5109–5121.

Reible D. D. (1982) Investigations of transport in complex atmospheric systems. Ph.D. thesis, California Institute of Technology, Pasadena, CA.

Russell A. G. (1983) Analysis of oxalic acid impregnated filters for ammonia determination. Open File Report 83-1, Environmental Quality Laboratory, California Institute of Technology, Pasadena, CA.

Schwartz S. E. and Freiberg J. E. (1981) Mass-transport limitation to the rate of reaction of gases in liquid droplets: application to oxidation of SO_2 in aqueous solutions.

Atmospheric Environment **15**, 1129–1144.

Seigneur C. and Saxena P. (1984) A study of atmospheric acid formation in different environments. *Atmospheric Environment* **18**, 2109–2124.

Waldman J. M. (1986) Depositional aspects of fogs and clouds. Ph.D. thesis, California Institute of Technology, Pasadena, CA.

Waldman J. M., Munger J. W., Jacob D. J. and Hoffman M. R. (1984) Chemical characterization of stratus cloudwater and its role as a vector for pollutant deposition in a Los Angeles pine forest. *Tellus* **37B**, 91–108.

Zeldin M. D., Davidson A., Brunelle M. F. and Dickinson J. E. (1976) A meteorological assessment of ozone and sulfate concentrations in southern California. Report 76-1, Southern California Air Pollution Control District, El Monte, CA.